Universidade do Minho
Escola de Engenharia

Henrique Lima Martins

Development and Manufacturing of a Device for Ultrasonic Assisted Milling

March, 2023

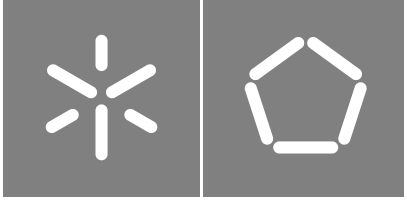

Universidade do Minho
Escola de Engenharia

Henrique Lima Martins

Development and Manufacturing of a Device for Ultrasonic Assisted Milling

Master's Dissertation
Integrated Master's in Mechanical Engineering
Specialization in Advanced Manufacturing

Work supervised by
Professor Hélder Puga

March, 2023

COPYRIGHT AND TERMS OF USE OF THIS WORK BY A THIRD PARTY

This is academic work that can be used by third parties as long as internationally accepted rules and good practices regarding copyright and related rights are respected.

Accordingly, this work may be used under the license provided below.

If the user needs permission to make use of the work under conditions not provided for in the indicated licensing, they should contact the author through the RepositóriUM of Universidade do Minho.

License granted to the users of this work

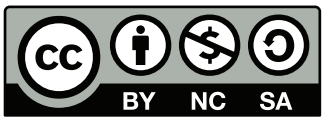

Creative Commons Attribution-NonCommercial-ShareAlike 4.0 International
CC BY-NC-SA 4.0

https://creativecommons.org/licenses/by-nc-sa/4.0/deed.en

STATEMENT OF INTEGRITY

I hereby declare having conducted this academic work with integrity. I confirm that I have not used plagiarism or any form of undue use of information or falsification of results along the process leading to its elaboration.

I further declare that I have fully acknowledged the Code of Ethical Conduct of the Universidade do Minho.

Acknowledgements

This thesis is the culmination of five years of learning and continuous growth, which are widely reflected in this work. I am grateful to several people who have provided their relentless support throughout this journey, to whom I cannot fail to give due recognition:

To my tutor, PhD Hélder Puga, not only for his unwavering patience and trust in my abilities, which allowed for the efficient yet extensive development of this project, but most importantly, for igniting a spark within me that grew into a special interest in the field of machining;

To my parents, Armanda and Joaquim, for their unyielding love and support through my brightest and darkest moments. Thank you for standing by me, supporting all of my decisions, and providing exceptional guidance that has brought me to this point in my life. Without you, I could not have achieved this;

I would like to express a special note of gratitude to my mother, who has taught me the true meaning of courage. Despite numerous challenges life has thrown her way, she has always found a way to overcome them, consistently proving to be the strongest person I have ever met. Thank you for inspiring me to face adversity with fortitude and for instilling in me the value of perseverance. I love you;

To my grandparents, Delmina and Joaquim, along with my uncle Carlos, for raising me with the fundamental values of humbleness, kindness, and wholeheartedness. Who I am today is the result of the invaluable lessons you imparted to me;

To Afonsina, my second family, for embracing me into their bohemian world and fostering an unparalleled environment in which we have shared countless beers, songs, and laughs;

To my three closest university friends, Cristiano, João Alves, and João Marques, who faithfully accompanied me through this ride. Thank you for your fellowship, friendship, and for all the endless nights of philosophical discussions occasionally overshadowing our academic commitments;

To my esteemed friends from “Casinha”, with whom I’ve shared unforgettable moments over the course of the last few years. Thank you for keeping me as part of the core of this phenomenal group, even during times when I have been absent. May our adventures never cease and our bond never break;

Lastly, but certainly not least, my most heartfelt appreciation goes to the light of my life, my beloved partner-in-crime Bárbara, with whom I profoundly wish to share the merits of this and future accomplishments. I kindly cherish every moment we have spent together. You are the definition of bliss;

I would also like to express my sincere gratitude to Bárbara’s wonderful family: Teresa, Palmira, António, Daniel, and João. I am grateful to each one of you for always treating me as one of your own;

To you all, I leave a note of eternal gratitude. These have truly been the best of times.

"The important thing is not to stop questioning. Curiosity has its own reason for existing." (Albert Einstein)

Abstract

Development and Manufacturing of a Device for Ultrasonic Assisted Milling

Machinability, along with all its involved aspects, is the most crucial machining cost-determining parameter. Its optimization is, however, fundamentally limited by the existing technology. To transcend such limitations, new alternative technologies arise, as is the case with Ultrasonic Assisted Machining (UAM). Therefore, the present thesis aims to reimagine a conventional milling tool holder to allow for the application of an ultrasonic vibration system, seeking to increase machining efficiency.

Chapter 1 serves as an introduction to the study, providing a brief overview of the project and its main objectives. General considerations and basic concepts of the machining technology are addressed.

Chapter 2 is dedicated to a comprehensive overview of the ultrasonic machining technology. Initial developments of ultrasonics applied to distinct machining operations are briefly mentioned. However, ultrasonic assisted machining is the main addressed technique, with the milling process being the primary point of focus. The influence of the technology in key machining parameters is explored, as well as its underlying principles and general considerations, such as frequency, amplitude, and resonance. Additionally, a definition of different types of ultrasonic assisted machining systems and a comprehensive kinematic analysis are also provided.

Chapter 3, the core of the document, describes the complete development of the ultrasonic assisted milling system. An existing system is analyzed and, through reverse engineering, its corresponding issues and efficiency-impeding factors are identified. Solutions for these limitations are proposed, and consequently, a complete redesign of the system is established, aiming for a more compact and functional design. Every aspect, from part design and optimization to production and consequent assembly, is addressed, recurring to an intensive FEA analysis to validate the proposed updated system. Three different studies are conducted: eigenfrequency determination, impedance curve plotting, and thermal expansion prediction for a shrink-fit type of tool fixation.

Finally, in Chapter 4, conclusions are drawn regarding the optimized system and its applications in the machining industry. The chapter includes a comprehensive overview of the project and suggestions for future improvements, providing valuable insights into the practical implications of this research and its potential for advancing the field of machining. Overall, the developed system yields a significant contribution to the machining field, presenting an innovative approach to ultrasonic assisted machining, having the potential to reduce cutting forces, improve surface finish and reduce tool wear, ultimately leading to cost savings and increased productivity.

Keywords: Frequency, Machinability, Optimization, Ultrasonics, Vibration...

Resumo

Desenvolvimento e Manufatura de um Dispositivo para Fresagem Assistida por Ultrassons

A maquinabilidade, em conjunto com os seus aspetos envolventes, é o principal fator determinante do custo de maquinagem. Porém, a sua otimização está limitada pela tecnologia existente. Variadas tecnologias de maquinagem não convencionais, como a Maquinagem Assistida por Ultrassons (UAM), pretendem transcender estas limitações. Deste modo, a presente dissertação visa a completa reimaginação de um cone de fresagem convencional para a aplicação de um sistema de vibração ultrassónica, a fim de aumentar a sua eficiência de maquinagem.

O Capítulo 1 contém a introdução ao estudo e um breve sumário do projeto e dos seus principais objetivos. São abordados conceitos básicos de maquinagem, assim como algumas considerações gerais.

Uma visão global sobre a maquinagem por ultrassons é dada no Capítulo 2. É efetuada uma abordagem cronológica da sua aplicação a diferentes tipos de operações. No entanto, a maquinagem assistida por ultrassons é o principal foco do estudo, com especial detalhe para o processo de fresagem. A influência da aplicação de vibração aos parâmetros de corte é investigada, assim como os princípios subjacentes da tecnologia e alguns conceitos como frequência, amplitude e ressonância. Vários sistemas deste tipo são apresentados e é feita uma análise cinemática integral do processo.

O principal foco da presente dissertação está incluído no Capítulo 3, o qual descreve o completo desenvolvimento do sistema de fresagem assistida por ultrassons. Um sistema do tipo é analisado e, através de técnicas de engenharia inversa, são identificadas as suas limitações. Soluções são propostas e o sistema é totalmente redesenhado, visando uma geometria mais compacta e funcional. Todas as etapas, incluindo a projeção, otimização, produção e montagem dos componentes necessários são descritas, sendo o sistema validado através de uma extensiva simulação por elementos finitos. São efetuados três estudos: determinação da frequência de ressonância, obtenção da curva de impedância do sistema e previsão da expansão térmica do cone para a introdução da ferramenta de corte.

Finalmente, no Capítulo 4, são apresentadas as conclusões acerca do sistema otimizado e sua respectiva aplicação na indústria. Além disso, o projeto é resumido e sugestões para trabalhos futuros são feitas, fornecendo informações sobre as implicações práticas do estudo, bem como seus principais contributos para a indústria de maquinagem. No geral, o sistema desenvolvido provou-se de elevado valor para a indústria, apresentando um método inovador na aplicação de vibrações aos processos convencionais, tendo o potencial para reduzir forças de corte e o consequente desgaste da ferramenta, melhorar o acabamento superficial e, deste modo, reduzir os custos e aumentar a produtividade.

Palavras-chave: Frequência, Maquinabilidade, Otimização, Ultrassons, Vibração...

Contents

List of Figures

List of Tables

Glossary

Antinode	A point on the tool or workpiece where there is maximum vibration or movement due to the interference of ultrasonic waves.
CAD	CAD refers to Computer Aided Design, which is the use of 3D modeling software in the creation and modification of designs, consisting of virtual representations of components, known as CAD models.
Delamination	Separation or splitting of layers in a composite material, often caused by stresses or forces acting perpendicular to the layers.
Eigenfrequency	A frequency that a system naturally tends to oscillate in without any external force interference. Also known as natural frequency.
Node	A point where there is little or no vibration or movement due to the interference of ultrasonic waves.
Resonance	A phenomenon that occurs if an externally applied frequency coincides with one of the system's natural frequencies, enormously amplifying the vibration amplitude.
Tensile strength	Material property that measures its resistance to breaking or deformation under tension. Expressed as the maximum stress a material can withstand before failure.
Yield strength	Material property that describes its ability to resist deformation under stress and specifically refers to the stress required to cause a material to deform permanently.
Young's modulus	A measure of the stiffness of a material, defined as the ratio of stress to strain within the linear elastic range of the material's stress-strain curve.

Acronyms

1D	One-dimensional
2D	Two-dimensional
3D	Three-dimensional
AC	Alternating Current
ATS	Actuated Tool System
AWS	Actuated Work System
BVD	Butterworth-Van Dyke
CFRP	Carbon-Fiber Reinforced Polymer
DOC	Depth of Cut
EDM	Electrical Discharge Machining
FEA	Finite Element Analysis
ID	Inner Diameter
MMC	Minimal Machining Cost
MPR	Maximum Production Rate
MRR	Material Removal Rate
OD	Outer Diameter

PV Peak-to-valley Roughness

PZT Piezoelectric

RUM Rotary Ultrasonic Machining

TWCR Tool-Workpiece Contact Ratio

UAM Ultrasonic Assisted Machining

USAM Ultrasonic Assisted Machining

USM Ultrasonic Machining

UVAM Ultrasonic Vibration Assisted Machining

VAM Vibration Assisted Machining

Symbols

a	Acceleration $[m/s^2]$
A	Amplitude [mm]
b	Width of cut [mm]
β	Applied frequency ratio [-]
c	Damping coefficient [-]
C_0	Capacitance of a piezoelectric transducer [F]
c_{cr}	Critical damping coefficient [-]
$\vec{D}$	Dipole moment
DC	Duty cycle [-]
D	Outer diameter [mm]
δ_{min}	Minimum displacement $[\mu m]$
d_P	Distance between equivalent points in a successive vibration cycle [mm]
η	Rake face angle [rad]
f	Frequency [Hz]
F	Force [N]
f_n	Natural frequency [Hz]
f_A	Anti-resonant frequency [Hz]
f_N	Nominal working frequency [Hz]
f_R	Resonant frequency [Hz]

γ	Cutting edge inclination angle	[rad]
h	Depth of cut	[mm]
HSR	Horizontal speed ratio	[-]
k	Spring stiffness	[N/m]
λ	Wave length	[mm]
d	Lever arm's length	[m]
m	Mass	[Kg]
ω_s	Spindle's angular velocity	[rad/s]
ϕ	Phase angle	[rad]
Q	Amplification factor	[-]
Q_1	Primary heat zone	
Q_2	Secondary heat zone	
Q_3	Tertiary heat zone	
Ra	Average Roughness	[μm]
ξ	Damping ratio	[-]
R	Radius of the cutting tool	[mm]
t	Time	[s]
T	Period	[s]

T_c Curie temperature [K]

τ Torque [Nm]

v Velocity [m/s]

v_c Cutting speed [m/min]

v_e Effective velocity [m/min]

v_f Feed rate [mm/min]

ω_n Angular natural frequency [rad/s]

x Linear displacement [mm]

x_c Complimentary solution [mm]

x_p Particular solution [mm]

Z Electrical impedance [Ω]

Z_A Electrical impedance at anti-resonance [Ω]

Z_R Electrical impedance at resonance [Ω]

1 Introduction

The total cost of machining a determined material is directly related to the machining parameters, primarily the machining time, tool cost, the generated cutting forces, and the surface quality of the machined piece. Such factors can be optimized to reduce the total machining time by increasing the overall machinability of said material. This will depend not only on simpler aspects, such as the selected machining process, but also on more specific, often overlooked characteristics, such as needed tools and all the remaining machining equipment and specifications, which will rely on the material's mechanical properties.

Nevertheless, one can analyze and enhance each and every one of the parameters in play to the maximum and still reach a point that will not allow for any further improvements, distinctive of the complete optimization allowed by the characteristics of the specific selected machining process. Hence, to transcend such limitations, new alternative machining technologies arise that aim to surpass said halt, as is the case with ultrasonic assisted machining. It is these alternative or non-conventional machining technologies that the study of the present document is focused on.

1.1 Motivation

Alternative machining technologies have been around for a while and are well-established in the manufacturing industry. Regarding vibration, one of the first developed technologies has been what is now known as conventional Ultrasonic Machining (USM), involving the usage of ultrasonic impacts on workpieces of brittle materials carried out by a medium of abrasive slurry [1].

On par with the constant technological evolution, computerization has been a crucial part of the industrial world, allowing for large leaps in technological advances, such as the opportunity to simulate systems without having to produce parts and build prototypes. Still and all, economics are one of the greatest driving forces of this progression, with the main focus of optimization being cost reduction.

Technologies such as conventional USM imply that a whole new machining station is created. Correspondingly, applying the beneficial aspects of this technology to conventional processes has been the main point of interest, since this would allow for the existing systems to be used while improving their machining capabilities. However, this topic is still in an embryonic stage, being mostly only yet empirically developed. Thus, in conjunction with the existing gap within this type of industry, the presented need for optimization and the possibility of developing a project that included the study and application of new technologies were the predominant factors in the writing of this thesis.

1.2 Project Goals and Adopted Methodology

The main objective of this work is to develop a device that aims to completely reimagine a default tool holder used in the conventional milling process to allow the application of an ultrasonic vibration system. Said device will permit a complete overhaul of the process while being perfectly applicable to ordinary existing milling stations, without the need for a complete machining station replacement.

The importance of an approach that can be applied to already established systems is directly related to the economic aspects of the industry. Obviously, having the possibility to take advantage of the existing equipment will prevent the retirement of the original parts to make way for upgraded ones, making the adaptation of conventional processes a much more interesting and economically viable perspective than completely reimagining the cutting process, adding to the fact that it enables the main points of interest of those technologies to be taken advantage of.

Undeniably, such a massive project is nothing but simple and should be broken into more straightforward, easier-to-understand parts, each one of them not more important than the others. These are explained in the upcoming section.

1.2.1 Thesis' Structure

To facilitate the reader's perception, the project has been organized in a way that each chapter denotes a distinct phase of the study. Smaller, simpler ones are present within each of these more comprehensive parts to provide further organization.

Best understanding of the thesis' content should come from the reading order that is presented in the document. Nonetheless, a brief summary of the project has been made and a diagram has been elaborated exhibiting each segment. This can be observed in Figure 1.

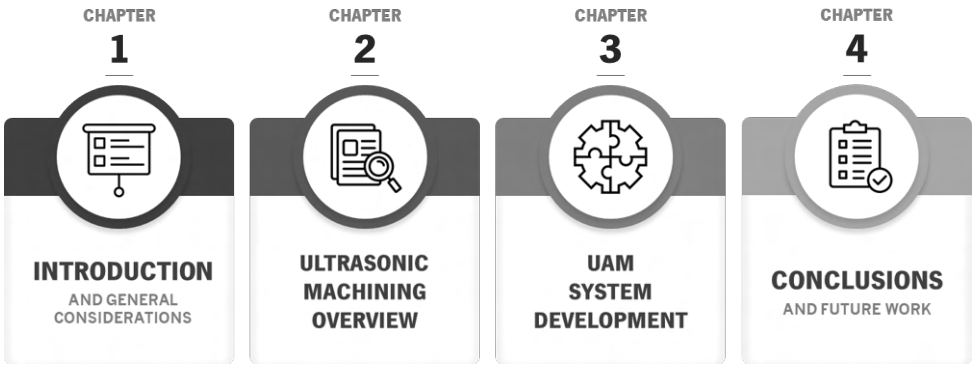

Figure 1: Structural arrangement of the document by chapters and respective contents.

The present chapter is dedicated to the introductory aspects of the study. A basic presentation of the project is performed and the main objectives the system targets are discriminated. In addition, a brief account of general considerations and key aspects of machining technologies is given. It is fundamental to address these aspects to understand the necessity of the study.

Chapter 2 consists of a complete review and thorough analysis of the ultrasonic technology. This can be considered as a summary of the research. A chronological outlook is carried out, and already established systems with the application of vibration to machining processes are presented.

Withal, the central aspect of the document is presented in Chapter 3. The project is described in its entirety, encompassing every aspect from the design of the parts to the production and consequent assembly of the whole system. Having conceived the CAD model, the system was validated via computational simulation methods with regard to the determination of the system's eigenfrequencies and subsequent impedance curve, as well as the predicted thermal expansion of a proposed shrink-fit tool holder. These aspects will be clarified in this section. Lastly, the designed parts were produced and assembled. Pivotal points such as design and project requirements are also addressed. A scheme of the process can be observed in Figure 2.

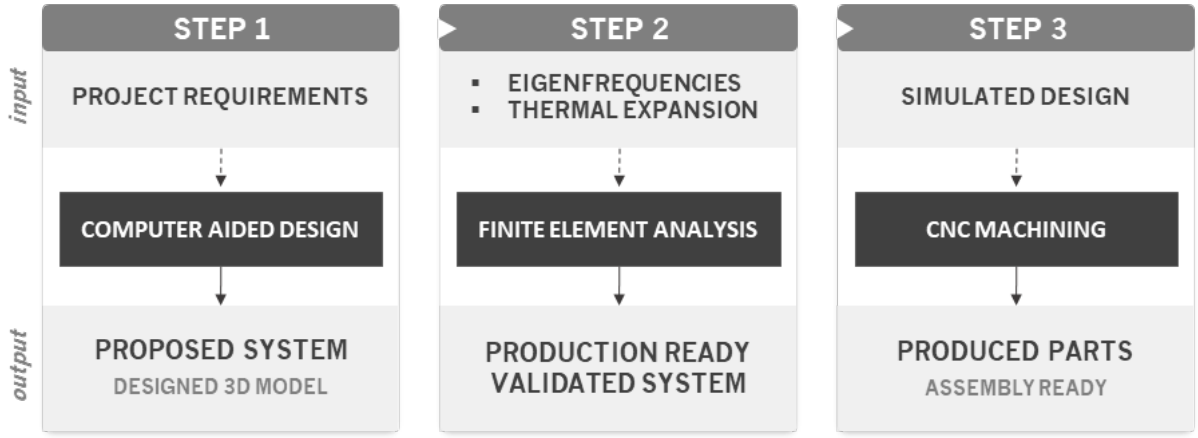

Figure 2: Schematic summary of Chapter 3, concerning the system's development.

In the project's final phase, the data presented in this document is synthesized in Chapter 4, where conclusions are drawn regarding the developed system and its applications in the machining industry, in conjunction with the theoretical concepts discussed throughout the course of the study.

A comprehensive overview of the entire project is given, including a discussion of any future improvements that could be made. To guide this discussion, three central questions are addressed: the project's central focus, its most significant contribution, and how it could be further improved. This chapter will serve as a critical section of this thesis, providing valuable insights into the practical implications of this research and its potential for advancing the field of machining.

1.3 General Considerations and Basic Concepts

Previous to the study of any system that aims to optimize a manufacturing operation, it is necessary to have a solid understanding of the basic concepts that define it, as well as every characteristic that it integrates. Accordingly, the framework of the presented topic should begin with the definition of concepts such as machining and machinability, crucial for the application of an ultrasonic machining system.

1.3.1 Machining Technology

Machining is a manufacturing process in which cutting tools are used to gradually remove excess material from a workpiece to achieve a desired shape and surface finish [2, 3]. As the cutting tool moves through the work surfaces, the material is deformed beyond its ultimate tensile strength until fracture is reached, occurring in the form of chips. Evidently, this is the case for ductile materials, since fracture occurs when the yield strength is reached for the brittle kind. These points are illustrated in Figure 3.

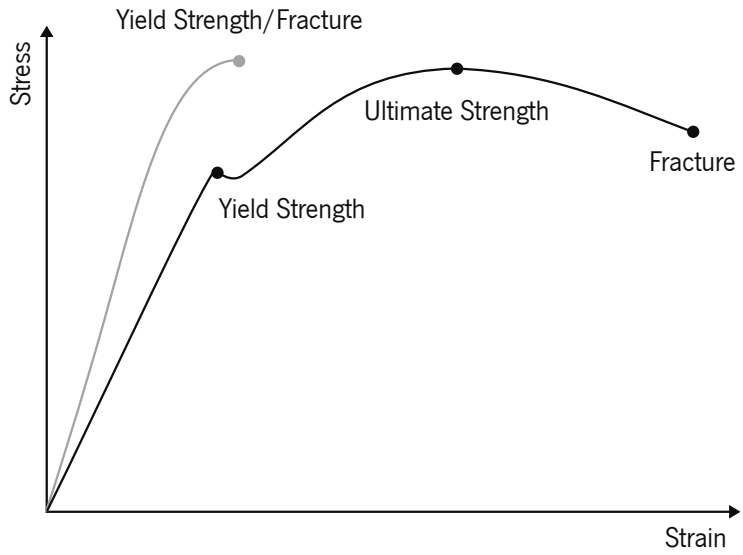

Figure 3: General stress-strain curve of a brittle material (grey) and a ductile material (black).

Being one of the most common manufacturing processes in the industry, numerous amounts of industrial components that require specific characteristics for their respective applications are manufactured through machining. Yet, there is an extensive array of pieces that are produced through these kinds of operations, given the fact that machining processes allow for the obtaining of complex geometries and dimensional characteristics, combined with the possibility of using different types of materials, ranging from metals to plastics, or even more complex alternatives, without hindering the piece production cost [2, 3].

Machining comprises several distinct processes, each having a specific use with respect to part geometry and surface texture. The main, most typical, would be turning, milling, and drilling. It is out of the context of this thesis to study each of these operations individually, as the main focus of the document is the optimization of the conventional milling process.

Milling involves a rotating tool with multiple edges in which its axis of rotation is perpendicular to the feed motion. While there are several distinct milling operations, the focal point of the document will be the end milling process. A basic schematic representation of this is presented in Figure 4.

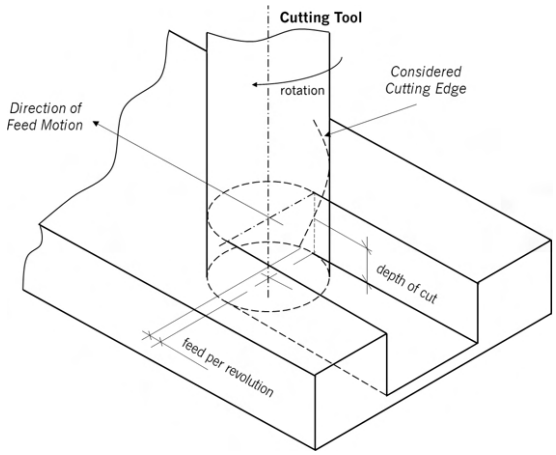

Figure 4: End milling schematic representation (adapted) [4].

A major general machining disadvantage is that there is a considerable amount of wasted material, which is a characteristic of subtractive manufacturing processes [2]. Although some of the resulting chips may be recyclable, there has been a growing interest in maximizing sustainability.

Cutting tool manufacturers, for example, have been producing tools with increasingly improved toughness, wear, and thermal resistance (resulting in longer tool lives). There is clearly a cap to this, however, as a too-high tool resistance could result in a reduction in sales and consequent financial drawbacks for these companies. Accordingly, efforts are also made within the process parameters to maximize process optimization, which is one of the most important reasons why it is essential to study alternative or non-conventional machining technologies, such as ultrasonic assisted milling.

There are countless factors that can affect the specified cutting operation's efficiency, adding to its overall complexity. Some of these factors are inherent in the machining process in question, including the cutting geometry of the process itself, the machining system used, and all the components involved. Others accrue from the machining parameters in play and the workpiece's mechanical properties [2].

Moreover, the stock (workpiece prior to being cut) can derive from a block of feedstock or from a preceding manufacturing process, like metal casting, in which the material is already in a predefined shape. An example is shown in Figure 5, regarding the turning process. Since machining is mainly a finishing operation, following specified requirements, workpieces usually possess a preliminary design.

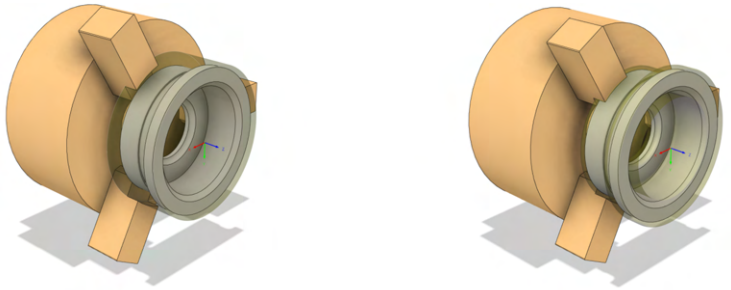

(a) (b)

Figure 5: (a) Stock from feedstock; (b) Stock from preceding manufacturing process.

Regardless of which machining process is used, however, it is crucial to understand the mechanics of the cutting process. A comprehensive study is necessary not only for the elaboration of a kinematic analysis but also for the correct interpretation of the heat zones generated in the process, which will later play a vital role when designing the desired system. Thus, a subchapter was developed with the purpose of highlighting the mechanics of the milling process.

1.3.1.1 Mechanics of the Cutting Process

There are two main movements that promote chip forming. First, a single rotation of the cutting tool removes a single chip of material. This is known as the cutting movement. Even so, if the tool continues to rotate without any additional motion, no further chip formation will occur. Therefore, a feeding motion is necessary for the removal of new material, generating the machined surface [2, 4]. Together, the two distinct movements culminate in the effective cutting movement, which is represented in Figure 6, where v_c, v_f and v_e represent the cutting speed, feed rate, and effective velocity, respectively.

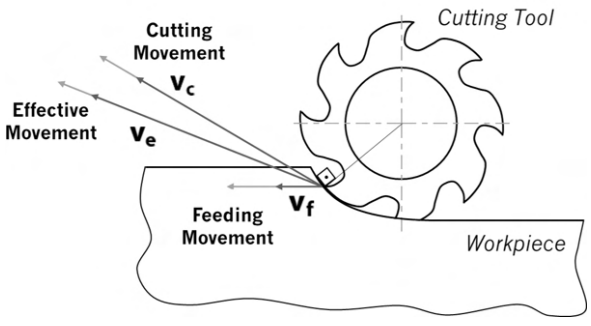

Figure 6: Movements promoting chip forming in milling [4].

Although the vectorial sum of cutting and feeding velocities results in an effective cutting direction angle, this is often neglected as there is substantial difference between the vectors' magnitudes.

In addition, there are movements that, despite not directly affecting chip formation or material removal, are also vital to the cutting process. These comprise the positioning movement (tool's approach to the workpiece, while not actually making contact) and the depth of cut, which determines the thickness of the removed material layer [2].

A three-dimensional study allows for a better understanding of all intrinsic parameters in the cutting process. Despite the fact that there are operations in which the orthogonal cutting model is an appropriate analysis, it is frequently used as a simplification to milling. In this model, the cutting edge is perpendicular to the cutting velocity [5].

Howbeit, an oblique cutting model would be the most correct approach, as the movement of the tool in relation to the workpiece is more accurately described. Although of increased complexity, it implies a more realistic chip flow representation. Both models can be observed in Figure 7.

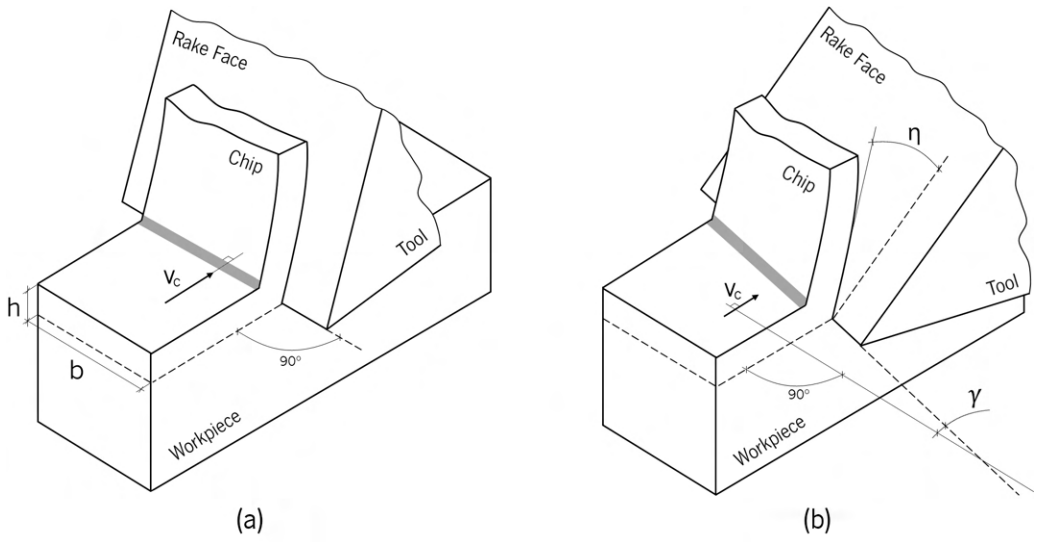

Figure 7: (a) Orthogonal cutting model; (b) Oblique cutting model [4].

In the orthogonal model, the area of the material removed by the cutting tool with velocity v_c is given by the multiplication of h (depth of cut) by b (width). The direction of the tool when it comes into contact with the surface of the workpiece results in higher cutting forces, increasing the cutting difficulty.

However, in the oblique variation, there is a cutting edge inclination angle, relative to the cutting velocity direction, given by γ. This geometry facilitates chip separation, resulting in lower cutting forces and inevitably lower required power for the machining system. The angle γ is directly related with the cutting force variation. The chip-flow angle is also present, between the rake face and the formed chip, given by η, which will not be discussed in detail.

The rake angle in relation to the machining surface is also of increased importance. Depending on the type of material, it can be beneficial to imply a positive or negative angle on the cutting tool, as it will directly affect the chip breaking process. A negative angle will promote chip separation and is often applied to ductile materials. Even so, this process could also be assisted by an increase in the cutting speed or the correct direction of the cutting fluid. On the other hand, in brittle materials, chip breaking occurs easily and does not require such attention to detail.

There are three main deformation zones during the cutting process, represented in Figure 8, that lead to heat accumulation due to the friction between the tool and the machining surface [6]:

- The primary heat zone, Q_1, corresponds to the plane normal to the rake angle. Its cause is the immense amount of energy that is converted to heat as the chip begins to form;
- The friction promoted by the sliding motion between the rake face of the tool and the forming chip leads to a localized temperature increase, resulting in the secondary heat zone, Q_2;
- Further heat generation is triggered by the friction between the tool and the newly machined surface. The point of contact between these two components corresponds to the tertiary heat zone, Q_3.

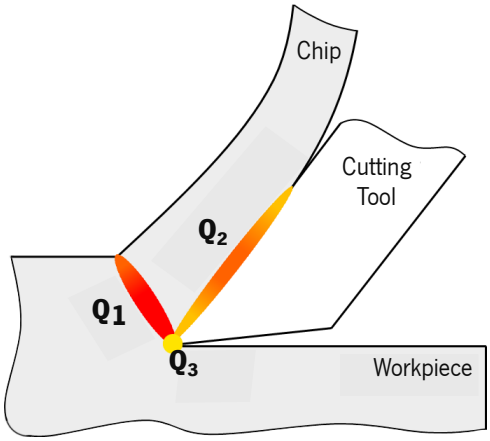

Figure 8: Distribution of heat sources in chip forming.

Evidently, the greater the depth of cut, the larger the heat zones. It is clear that higher temperatures contribute to the ductility of the material, which promotes chip formation. However, the greater the surface of contact is, the greater the forces on the flanks of the tool will be.

Reducing heat will be a key factor of study when designing the system, as the increase in the material's ductility can limit the benefits of the application of ultrasonic vibration.

1.3.2 Machinability and Project Optimization

Simply put, machinability denotes how easy it is to cut a certain material. When speaking of machining efficiency, it is the pivotal factor to be taken into consideration. Whilst it might seem simple at first glance, mainly dependent on the material's mechanical and thermal properties, it is a fairly complex concept that relies on the entirety of parameters and general considerations regarding a machining process.

Figure 9 includes a list of the predominant factors that affect machinability.

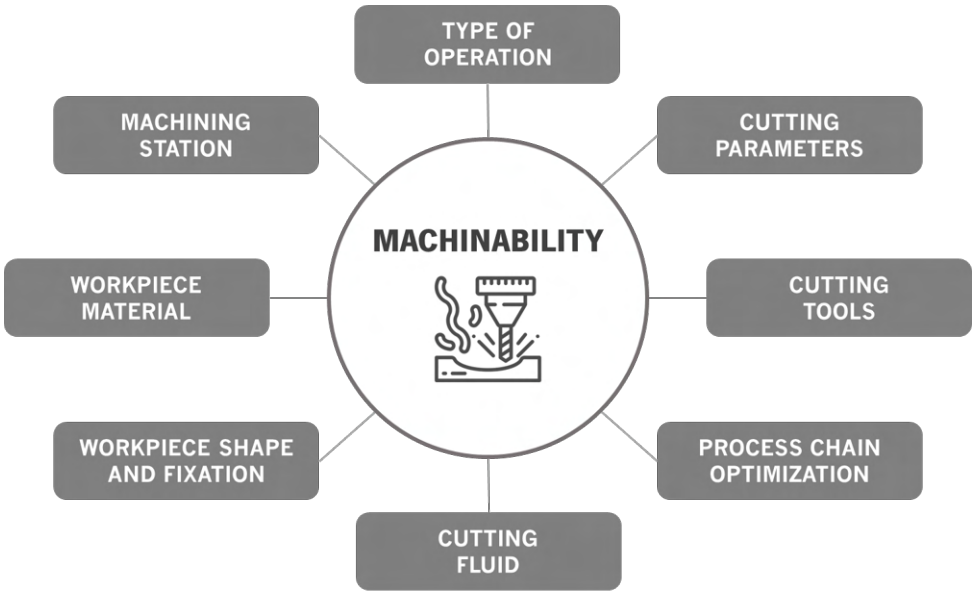

Figure 9: Summary of machinability affecting factors [2, 7].

The definition of an adequate station for the selected machining process is a preponderant factor regarding machinability. The type of operation should be in accordance with the desired cutting process. Not only is this selection crucial, but the correct utilization of the machine is necessary to take full advantage of its potential. A scientific approach should be followed at all times, albeit being often neglected [7]. Under-utilizing the machine's capabilities hinders the machinability of the workpiece.

The cutting parameters are also a critical aspect that influences machinability, including cutting speed, feed rate, and depth of cut. While it may seem obvious that an increase in these variables reduces the total machining time, it does not necessarily mean that this will be favorable. Exaggerated values lead to premature tool wear, surface imperfections on the workpiece, and greater required machining power.

Evidently, the machinability of a certain material will also be regulated by its own mechanical and thermal properties. Although soft materials, such as aluminum alloys, benefit from increased cutting parameters, harder materials require these to be adjusted. At higher temperatures, for example, titanium and nickel-based alloys have a high chemical affinity with the tool material while maintaining low thermal conductivity. Thus, cutting speeds should be reduced to ease heat dissipation [7].

Hence, a detailed study of the correct cutting parameters is mandatory for each situation. The cutting path should equally be optimized to minimize the cutting time.

Harder materials will also require more rigid tools. Having each tool a specific purpose, whether it is the respective cutting operation or the suggested workpiece material, this component should be adequately selected. Since distinct tools can comprise different materials and coatings, the tool choice will directly influence the cutting process. Moreover, the rake angle, previously mentioned in Subchapter 1.3.1.1, should equally be considered. Additionally, the cutting routine is expected to include minimal tool changes, as these also affect the total machining time.

A synthesis of proposed cutting tool materials in relation to cutting speeds and the material hardness of the workpiece is shown in Figure 10.

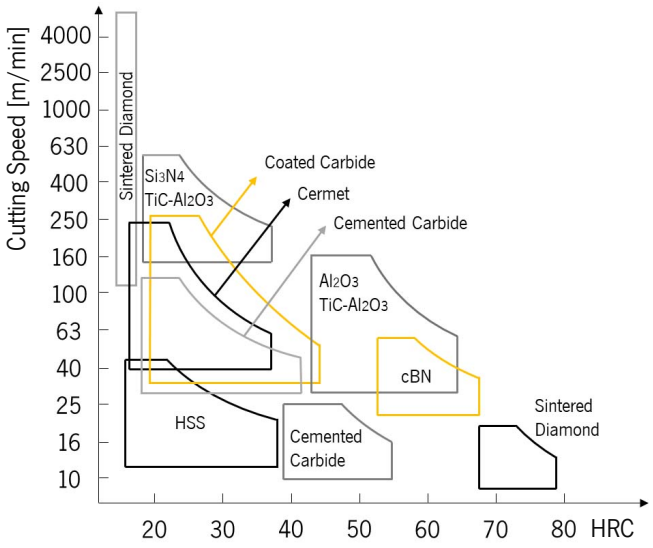

Figure 10: Overview on proposed cutting speeds regarding machined material's hardness [2].

Moving over to the component's fixation, this will be directly influenced by its own shape. Depending on how complex the geometry of the component is, it might be necessary to design a specific support to hold it. This should be done with the optimized cutting path in mind to achieve the best possible results. From a broader perspective, if several parts are to be machined successively, process chain optimization can potentially play a major role in the overall machinability as well.

Finally, the selection of the optimum cutting fluid and its correct orientation can benefit the machining process greatly, as it eases chip removal while increasing material removal rates. The surface finish will consequently be superior [7].

Taking all of the above factors into account, a reverse analysis can be performed in a way that machinability directly influences tool life, surface quality, cutting forces, and the chip-forming process.

Machining efficiency, however, will be dictated by the machining cost of the component in question, as project optimization is also directly related to the economic facet of the manufacturing industry. Undoubtedly, the total production time will profoundly affect the machining cost. A simple way to visualize the behavior of the main cost and production time influencing parameters is to analyze their evolution in relation to the cutting speed variation. Thus, Figure 11 shows this conduct.

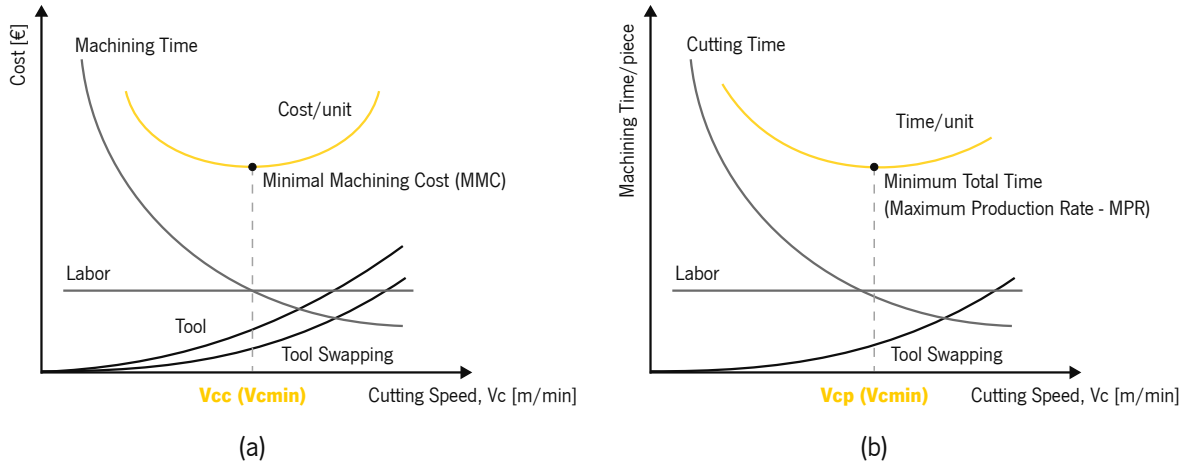

Figure 11: (a) Machining cost variation; (b) Machining time variation [2].

A quick analysis of both presented graphs is enough to understand that the increase in cutting speeds will affect the studied parameters differently. Machining time benefits greatly from increased cutting parameters. Consequently, the longer it takes to cut a certain material, the higher its machining cost will be. On the other hand, the increase in factors such as tool cost with increased cutting speeds is obvious. As previously mentioned, harder materials will require harder cutting tools, which are evidently more expensive. Naturally, as the wear increases, tool replacement will be more frequent.

However, there will be a sweet spot in which the cutting speed is optimal for both machining time and machining cost, respectively coinciding with the Minimal Machining Cost (MMC), and minimum total machining time, which is interpreted as the Maximum Production Rate (MPR). Ultimately, a company will focus on reducing the machining cost of any given component. On that account, the decisive machining optimization factor is generally going to be the MMC, being all the efforts done to further decrease it, in a way that the presented parameters will be of crucial importance for its viability.

With this in mind, and as can be observed in Figure 11, said parameters will only allow the project optimization to be performed to a certain extent. This optimization plateau can solely be surpassed with the development of new methods and techniques, opening the door to more optimal machining of complex materials, in which the cutting efficiency would, conventionally, be reduced.

It is at this point that alternative machining technologies come in.

1.3.3 Complex Materials and Alternative Machining Technologies

The main purpose of the development of alternative machining technologies is to overcome inherent obstacles in conventional machining, as traditional machining techniques show a clear bottleneck in improving machining performance.

There is an extensive array of non-conventional technologies. Although several distinct methods have been developed over the years, they all share the same purpose, which is to reduce the MMC of any said component. Taking into account the cost variation graph in Figure 11, these methods will push the cost/unit curve further below what was previously accepted as being fully optimized. A visual representation of this is present in Figure 12. Manifestly, employed process parameters may shift said curve horizontally, affecting also the tool swapping cost (as later discussed in Chapter 2).

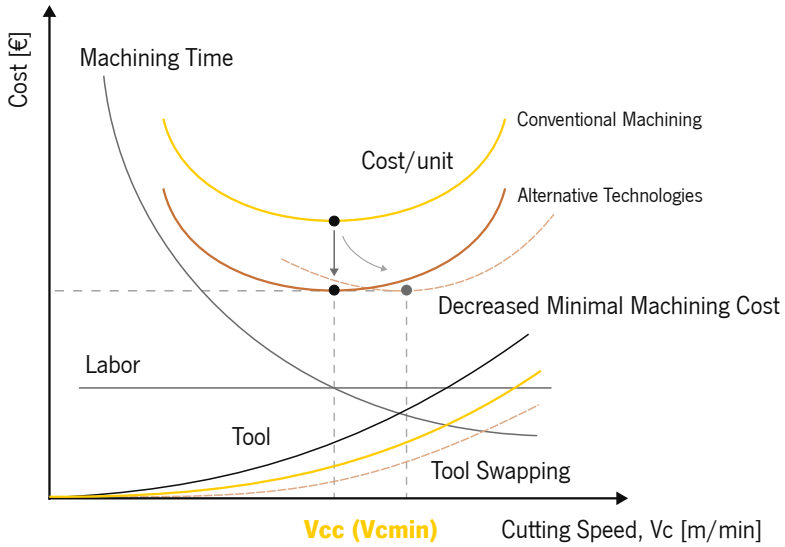

Figure 12: Further machining cost reduction through alternative technologies (adapted) [2].

Alternative machining methods usually target difficult-to-cut materials, while not being at all limited to them. The constant growing interest in the machining of complex materials is a result of their excellent physical and chemical properties, making them particularly exceptional alternatives for numerous uses in diverse yet fundamental fields of modern industry. Some examples of these types of materials include titanium alloys, Inconel (nickel-based superalloys), composites, and ceramics.

Titanium alloys are especially known for their impressive strength-to-weight ratio, and extraordinary fatigue and corrosion resistance [8, 9]. However, they are particularly difficult to machine because of titanium's tendency to work-harden. In addition, these alloys are not only resistant to temperature changes, given their high thermal resistance, but also have increased difficulty in heat dissipation, given their low thermal conductivity. These factors further increase this material's machining difficulty [8]. One of the most widely used titanium alloys is titanium grade 5 (Ti6Al4V).

Regarding Inconel, a group of high-performance nickel-based alloys that are also known for their unique strength and corrosion resistance at high temperatures [9], their tendency to work-harden makes them particularly difficult to cut.

Composites are made up of two or more different materials with unique characteristics, offering the opportunity of the combination of several beneficial mechanical properties, creating a conjunction that would not otherwise be possible. For example, metal matrix composites combine the high strength and stiffness of metals with reinforcement materials such as ceramics, resulting in improved properties like wear and corrosion resistance. Other examples of common composites are ceramic matrix composites, fiber-reinforced plastics, and polymer matrix composites [10, 11].

An appreciable advantage of composite materials is that they can be purposely designed to meet specified requirements, even though enhanced properties increase their machining difficulty. Naturally, machining tools and processes must complement the demands of each specific combination, which denotes an added drawback in their machining [12].

Finally, ceramics include diverse characteristics that allow for multiple applications. Although mainly known for their high hardness and excellent wear and corrosion resistance [13], they exhibit exceptional chemical stability [12–14] and elevated thermal conductivity while maintaining a low mass density. This allows for an outstanding mechanical performance at high-temperature environments [12, 14, 15]. However, their brittleness and toughness make them a difficult material to machine. Examples of these are alumina (Al2O3), zirconia (ZrO2) and silicon carbide (SiC).

There are many application fields that rely on these types of materials for various uses due to their specific properties, including the aerospace and aeronautic industries (e.g. Ti6Al4V in lightweight structures that improve engine efficiency and performance) [3, 8, 9, 12–17], the mechanical and automotive industries (e.g. ceramics in bearings and other rotary parts; brake pads) [9, 14–16] and even the medical industry (e.g. ceramics for tooth implants) [3, 12, 16]. These materials can also be found in the energy [3], electronics [14], and optical [13, 15] industries, along with general usages in precision machining for the production of microscale components [18].

Although the above-mentioned groups of materials are the most common, numerous others used in alternative cutting processes can be found in the literature. Examples of these are aluminum alloys used in the aeronautic industry [8, 17] (challenging to work with due to their low melting point and high thermal conductivity, consequently hindering surface finish), and austenitic stainless steels (such as AISI 316L, with various usages due to its great ductility and resistance to corrosion [19]). The versatility and unique properties of these materials make them essential in modern society.

Moreover, and since the aeronautic industry is a common application field for these types of materials, as presented in the preceding paragraphs, a clear way to visualize said information is by analyzing the percentages of the constituting materials of a Boeing airplane, as shown in Figure 13.

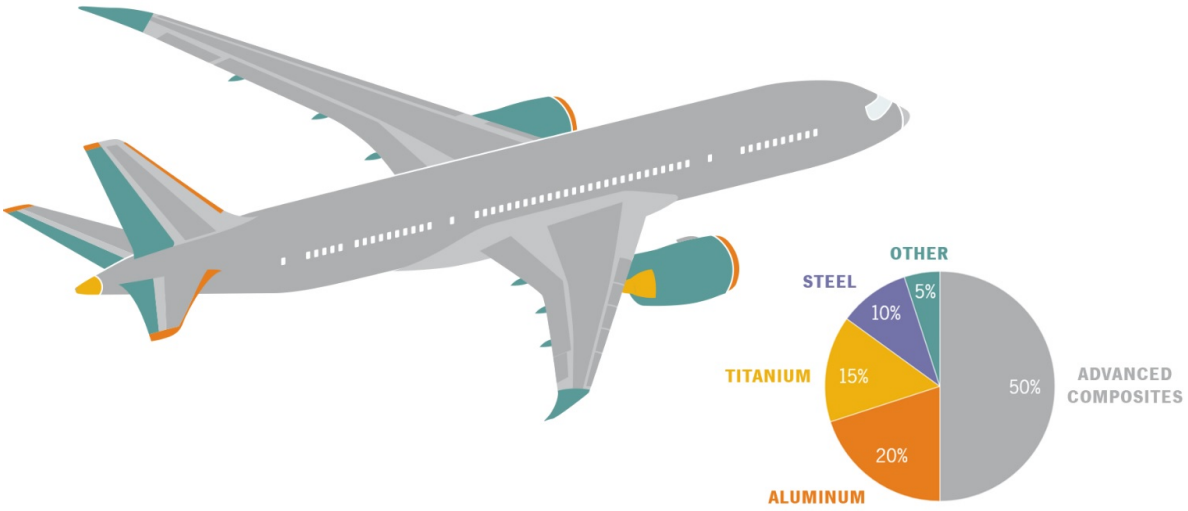

Figure 13: Percentages of the constituting materials of a Boeing 787 airplane [20].

The use of advanced composites in the body of the airframe (including carbon fiber-reinforced plastic) results in weight savings of nearly 20% compared to conventional aluminum designs. Additionally, due to the excellent mechanical and thermal properties of these advanced materials, the need for both preventive and condition-based maintenance is reduced, thus lowering overall costs [20].

In general, complex machining materials require specialized tools and techniques to machine effectively, and there is a need for the constant study and perfection of techniques in this type of technology. Having exceptionally poor machinability (resulting in increased cutting forces and surface roughness, low machining accuracy, and rapid tool wear), they are very demanding for conventional machining technologies, where the key requirements are productivity (large material removal rate and minimized surface roughness), part quality and reduced tool costs [12, 21].

It is also important to note that process stability and reliability are required when dealing with small series of parts, specifically due to operational costs and time consumption. In addition, reliability is also vital for geometries with great complexity levels [12], which makes the designing of such techniques much more challenging.

Ultimately, there is a great demand for cost-effective machining technologies that improve the machining efficiency of complex materials, resulting in a profitable cutting process. To transpose such obstacles, the application of ultrasonics to the cutting process has been shown to be one of the most popular non-conventional techniques, in conjunction with Electrical Discharge Machining (EDM) [2].

In addition, the manufacturing of structural components continues to face challenges in finding effective additive manufacturing methods that can match the performance of classical subtractive alternatives. Said techniques often exhibit low fatigue resistance, making them unsuitable for critical applications, such as in the aeronautical industry.

Consequently, the subtractive manufacturing method remains the focal point of the machining industry, not only for the development of new technologies but also for the optimization of existing ones, underscoring the need for alternative techniques, given the demand for high-quality components that can withstand the rigorous requirements of various industries. Thus, Figure 14 comprises a summary of the present subchapter.

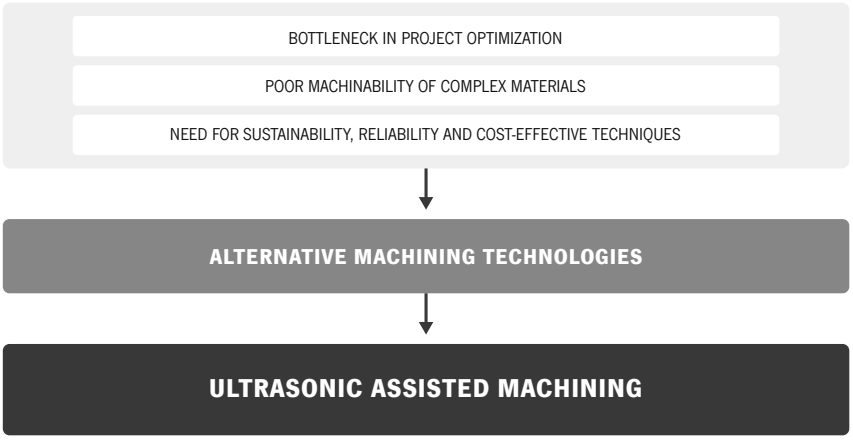

Figure 14: Machinability issues leading to the development of alternative machining technologies.

Throughout the years, various investigations have explored the utilization of ultrasonic vibration in conventional machining techniques. Nevertheless, the scarcity of research on the implementation of these methods prompted the development of the current thesis.

In light of the aforementioned, this thesis seeks to examine the design and impact of ultrasonic technology on the milling process. Specifically, it aims to scrutinize the potential advantages and drawbacks of ultrasonic vibration and identify the factors that may affect its efficacy. Therefore, a comprehensive and thorough investigation of the ultrasonic domain is imperative.

Hence, the present study reviews relevant literature and critically analyzes empirical studies that have investigated the application of ultrasonic vibration in machining operations.

Concluding, this research contributes to the understanding of the potential of ultrasonic technology and its applicability in milling operations. The study's findings are expected to provide valuable information for industry practitioners, researchers, and academicians, as well as contribute to the advancement of knowledge in the field of machining technology.

2 Ultrasonic Machining Overview

The usage of ultrasonic vibration in the machining world has been well present for over 60 years [8, 14, 17, 18, 22, 23]. Although the first patent on the application of ultrasounds to machining was only granted to *L. Balamuth* in 1945 [14], there are records of academic research on this matter dating as far back as 1927, with the submission of a paper by *R. W. Wood* and *A. L. Loomis* [14, 17].

The ongoing development of the machining industry has facilitated the emergence of a wide range of ultrasonic systems, which are a particularly effective machining technique due to their ability to produce minimal residual stress levels on the surface of the workpiece. Obviously, this especially makes Ultrasonic Machining a great option for machining brittle materials [14]. This process is generally associated with low material removal rates, being mainly used as a finishing operation [18].

Said evolution has ultimately resulted in the creation of various designations for the technology. Nevertheless, Ultrasonic Machining has become the most widely used variation since the 1950s [14]. There is an exception to this, however, when it comes to the application of this technology to traditional machining processes. As a result, two large groups are formed depending on the type of applied vibration, corresponding to two entirely different processes: Conventional Ultrasonic Machining (USM) and Ultrasonic Assisted Machining (UAM).

Conventional USM, which was briefly mentioned in Subchapter 1.1, requires the development of a specialized structure. A representation of this type of operation is present in Figure 15.

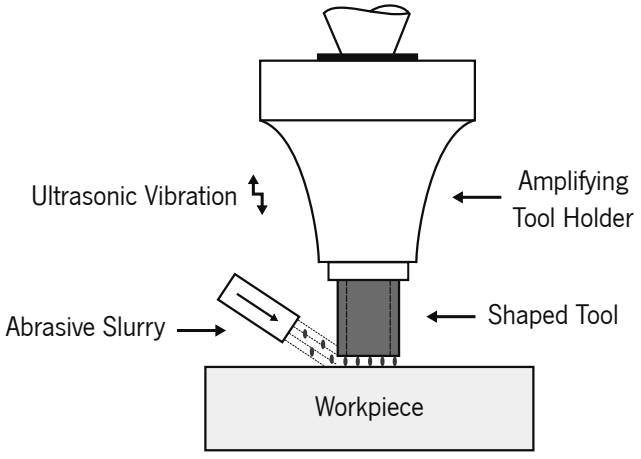

Figure 15: General representation of an Ultrasonic Machining system (adapted) [23].

A transducer is used to convert electrical energy into mechanical vibrations on the longitudinal axis of the tool. The tool holder is used as an amplifier (commonly referred to as booster) to achieve high-frequency values (over $20\ kHz$, entering the ultrasonic range) while maintaining a low vibration amplitude, in the range of microns [1, 5, 14].

In conjunction with a static load applied to the tool (which has no cutting edges), an abrasive mixture (such as SiC and water/oil) is used to remove material from the workpiece. Thus, the generated vibroimpact regime is the primary cutting process. Involved material removal mechanisms comprise mechanical abrasion and microchipping (impacts of the abrasive particles on the workpiece surface), cavitation (effect of the slurry), and chemical reactions (due to the employed fluid) [1, 8, 14, 17, 23].

Not only the slurry contains abrasive particles, it also acts as a coolant for the vibrating system. Furthermore, the constant fluid supply will aid in the removal of debris from the cutting area [14].

On the other hand, UAM involves the use of ultrasonic vibrations to enhance traditional machining processes. In this case, key components of the selected process are modified to incorporate the use of ultrasonic vibration. Both conventional Ultrasonic Machining and Ultrasonic Assisted Machining have specific applications and advantages in the manufacturing industry.

T. B. Thoe et al. have established a great rundown of the main ultrasonic vibration using techniques, noting some less common technologies still worth mentioning. Included in these are Rotary Ultrasonic Machining (RUM), the combination of USM with EDM, and even non-machining ultrasonic applications (cleaning, plastic/metal welding, chemical processing, coating and metal forming) [14].

In this context, RUM is a technique in which the tool rotates over its own axis, while material removal still occurs in the form of abrasion. The tool takes on a different arrangement in this variation, as can be seen in the general representation present in Figure 16.

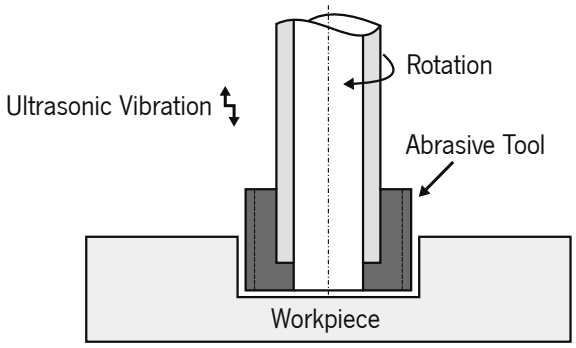

Figure 16: General representation of a Rotary Ultrasonic Machining system [24].

It is worth noting that there are some types of RUM applications where the workpiece is the rotated component, in contrast to those in which the tool comprises both vibration and rotation movements. Evidently, a whole table setup is needed for the workpieces to be fixed in these kinds of systems, including a motor to provide the desired component's movement [1].

Compared to conventional USM methods, the Material Removal Rate (MRR) of RUM is around four times superior, increasing with the applied rotation speed. This is mainly by virtue of the contact mechanisms potentiated by the added rotation movement. For this reason, RUM is clearly considered superior to the traditional variation [1, 18].

It can be clearly understood that there are various drawbacks with the implementation of RUM and conventional USM techniques. Although RUM has been shown to be a much more effective process, these still essentially consist of abrasive machining operations, being limited to certain applications and workpiece requirements. Furthermore, having to develop specialized structures for their application is economically unfeasible when compared to the possibility of redesigning already established machining systems, added to the fact that the application to distinct methods will evidently widen the range of machining possibilities, using the technique merely to enhance these operations' inherent capabilities.

Nevertheless, some clarifications must be addressed prior to any detailed system characterization, since it is necessary first to establish a clear understanding of what constitutes the basis for these alternative machining methods. Accordingly, Subchapter 2.1 not only contains a thorough analysis of the UAM technology, which coincides with the main topic of the document, but also includes a study on the theoretical and technical aspects of the principles involved in its implementation.

2.1 Ultrasonic Assisted Machining

The application of ultrasonic vibration to conventional machining processes can be traced almost as far back as the first developed ultrasonic machining technologies. Being turning the initial process to benefit from the technology, the consequent employment of these methods to other traditional machining techniques has increased with the exponential growth of the machining industry, on par with the evolution in ultrasonic transducers and horn structures over the years. In other words, UAM systems can be viewed as a natural evolution from conventional USM techniques [8, 18, 22, 25].

Instead of relying on an abrasive mixture for material removal, UAM systems consist of the application of high-frequency vibration to one or more components of a machining operation. A traditional tool with cutting edges is used to remove material, while applied vibration causes discontinuity in the tool-workpiece interaction, increasing the efficiency of the process in question [2, 9, 17, 18, 21, 22, 25–27]. Generally, vibration is applied to the tool, with UAM systems often studied based on the motion of the cutting tooltip.

Said discontinuity between the two surfaces consists of four essential movements, as illustrated in Figure 17, repeating cyclically with the applied frequency: Approach, contact, immersion, and back off.

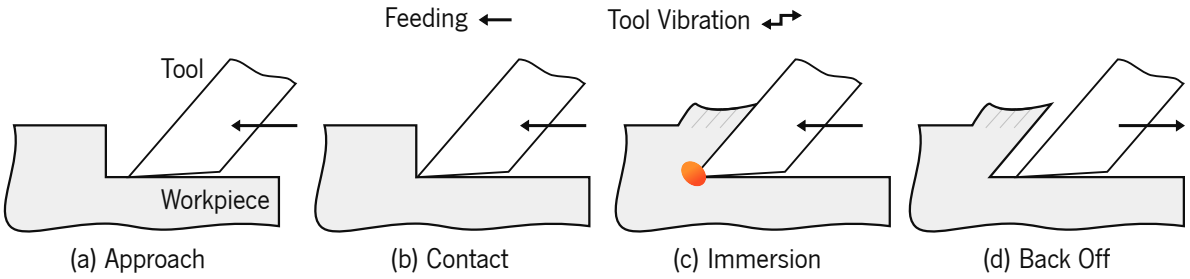

Figure 17: Fundamental stages of the tool's movement in a vibration cycle [9].

At present, UAM is widely used in an extensive range of the machining industry, most common in turning and drilling processes, where better performance is consistently reached [19, 28]. However, there are clear limitations in the correct comprehension of the technology, especially for the milling process, as there is a scarce investigation of the technique's dynamics and cutting characteristics. Theoretical research still lacks predictive theories and quantitative models that would allow further optimization of machining processes for operating conditions, especially for complex materials [17–19, 25].

Figure 18 shows an example of the application of UAM techniques to drilling, turning, and milling. There are several degrees of vibration that can potentially be applied, as already stated, either to the tool or to the workpiece. Vibration can be applied to one, two, or even three dimensions.

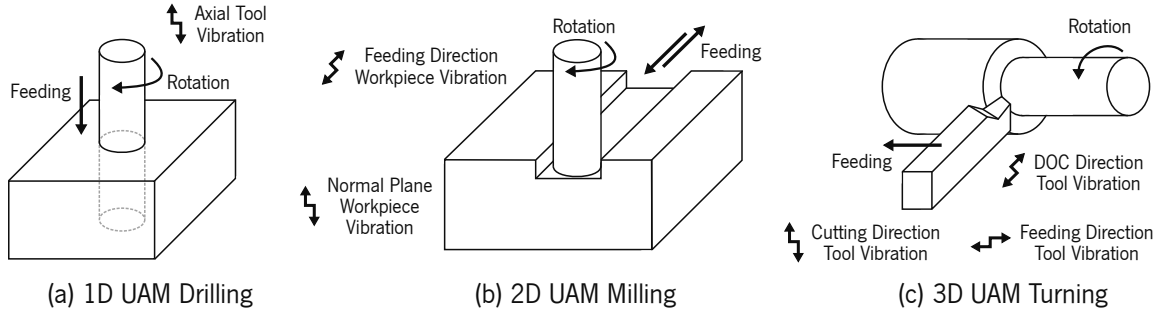

Figure 18: UAM application to conventional machining methods (adapted) [2].

For instance, and as shown, it is fundamentally easier to implement 3D vibration to the cutting tool in the turning process rather than in milling, given to the cutting tool's stationary configuration. In drilling operations, on the other hand, an axial vibrating tool would naturally make more sense.

It is necessary to note that the presented configurations are merely illustrative and should not be taken into account as fixed vibration systems, since there are countless variations depending not only on the type of technology in which the vibration is applied but also on the desired purpose of the system.

Although the greatest challenge of UAM is essentially developing a fundamental understanding of the process, promoting optimal and consistent results [17], there is a particular interest in the study and development of these types of systems, given not only their proposed advantages but also their applicability and consequent economic viability.

2.1.1 Influence on Key Machining Parameters

The particular interest in UAM is derived of the distinct benefits the technology proposes over diverse operating conditions, machining parameters, and involved cutting tool and workpiece materials.

As the ultrasonic vibrations aid in the breaking of the workpiece material, a more favorable cutting environment is created since the reduced cutting resistance results in the improvement of the machining parameters and, consequently, in a more precise, efficient, and cost-effective cutting process.

In short, the intermittent contact promotes easier chip separation (and breaking), as well as consequent extraction from the cutting area (preventing the clustering of generated particles in tooling surfaces), along with friction reduction between the tool and the workpiece [12, 22]. This ultimately results in reduced heat generation and consequently diminished cutting forces, reduced tool wear (longer tool lives), and reduced workpiece surface roughness, consisting of an improved surface finish. Other advantages include minimal burr formation (facilitated chip breaking) and a greater critical value for the depth of cut in the ductile regime machining of brittle materials. [2, 8, 9, 17, 18, 25–27].

Such UAM benefits ultimately result in greater quality and flexibility of parts, superior dimensional accuracy, as well as increased machining productivity [5, 12]. Obviously, this gives this alternative machining technique immense potential for industrial applications.

Figure 19 contains a schematic representation of the main proposed UAM advantages, from which the mentioned subsequent benefits derive.

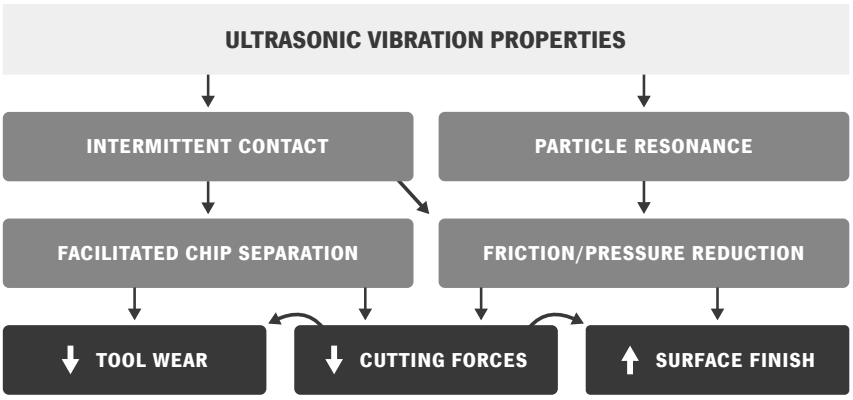

Figure 19: Main proposed advantages of UAM systems.

Apart from the presented general UAM benefit introduction, however, the complete understanding of the technology's advantages should come from a comprehensive examination of their essential tenets in an effort to comprehend what causes said enhancements. Manifestly, these arise due to extensive research having been carried out by diverse authors on the topic.

Although every benefit will be interconnected, the most predominant advantage of the process will be the reduction in cutting forces. As vibration is applied, there will be a reduction in the Tool-Workpiece Contact Ratio (TWCR), given the nature of the intermittent contact between the tool and the uncut material. The cyclic cutting interruption will reduce the effective cutting time, as well as the inherent cutting forces. As a consequence, excessive heat accumulation will be avoided, preventing thermal burns and physical/chemical properties change in the workpiece [13, 18, 21].

Average cutting forces have been shown to be decreased with the application of ultrasonic vibration to conventional processes by values reaching over 50% [19, 29]. However, superior results are connected with vibrations imposed in the same direction of the cut [18]. Table 1 comprises some studies on cutting force reduction with the application of ultrasonic vibration to conventional processes.

Table 1: Experimental studies on cutting force reduction.

Process	Material	Frequency [kHz]	Amplitude [μm]	Force	Reduction	
Drilling	Ti6Al4V	17.7	0 - 9	Feed F_z	20% - 50%	[8]
Turning	Ti6Al4V	20.0	12	Tangential F_y	26%	[30]
		20.0	12	Feed F_z	26%	
		20.0	12	Radial F_x	38%	
Side Milling	AISI 420	23.5	20	Resultant	8% - 22%	[31]
End Milling	AA	19.6	0 - 8	Axial F_x	41%	[28]
		19.6	0 - 8	Feed F_y	45%	

The impact of ultrasonic vibration on the reduction of cutting forces is evident, particularly in the presented end milling process, where the most favorable and consistent outcomes are achieved. Notably, the force reduction intervals presented for the drilling and side milling scenarios are contingent upon variations in amplitude and feed rate, respectively, whereby an increase in these parameters is directly associated with a decline in the analyzed forces.

Facilitated heat dissipation will allow for better cooling of the cutting tool within each cycle of interrupted cutting, which, in addition with the reduction in cutting forces and stresses (as well as the frictional forces between the tool and the workpiece), will effectively reduce the tool wear, ultimately resulting in a more durable, longer-lasting tool [9, 18]. Tool wear reduction ranging from 20% to 30% is attainable, depending upon the specific tool geometry and employed machining parameters [12].

Longer tool lives undeniably result in a substantial reduction of tool maintenance and replacement costs, thereby constituting one of the most salient advantages of the UAM technology. It's important to note, however, that there is a limit amplitude value over which tool wear increases, being a consequence of the reached impact regime [8, 32].

Chip geometry will evidently be modified with the applied vibration, with UAM systems producing thinner, more consistent chips [18]. Thus, chip formation will be intermittent, provided by the reduction of instantaneous pressure-bending stresses along with the diminished cutting forces [9].

Figure 20 shows chip formation of Ti6Al4V with and without application of ultrasonic vibration to conventional drilling [8]. As can be seen, UAM results in non-continuous chips of smaller dimensions.

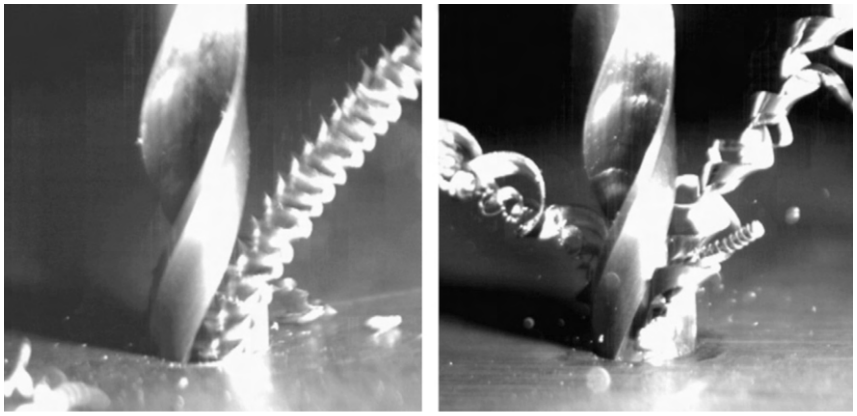

(a) (b)

Figure 20: (a) Chip formation in conventional drilling; (b) Chip formation with ultrasonic assistance [8].

Since burr formation is the result of instantaneous compressive and bending stresses in the deformation zone, the reduction in cutting forces will also result in minimal burr formation in parts machined with the UAM technology, as said stresses are vastly reduced [18].

The reduction in cutting forces will also minimize the formation of thermal cracks and plastic deformation in the workpiece, resulting in improved surface integrity due to the arrangement of the component's microstructure (lower residual stresses). Accordingly, with non-continuous chip formation and reduced subsurface cracks triggered by the low temperatures of the process, the uniformity of the cut will be increased, resulting in a smoother machined surface with reduced roughness [13, 18].

Reduced tool wear also implies decreased adhesion of workpiece material to the cutting tool, meaning that fewer particles remain to cause secondary damage to the machined surface [18]. As such, surface finish and dimensional accuracy greatly benefit from the UAM process.

Analogous to the tabulated data on cutting forces, Table 2 highlights the significant impact of UAM on improving surface quality, summarizing experimental research and underscoring the technology's potential. DOC refers to depth of cut, PV to peak-to-valley roughness and Ra to average roughness.

Table 2: Experimental studies on surface finish improvement.

Material			Surface Roughness [μm]		
Workpiece	Tool	DOC [μm]	Conventional Machining	UAM	
Al-SiC	SCD	1	0.86 PV	0.58 PV	[33]
Brass	SCD	1	1.00 PV	0.04 PV	[34]
Inconel	Carbide	50	60.00 PV	4.50 PV	[35]
SS	Carbide	50	20.00 PV	4.30 PV	[35]
AA LY12	PCD	150	0.94 Ra	0.63 Ra	[36]
CFRP	SCD	200	4.00 Ra	2.80 Ra	[37]
Inconel	Carbide	800	0.51 Ra	0.28 Ra	[38]

Further, Figure 21 shows the surface finish improvement with ultrasonic vibration in unidirectional milling of CFRP with ultrasonic assistance. As can be seen, vibrations reduce delamination of the composite layers and consequently improve the machined surface quality [12].

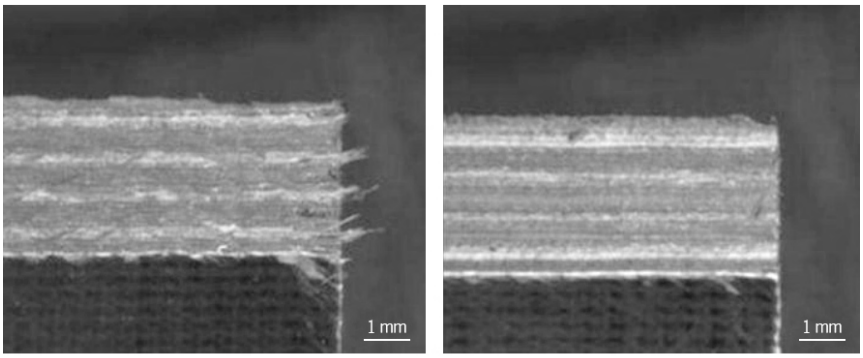

(a) (b)

Figure 21: (a) Edge quality for conventional milling; (b) Edge quality with ultrasonic assistance [12].

Moreover, as the MRR is increased with machining parameters such as the spindle speed, feed rate (not excluding vibration settings such as frequency and amplitude), resulting lower cutting forces can allow for an increase in the feed rate if a reduction in the machining time is required [12].

Process reliability can also be increased, especially for intricate geometries and very fine structures in difficult-to-cut materials. Complex textural patterns can be accurately created at micro and nano levels based on the direction of applied vibration, which would otherwise be very difficult to obtain recurring to conventional machining processes [22, 39, 40].

Regarding brittle materials, and as they tend to fracture easily under the great stress and strain conditions of the machining process, cutting in the ductile regime is going to improve machinability, more specifically extending tool life and producing parts with superior surface quality. In this domain, the material undergoes plastic deformation, absorbing part of the stress and strain and consequently preventing fracture. Chips will be produced by means of plastic flow.

This regime can be achieved by carefully controlling machining parameters such as the cutting speed, feed rate, and depth of cut. The critical value for the DOC variable is extremely low, however, in the order of microns, which will ultimately turn impractical due to the reduced MRR and extremely high machining times [18]. Furthermore, excessive plastic deformation can also lead to increased tool wear.

Nonetheless, the economic viability of machining in the ductile regime is also greatly improved with UAM techniques, as these have shown to vastly increase the critical DOC at which is regime occurs, being also a consequence of the resultant diminished cutting forces [9, 18].

Based on the proven substantial cutting force reduction, reduced tool wear allowing for extended tool life, and remarkable obtained surface finish, not neglecting the additional presented advantages inherent of UAM techniques, this technology has shown to be not only one of the most flexible and efficient methods of machining difficult-to-cut materials, with no comparable technique existing to date [12].

When compared to traditional methods, it is evident that UAM is applicable to a wider range of materials, improving their machinability, as ultrasonic vibrations aid in breaking down the workpiece material, reducing cutting resistance. Thus, Ultrasonic Assisted Machining consists of a more effective and efficient cutting process. Of course, presented enhancements follow the necessity for alternative machining technologies, as discussed in Subchapter 1.3.3.

For a better comprehension of process operation to ensure reliable performance, the study shall proceed with an analysis of the essential principles of ultrasonic vibration, not excluding system design, which is an essential step for a successful implementation of the technology.

It is also worth mentioning that the literature includes several designations for Ultrasonic Assisted Machining, depending mainly on the author. Specifically, concerning vibration applied to conventional processes, the two most typically used terms are UVAM (Ultrasonic Vibration Assisted Machining) and UAM/USAM (Ultrasonic Assisted Machining). In any case, they all refer to the same technique.

2.1.2 Underlying Principles and General Considerations

The ultrasonic designation comes from the implied vibration frequency values in the audio frequency spectrum. Electrical energy is converted into mechanical vibrations using an ultrasonic transducer, which is frequently piezoelectric or magnetostrictive, being consequently transmitted to the desired component. In short, vibration frequency belongs in the ultrasonic range, beyond the upper limit of human hearing, generally over 20 kHz [22, 26].

Figure 22 shows a representation of this.

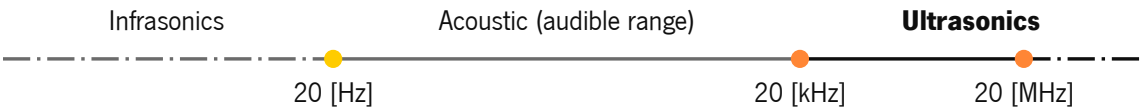

Figure 22: Audio frequency spectrum.

There are also systems with the Vibration Assisted Machining (VAM) denomination, in which the applied vibration values may not be limited to the ultrasonic range. These will not be taken into account in the present study, as the focal point is specifically ultrasonic technology. Moreover, vibration in the ultrasonic range enhances system stability, while low-frequency vibrations could have the opposite effect [22].

Within ultrasonic systems, as alluded to earlier, vibration can be applied either to the cutting tool, namely Actuated Tool System (ATS) (also known as "Direct Approach"), or to the workpiece, namely Actuated Work System (AWS) (also known as "Indirect Approach"), depending on the desired system specifications and will correspond to one of the main system-defining characteristics [2, 17, 25, 41].

The ultrasonic wave propagates through different mediums, provoking infinitesimal displacements of the molecules of the transposed medium, disturbing their equilibrium state. Said wave is characterized by its intensity, determined by the ultrasonic frequency (number of complete oscillations generated per second), and vibration amplitude. Together, they describe how much power transposes a unit cross-section area [22]. Since vibration is transmitted to a specified component, whether it may be the tool or the workpiece, the applied frequency value generally coincides with one of its natural frequencies[1].

A natural frequency (or eigenfrequency) is a characteristic frequency in which a system tends to naturally oscillate in when disturbed from equilibrium, without any external force interference. If an applied external frequency coincides with one of the system's eigenfrequencies, vibration amplitude is enormously amplified. This phenomenon is called resonance, consequently leading to more energy-efficient systems [25].

[1] Multiple natural frequencies can be present in a component, each corresponding to a specific degree of freedom. Some of them have a more pronounced effect than others.

Although it is true that systems involving resonance are by far the most common within this type of technology, given their optimal approach, there are several alternative vibration application methods not limited to this phenomenon. For example, *J. Cuttino* and *J. Overcash* developed a system in which the frequency can be tuned within a wide range of ultrasonic frequencies [18, 42].

Non-resonant systems also operate in a continuous frequency range, though generally with values below the ultrasonic domain, with a working amplitude greater than that in the resonant type [25, 26]. Resonant systems, however, have the advantage of operating far above certain natural frequencies that could potentially cause unwanted and uncontrolled resonance. It is important to emphasize that employed frequency is solely intended to enhance the cutting process.

The literature also contains some self-regulating systems. An example of this is a method developed by *Babitsky et al.* that uses the feedback given by the system's reactive energy, enabling the tuning and maintenance of optimal resonant frequency values, managing to improve the surface finish in the machining of Inconel components by 50% compared to standard ultrasonic systems without this type of regulation [18, 43, 44].

In ATS type methods, vibrations generated by the transducer are transmitted to the tool via an energy-focusing device, as is the case with conventional USM systems [26]. The booster, horn and sonotrode terms also apply to UAM techniques. The cutting tool will then vibrate according to the imposed direction(s).

As a consequence, while in ATS systems the optimization of the material removal rate is largely dependent on both the tool and the horn, directly impacting the vibration environment, AWS alternatives will rely on a more challenging design, as the practicality of tuning the system specifications to the cutting tool is superior when compared to actuating on the workpiece, especially for larger components.

AWS methods will benefit from workpieces with thinner walls, given the nature of the acoustic transmission. This makes ATS setups overwhelmingly more common, as they do not depend on workpiece configuration whatsoever [2, 17]. Hence, the restriction of the study to vibrating tool systems will be a default assumption for the present analysis, disregarding the AWS approach.

The developed UAM system is of the resonant type, contemplating 1D axial vibration.

2.1.2.1 Vibration Fundamentals

To understand complex concepts like resonance, it's important first to grasp the basics of vibration. The analysis shall hence start with a naturally vibrating system that is not influenced by any external forces.

The complex behavior of vibration systems can usually be simplified by establishing parallelism to a simple model that approximates their dynamics. One of the most frequent simplifications is the reduction to a mass-spring system, given its mechanical simplicity.

A visual representation of the described system can be observed in Figure 23.

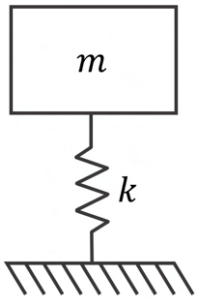

Figure 23: Mass-spring system.

The analogy involves simplifying the overall mass of the system to a single point mass, represented by m, and reducing its total stiffness to that of a spring, represented by k, assuming a single degree of freedom due to the spring's retraction/extension. Note that gravity and energy dissipation (damping) are neglected in this analysis.

The presented system can be defined recurring to Hooke's law of elasticity, which states that an applied force, F, equals the product of the spring's stiffness and its change in length, x, acting as the displacement of the point mass. This correlation is shown in Equation 1.

$$F = k \cdot x \quad [N] \tag{1}$$

As there are no externally applied loads, the only acting force will be that of the spring. Figure 24 contains the system's free-body diagram.

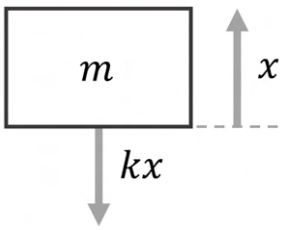

Figure 24: Free-body diagram of the mass-spring system.

In a similar manner, Newton's second law of motion states that the sum of the forces applied to the system is equal to its mass, m, multiplied by its acceleration, a, as shown in Equation 2.

$$F = m \cdot a \quad [N] \tag{2}$$

A relationship between the two equations can now be established. Since position is the second derivative of acceleration, the equation can be rewritten using only spring stiffness, point mass, and corresponding position (displacement). Thus, the resulting equation of motion for the system is illustrated in 3, completely defining its dynamics according to the proposed assumptions.

$$\sum F = ma - kx \quad \Leftrightarrow \quad m\ddot{x} + kx = 0 \tag{3}$$

Such correlation, however, can only be drawn given that the mass displacement and the force exerted by the spring have contrary directions.

The solution of the differential equation can be reformulated by expressing the relationship between spring displacement, x, and vibration amplitude, A, by the form of a sinusoidal function shown in 4.

$$x(t) = A \sin\left(\sqrt{\frac{k}{m}}t + \phi\right) \tag{4}$$

Note that ϕ refers to the phase angle, while t refers to time.

The natural angular frequency of an elementary system like the one in question, ω_n, can be calculated by the root of the ratio of the spring stiffness to its mass as shown in Equation 5. Evidently, this will be independent of any initial system conditions.

$$\omega_n = \sqrt{\frac{k}{m}} \quad [rad/s] \tag{5}$$

This value can then be easily converted to the linear natural frequency of the system, f_n, by the operation shown in 6.

$$f_n = \frac{\omega_n}{2\pi} = \frac{\sqrt{k/m}}{2\pi} \quad [Hz] \tag{6}$$

Therefore, the sinusoidal function can be adjusted both to the system's angular and linear natural frequencies, as shown in 7 and 8.

$$x(t) = A \sin\left(\omega_n t + \phi\right) \tag{7}$$

$$x(t) = A \sin\left(2\pi f_n t + \phi\right) \tag{8}$$

Expressions 7 and 8 define the harmonic movement of the naturally vibrating system. Evidently, displacement x will only be dependent on the system's initial conditions.

It is also worth noting that the vibration period, T (time needed for a complete single oscillation of a system), can be calculated by the ratio of 1 to the natural frequency f_n, as shown in 9.

$$T = \frac{1}{f_n} \quad [s] \tag{9}$$

The comprehension of the fundamental system equations can be greatly facilitated by drawing a visual representation of the sinusoidal function, as shown in Figure 25.

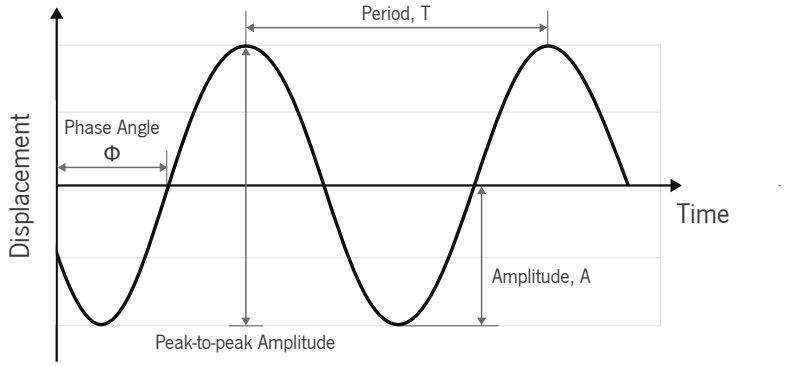

Figure 25: Sinusoidal wave of harmonic vibration.

Naturally, in a real-life situation, damping occurs, and energy is dissipated over time, due not only to the relative motion of the involved system components but also to the interactions at their molecular level. Therefore, a more accurate representation of a naturally vibrating system can be achieved by adding a damper to the previous simplification, resulting in a mass-spring-damper system, as shown in Figure 26.

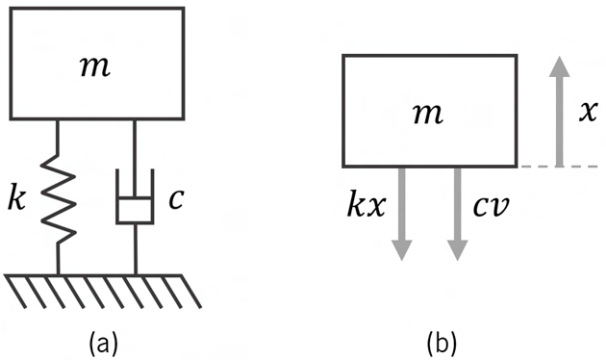

Figure 26: (a) Mass-spring-damper system; (b) Free-body diagram.

Following the line of thought applied previously, in the expressions relative to the system's point mass and point stiffness, the same procedure can be applied to the case of the introduced damper. In this way, the damping force can be defined by Equation 10, using a viscous damping model in which c refers to the damping coefficient and v to the velocity.

$$F = c \cdot v \quad [N] \tag{10}$$

Consequently, the equation shown in 3 can be easily readjusted to the addition of the new component, as shown in 11. Note that the displacement x is the derivative of velocity v.

$$\sum F = ma - kx + cv \quad \Leftrightarrow \quad m\ddot{x} + c\dot{x} + kx = 0 \tag{11}$$

Unlike with the simpler mass-spring system, the addition of a damper will imply that the solution of the system's equation of motion depends on the amount of applied damping. Therefore, it is necessary to comprehend that there are essentially three distinct damping scenarios.

The damping ratio, denoted by ξ, is a dimensionless parameter defined as the ratio of the damping coefficient, c, to the critical damping coefficient, c_{cr}. The critical damping coefficient can be written in terms of the system's mass and natural angular frequency. The algebraic expression is present in 12.

$$\xi = \frac{c}{c_{cr}} = \frac{c}{2m\omega_n} \tag{12}$$

The three main scenarios of damping in mechanical systems include critically damped, overdamped, and underdamped, each one with an associated damping ratio ξ, respectively equal to 1 (critical damping), greater than 1, and less than 1. The resulting curves can be observed in Figure 27.

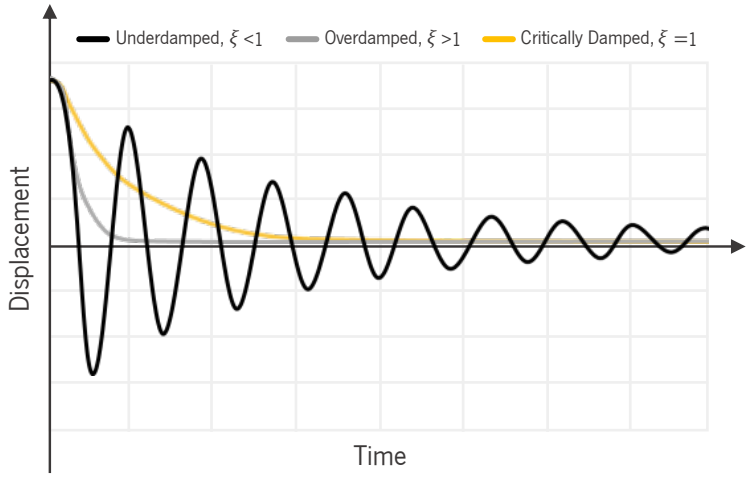

Figure 27: Representation of the three distinct damping scenarios.

The transient state is quickly surpassed in critically damped systems, and equilibrium is reached in the shortest possible time. The equilibrium state is known as the steady-state response. There are also no visually present oscillations in overdamped systems. However, these don't return to their equilibrium state as quickly as in the critically damped type. In underdamped systems, alternatively, the oscillations are slow to fade, and the system takes the most time to achieve the steady-state response. As can be observed, its behavior represents an exponentially decreasing harmonic function.

It is important to note that a damping ratio of zero corresponds to an undamped system, which is only possible theoretically, as no matter how well-engineered or optimized systems may be, they will always have some form of damping.

Applying the above information to a scenario in which the system is affected by an external harmonic load f_e with intensity F_e and angular frequency ω_e, as is the case with the usage of ultrasonic transducers in UAM systems, maximum vibration amplitude at resonance can be empirically proven. Expression 13 defines the forced load, while Figure 28 presents the system's free-body diagram.

$$f_e(t) = F_e \sin(\omega_e \cdot t) \tag{13}$$

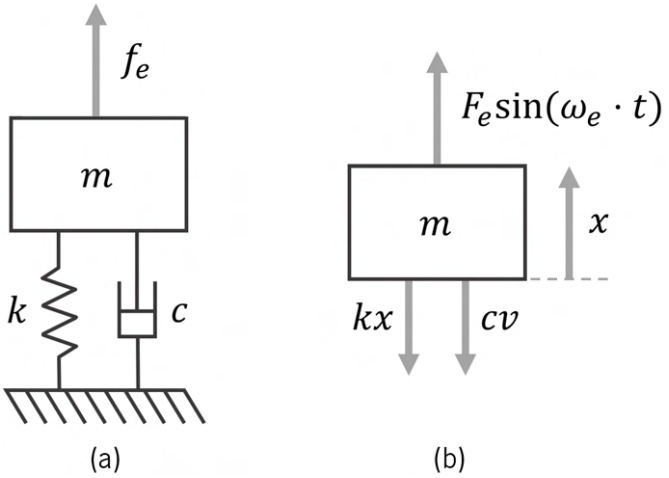

Figure 28: (a) System with an externally applied sinusoidal load; (b) Free-body diagram.

The system will be defined by a non-homogeneous differential equation, as shown in 14.

$$m\ddot{x} + c\dot{x} + kx = F_e \sin(\omega_e \cdot t) \tag{14}$$

In this case, the solution of the equation of motion of the system will consist of the sum of two functions, x_c, referring to the *complementary solution* (transient response), and x_p, referring to the *particular solution* (steady-state response). The complementary solution is the solution to the homogeneous form of the equation, as previously shown in 11, in which the system is in free vibration.

On the other hand, the particular solution captures the effects of the external load, denoting the system's forced amplitude response, as expressed in 15.

$$x_p(t) = \frac{F_e/k}{\sqrt{(1-\beta^2)^2 + (2\beta\xi)^2}} \tag{15}$$

Note that β refers to the ratio of the forced frequency to the natural frequency, as shown in 16.

$$\beta = \frac{\omega_e}{\omega_n} \tag{16}$$

As the system stabilizes, the complimentary solution will eventually reduce to zero, given that free vibrations fade due to damping. Thus, as solely forced vibration remains, the particular solution will completely define the motion of the system (steady-state response). This equilibrium state will contain the same frequency as the applied harmonic load, yet offset by a response lag, as shown in Figure 29.

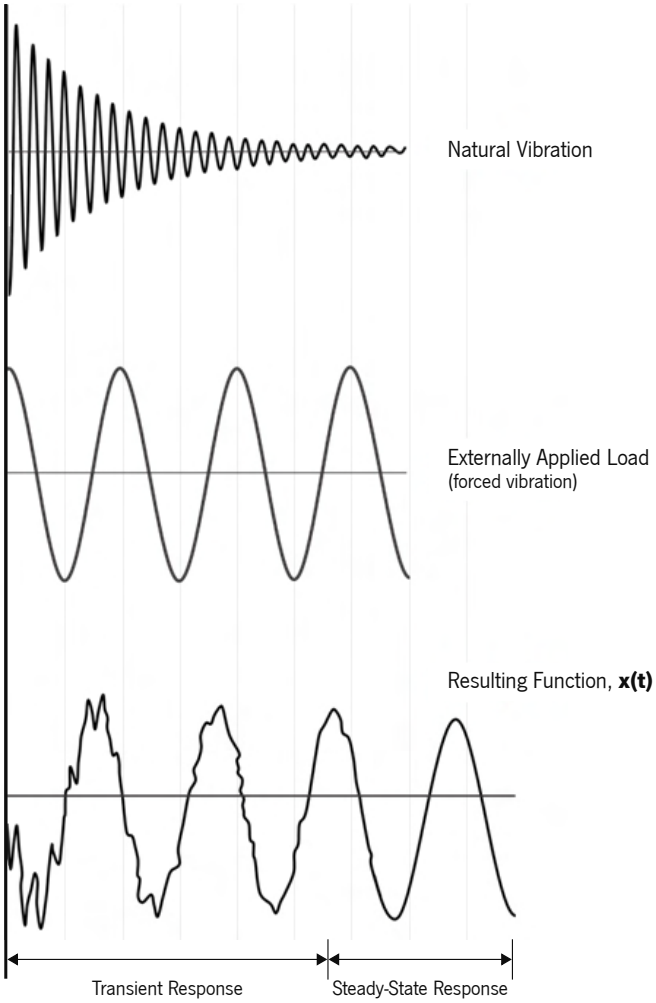

Figure 29: Representation of the system's harmonic response to the applied sinusoidal load [45].

The presented delay corresponds to the phase angle ϕ, given by Equation 17.

$$\phi = \tan^{-1}\left(\frac{2\xi\beta}{1-\beta^2}\right) \quad [rad] \tag{17}$$

Accordingly, the resulting solution to completely define the system's amplitude, x, will coincide with the mentioned particular solution x_p, as shown in 18.

$$x(t) = x_p(t) = \frac{F_e/k}{\sqrt{(1-\beta^2)^2 + (2\beta\xi)^2}} \quad [m] \tag{18}$$

If the frequency of the applied sinusoidal load approaches the natural frequency of the system (resonance), frequency ratio β will tend to 1. In conjunction with minimal damping values, in which the damping ratio ξ tends to 0, the denominator in Equation 18 will consequently also tend to 0, resulting in the displacement x being enormously amplified. Theoretically, if damping was non-existent, vibration amplitude at resonance would be infinite.

A representation of this amplification with different values of the damping ratio is shown in Figure 30.

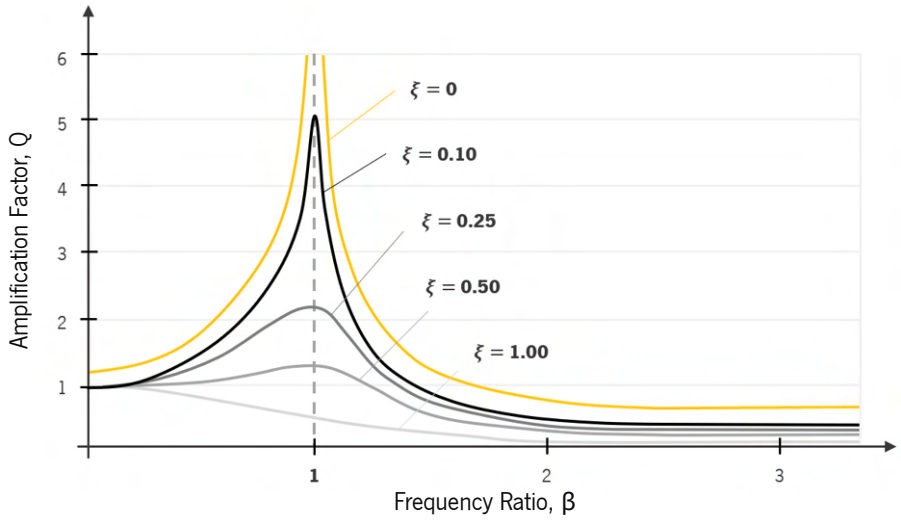

Figure 30: Variation of vibration amplitude with distinct damping ratio values.

Note that Q corresponds to the amplification factor, which is a measure of how much the system output changes overtime, defined as the ratio of the steady-state response to the transient response of the system, as given by 19.

$$Q = \frac{x_p}{x_c} = \frac{1}{\sqrt{(1-\beta^2)^2 + (2\beta\xi)^2}} \tag{19}$$

Thus, the maximized amplitude values for reduced damping ratios at resonance demonstrate resonant systems' improved energy efficiency, although being limited to a discrete natural frequency.

It's worth emphasizing that the foundation of this section is rooted in the seminal contributions of researchers *J. Meireles* [45] and *J. L. Humar* [46] on structural dynamics, as well as the work of *J. He and Z. Fu* on modal analysis [47].

System stability will fundamentally depend on parameter control. As frequency takes on immense values, amplitude belongs in the micron range, generally below 50 μm [1, 9, 16, 18, 21, 25, 26, 31]. Regardless of resonance resulting in maximum displacement, vibration amplitude will ultimately be limited by the relationship between the excitation and mechanical response of the transducer, adding to the difficulty of controlling the tool trajectory due to phase lag [25]. Such limitations increase the importance of energy efficiency in resonant systems.

One large disadvantage of conventional UAM resonant systems, however, is that the natural frequency will fundamentally change with alterations to the applied load and to the tool's cutting edges (due to tool wear). This can also be caused by inadequate system setup. Without an auxiliary system providing information, there is a risk of a UAM system working in a non-optimal state. If this is the case, the amplitude will be reduced and most of the power that is output by the power supply is converted into heat, excluding the benefits of the applied technology [25, 48–50].

To address this issue, and as briefly mentioned, self-regulating systems have been consequently studied by researchers. Notwithstanding, the developed milling system is of the resonant kind and does not contemplate any kind of regulation, as this would be over-complicated for the scope of this thesis.

2.1.3 Specifications of UAM Systems

The vibration mode is generally the key characteristic in which UAM systems are divided into. Three categories arise, including vibration in one, two, or three dimensions, as previously outlined [18, 25, 26].

Figure 31 shows a historical perspective of the first UAM developments in different vibration modes.

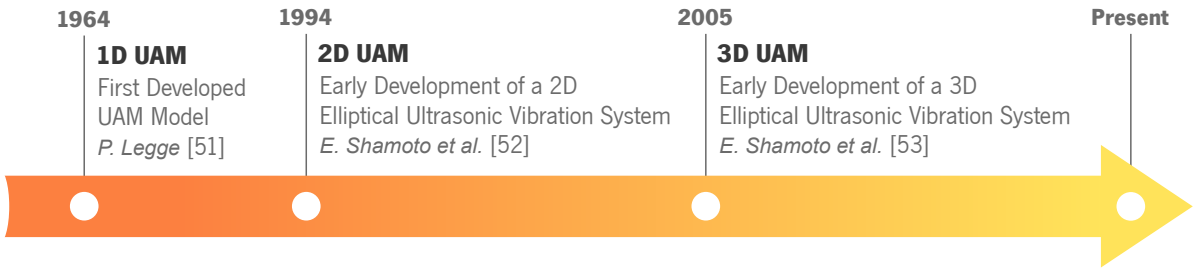

Figure 31: Historical timeline of the initial developments in distinct UAM vibration types [25, 51–53].

It can be naturally comprehended that applying vibration in a single direction is a far less challenging approach than designing a system that comprises two or more vibration axes. Accordingly, 1D UAM systems have preceded 2D and 3D alternatives for an extended period of time.

In 1D UAM systems, the tool can either vibrate in the cutting direction or any other direction perpendicular to it. For example, an axial vibrating tool will coincide with the feeding direction in the drilling process while being perpendicular to the feeding motion in a milling operation. This superimposed movement will occur harmonically in a linear path [18].

Regarding the two-dimensional approach, the application of harmonic waves occurs in two distinct directions. Vibration in the tool's supporting structure is generated, consequently creating an elliptical motion in the tooltip. The introduction of a new vibrating axis has been shown to further enhance the already attained advantages of 1D UAM systems, particularly regarding improvements in surface finish quality, reduction in cutting forces, and extension in the tool's life [25, 26].

Additionally, while the tool comprises a plane elliptic curve trajectory in 2D UAM systems, the introduction of a third vibration axis in 3D UAM systems generates a spatial elliptic curve [26].

The application of vibration in two or three dimensions is still comparatively recent, and further research is required to validate its effectiveness. Current challenges of the technology, not limited to multi-axial vibration system types, consist in stabilizing control signals and improving transducer efficiency [25].

Despite their simplicity, 1D UAM systems have consistently demonstrated their efficiency throughout the years and have continued to evolve constantly. At present, these are undoubtedly the most common.

Note that the presented milestones solely focus on UAM, disregarding conventional USM techniques.

2.1.3.1 Kinematic Analysis

The combination of the applied harmonic load with the tool's rotating motion during the cutting process will fundamentally result in a complex movement of the tooltip. In reality, in 1D UAM systems with axial tool vibration in operations where the tool is rotated, torsional vibration will be present at the bottom of the cutter, being a result of the conjunction of the imposed vibration and the rotating nature of the tool. Depending on the tool's geometry, this can also contribute to the reduction of cutting forces [54].

A comprehensive analysis of the kinematics of UAM milling can be developed for a better comprehension of the tool's movement. Nonetheless, mentioned torsional vibration will not be included in the present study due to its minimal influence. As vibrating tool systems have been an assumed premise for the document, the 1D vibration mode will follow the same principle, given the nature of the developed UAM system, with every succeeding analysis being established regarding the milling process.

The three directions in which vibration can be applied in a milling operation can be observed in Figure 32, consisting in the primary cutting (feed) and crossfeed directions, as well as the DOC direction. These are respectively represented by the x, y, and z axes.

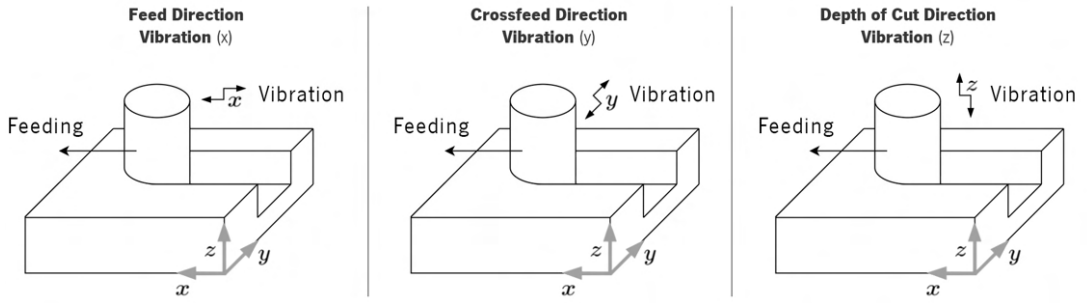

Figure 32: Vibration application to the three coordinate axes in a milling operation.

The tool's movement will be completely defined by the conjunction of the cutting tool's feed rate v_f with the applied harmonic load. However, the vibration direction will dictate which of the coordinate axis the analysis needs to be carried out in.

In the case that vibration coincides with the feed direction, only the x axis needs to be studied. Taking the representation shown in Figure 17 and included stages into consideration, the tool's position can be related to the vibration amplitude. Such a scenario is presented in Figure 33.

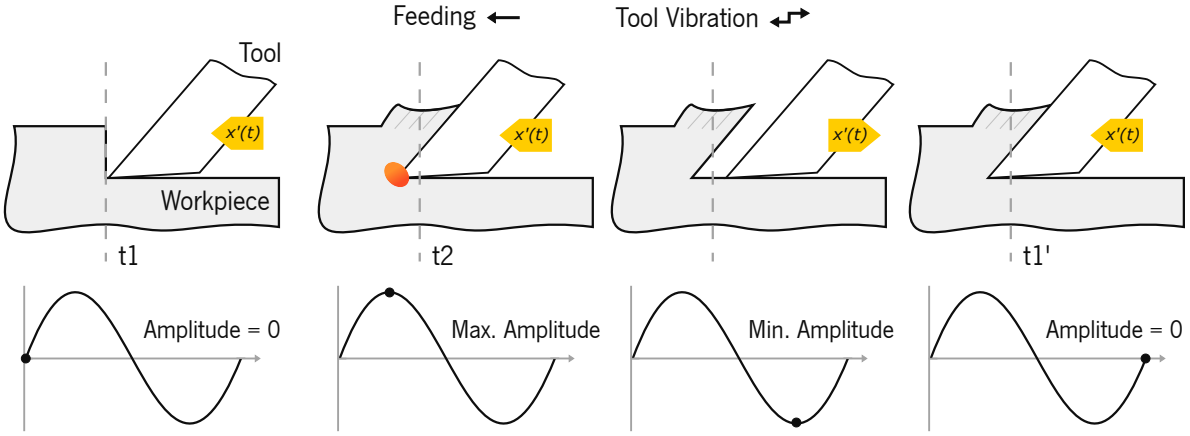

Figure 33: Phases of a vibration cycle in 1D UAM [18].

A similar expression to Equation 8 can be used as the motion equation while disregarding phase angle ϕ (unnecessary for this analysis) and including the feeding motion, as shown in Equation 20.

$$x(t) = A\sin(2\pi f t) + v_f\, t \tag{20}$$

Consequently, through differentiation, the tool's velocity can be defined by Equation 21.

$$v(t) = x'(t) = 2\pi f A \cos(2\pi f t) + v_f \tag{21}$$

Under these specific circumstances in which movement occurs in a single direction, there will be a critical value for v_f above which the tool will permanently contact the work surface, given by Equation 22.

$$v_{f\ crit} = 2\pi f A \tag{22}$$

As desirable UAM advantages derive from the interrupted cutting motion, these will only manifest if the applied feed rate is below this critical value. Alternatively, if $v_f \geq v_{f\ crit}$, the cutting process becomes continuous, similar to that of conventional cutting. Nonetheless, the harmonic variation of the relative velocity between the tool and the workpiece will still occur [18].

The horizontal speed ratio, HSR, can then be defined as the ratio between the feed rate v_f and the critical feed rate above described, as shown in Equation 23 [18, 25].

$$HSR = \frac{v_f}{v_{f\ crit}} \tag{23}$$

Naturally, continuous cutting will occur for $HSR \geq 1$.

Moreover, the distance traveled by the tool between two equivalent points in a successive vibration cycle, represented by d_P, can be defined by the ratio of the feed rate v_f to the vibration frequency f, as shown in Equation 24.

$$d_p = \frac{v_f}{f} \tag{24}$$

The two-time variables that define the interrupted contact between the tool and the workpiece are instants t_1 and t_2, respectively referring to the instant when the tool contacts the surface of the uncut material and the instant when such contact is terminated. These can be observed in Figure 33.

The time frame between mentioned instants is the portion of a single vibration cycle in which material removal happens, being designated as the duty cycle, represented by DC. When related to the harmonic period T or its reciprocal frequency f, it can be defined by Equation 25.

The cutting duration within a vibration cycle will be proportional to the value of this parameter. Inherently, it will also specify the nature of the cutting process, as continuous cutting happens if $DC = 1$.

$$\mathrm{DC} = \frac{t_2 - t_1}{T} = f\left(t_2 - t_1\right) \tag{25}$$

To define instants t_1 and t_2 according to the presented variables, however, two slightly more intricate expressions arise, as presented in Equations 26 and 27 [18].

$$A\sin\left(2\pi f t_1\right) = A\sin\left[\arccos\left(\frac{-v_f}{2\pi f A}\right)\right] - v_f\left[t_1 - \frac{\arccos(-v_f/2\pi f A)}{2\pi f}\right] \tag{26}$$

$$t_2 = \frac{\arccos(-v_f/2\pi f A)}{2\pi f} \tag{27}$$

If, alternatively, vibration is applied perpendicular to the feed direction, whether coinciding with crossfeed or with the direction of the depth of cut (axial tool vibration), the analysis requires the division of the tool's movement between the two corresponding coordinate axes. Movement in direction x is now solely defined by the feed rate v_f, as shown in Equation 28.

$$x(t) = v_f \cdot t \tag{28}$$

The harmonic movement of the tool will be defined in directions y and z, the former referring to vibration in the crossfeed direction and the latter to vibration in the tool's axial direction.

Thus, for systems where vibration coincides with the crossfeed direction, the harmonic movement of the tool will be defined by the expressions presented in 29.

$$\begin{cases} x(t) = v_f\, t \\ y(t) = A\sin(2\pi f t) \end{cases} \tag{29}$$

As for vibration in the tool's axial direction, the respective expressions are shown in 30.

$$\begin{cases} x(t) = v_f\, t \\ z(t) = A\sin(2\pi f t) \end{cases} \tag{30}$$

Manifestly, velocity in these cases can also be defined by the differentiation of the above-presented equations in 29 and 30, for crossfeed and axial vibration, respectively.

A summary of the presented kinematic analysis for different 1D UAM systems in the three coordinate axes can be observed in Figure 34, including a representation of the tooltip's displacement.

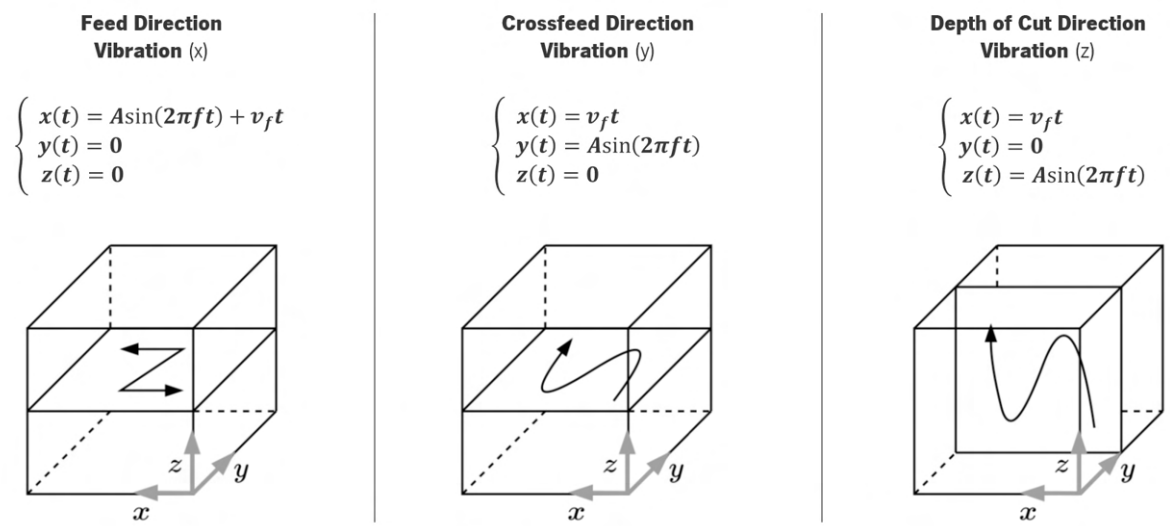

Figure 34: Summary of tool motion definition for 1D UAM milling systems.

The analysis shall now proceed by narrowing its scope to axial vibrating tool systems.

Figure 35 (a) includes a schematic representation of a system of this kind with the addition of point P, referring to a randomly selected point within the tool's cutting edge, while Figure 35 (b) entails a top view of the plane normal to the applied vibration direction.

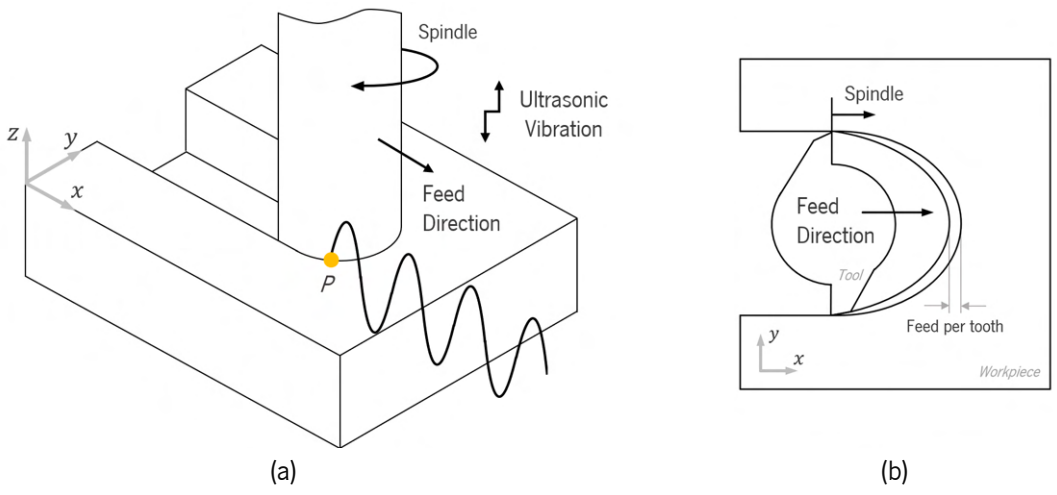

Figure 35: Analyzed system representation: (a) isometric view; (b) top view of cutting plane.

The spatial trajectory of point P within a single tool rotation with vibration should also be considered for comparison with an equivalent point without the applied harmonic wave, as depicted in Figure 36.

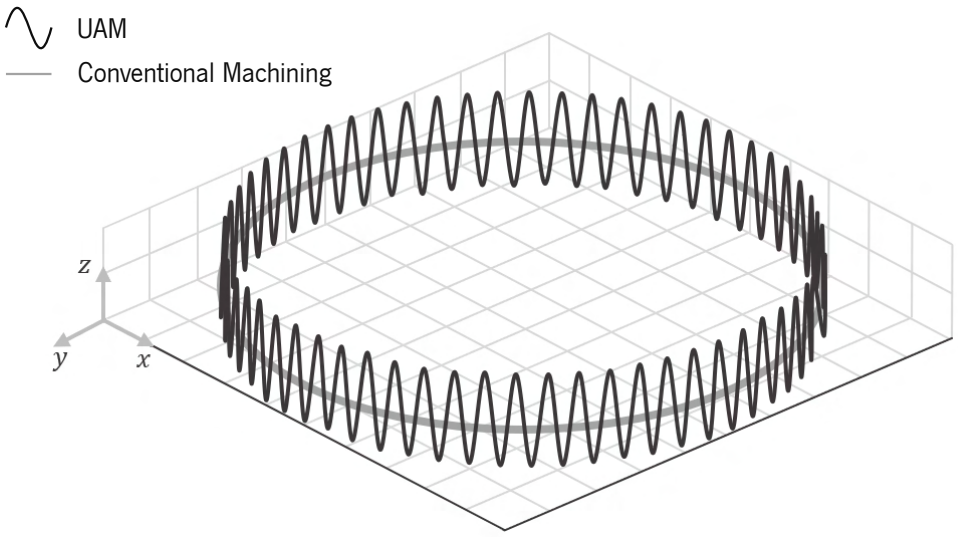

Figure 36: Trajectory of point P in a single rotation.

In reality, considering spindle rotation with a cutting velocity v_c will generate hybrid movement in the tooltip. It is indispensable to consider this parameter, as no cutting action occurs if the tool does not rotate.

Consequently, the tool's motion is completely defined by the equations shown in 31 [16].

$$\begin{cases} x(t) = v_f\, t + R\sin(\omega_s t) \\ y(t) = R\cos(\omega_s t) \\ z(t) = A\sin(2\pi f t) \end{cases} \tag{31}$$

Parameter ω_s refers to the angular velocity of the spindle, while R refers to the cutting tool's radius.

From this, the kinematic study can be concluded through the differentiation of above-presented expressions, resulting in velocity definition over the three coordinate axes, as shown in Equation 32.

$$\begin{cases} x'(t) = v_f + R\omega_s\cos(\omega_s t) \\ y'(t) = -R\omega_s\sin(\omega_s t) \\ z'(t) = 2\pi f A\cos(2\pi f t) \end{cases} \tag{32}$$

Evidently, optimization will be a significant factor in the design of UAM systems. Therefore, a comprehensive understanding of piezoelectricity and the operating principles of ultrasonic transducers is also essential, not neglecting other involved components for the correct design of a vibration system. It is on these subjects that the study shall subsequently focus.

2.1.4 Comprehensive Analysis of Required Components

There are several components involved in the application of ultrasonic vibration to a conventional machining system, some of which are mandatory for the process. In the case of this thesis, as already stated, the analysis focuses on a resonant 1D ATS UAM system for milling, in which the tool is driven harmonically in one dimension, coinciding with its axial direction.

The design of the system should focus mainly on the ultrasonic generator (which generates high-frequency electrical energy, acting as a power supply), the transducer (which converts the electrical energy of the generator into mechanical vibrations), the sonotrode (which amplifies the vibrations generated by the transducer, acting as an energy-focusing device) and the vibrating cutting tool [14, 18, 22, 26]. Additionally, a control system regulates the power and frequency of the applied vibrations.

The efficiency of the vibrating system will largely depend on ensuring consistent contact among all components involved, reducing any potential electrical and mechanical losses [22]. Note that the cutting tool should be perfectly aligned at the end of the sonotrode (which will act as the tool holder), ensuring that the applied vibration direction matches the system requirements [18, 26].

Figure 37 shows a general representation of the components of 1D ATS UAM system.

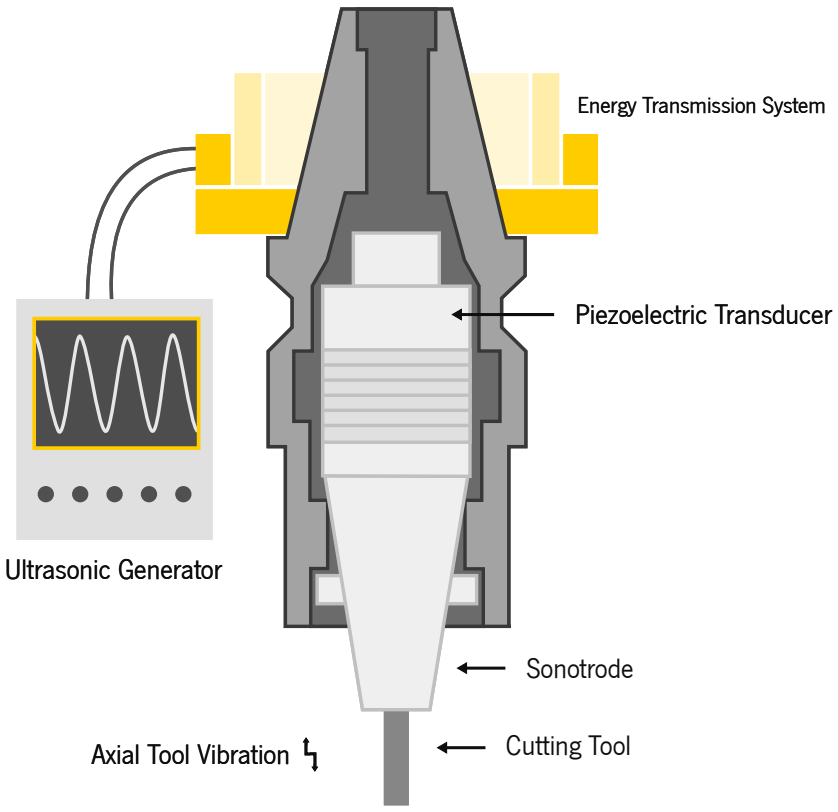

Figure 37: General 1D ATS UAM system.

2.1.4.1 Ultrasonic Generators

An ultrasonic generator is used to convert the standard power of the network (120-240 V, 50/60 Hz) into AC electric energy at the desired ultrasonic frequency, within its range of working operation [3].

Figure 38 includes a functional schematic representation of an ultrasonic generator.

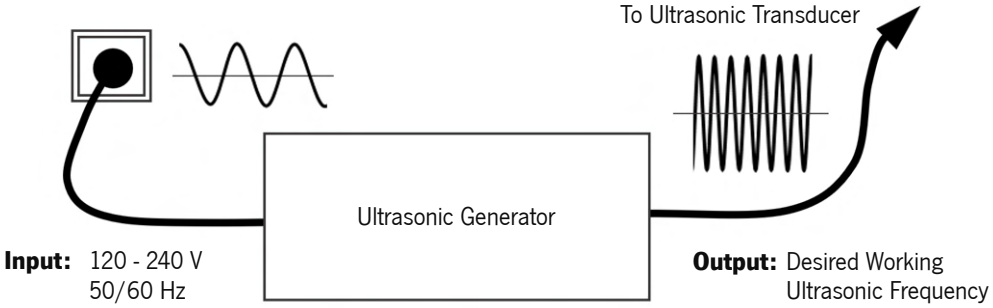

Figure 38: Schematic representation of how an ultrasonic generator operates [55].

Ultrasonic generators operate in the discrete frequencies required by UAM systems, reaching values up to 40 kHz in the ultrasonic range. These consist in high Q[2] resonant systems [18].

However, as the applied frequency will depend on the design of the rest of the system, and given the risk of non-optimal working frequencies due to possible setup errors and tool wear, some resonance following generators have become available, automatically tuning the output frequency to match the natural frequency of the assembly. These also minimize acoustic energy loss and heat generation, having the possibility to include safety features [14].

2.1.4.2 Piezoelectricity and Ultrasonic Transducers

Once the frequency is converted to the system's desired values, the transducer will begin to function. As previously mentioned, this component will use the electrical energy it receives to generate a reciprocating harmonic high frequency, low amplitude mechanical motion [3].

For ultrasonic industrial applications, as already stated, transducers are generally piezoelectric or magnetostrictive. The latter essentially squeezes the atoms of a magnetic material via an applied oscillating magnetic field, creating a periodic change in the material's length and consequently producing a high-frequency mechanical vibration [56].

A major disadvantage of magnetostrictive transducers is their reduced working efficiency (under 55%), due to major losses in the form of generated heat [14].

[2]High Q indicates that the system is able to store more energy in its oscillations and to have low rates of energy dissipation, consisting of a more pronounced resonance and a longer decay time.

Piezoelectric (PZT) transducers, on the other hand, are overwhelmingly more popular in UAM systems. Not only do they have a higher working efficiency (over 90%) compared to the magnetostrictive alternative, but they also include higher achievable frequency values, better temperature stability, smaller size, easier construction, and overall longer durability [14]. Even though having a reduced dimensional displacement, a commercial 20 kHz PZT transducer can output a force of 3000 N [3].

The piezoelectric effect is the ability of certain materials to generate an electrical charge when mechanical stress is applied to them. Inversely, as PZT materials are smart materials, their shape will change as they expand or contract (depending on the polarity), generating mechanical energy as soon as voltage is applied to them. This is known as the converse piezoelectric effect, and it is the working principle of a PZT transducer.

A representation of the converse piezoelectric effect can be observed in Figure 39.

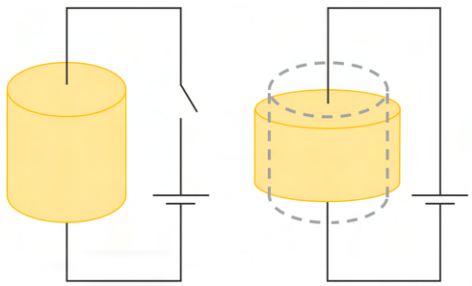

Figure 39: Representation of the inverse piezoelectric effect.

The piezoelectric crystals within a PZT transducer are ceramics, generally lead zirconate and lead titanate. These come usually in a form of discs, each with an approximate thickness not over 10% of the total transducer's length [14].

Multiple PZT discs (or actuators) are stacked inside the transducer in order to achieve high working frequencies without the need of active cooling, recurring to a phased actuator activation sequence in which each individual disc works at a lower frequency than the higher output frequency value [18].

The piezoelectric effect is a result of how the material's crystalline structure behaves when an external electrical field is applied to it, becoming slightly distorted. This deformation causes the positive and negative charges within the material to become separated, creating a dipole moment $\vec{D}$ [57].

The dipole moment is a measure created in the distorted structure (wherein the center of positive and the center of negative charges don't coincide with each other), and its magnitude is directly proportional to the strength of the applied electric field and the amount of charge separation. Polarization will consequently lead to the material's contraction or expansion, depending on the direction of the applied electric field.

However, this phenomenon only takes place for temperatures below the Curie temperature, represented by T_C, above which the material will lose its piezoelectric properties due to its crystalline structure becoming disordered and the dipole moments consequently becoming randomized. This temperature is relatively high for most PZT materials (typically above 1000 $°C$) [3].

Figure 40 shows a representation of the crystalline structure of a material above and below the Curie temperature, including the involved charges, for a better comprehension of the polarization phenomenon.

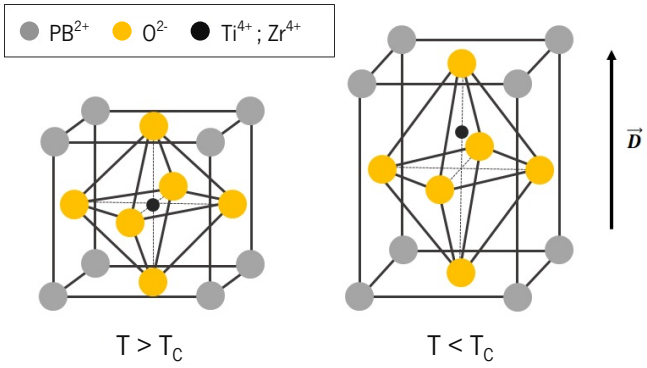

Figure 40: Crystalline structure of a piezoelectric material at different temperatures [58, 59].

Although the temperature might be favorable and each grain of the material having its own dipole moment, the overall macroscopic structure may be considered unpolarized. Polarization occurs when the dipoles align in the same direction due to the application of the electric field, leading to a polarized macroscopic structure without modifying the grains themselves [3].

In similarity to what was done in Subchapter 2.1.2.1, a mass-spring-damper system can also be used to mechanically represent a piezoelectric transducer. The spring stiffness k will correspond to the Young's modulus of the material, and the damping coefficient c will represent loss factors due to the system's dissipated energy. Nonetheless, a more accurate representation would be from an electrical perspective.

For PZT transducers, the electrical equivalent is known as a Butterworth-Van Dyke (BVD) circuit, and the two most widely used lumped-parameters impedance models are presented in Figure 41 [60].

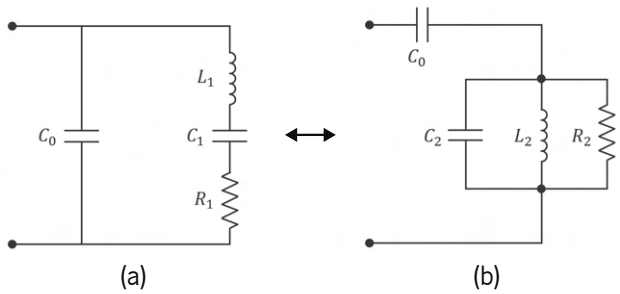

Figure 41: Mechanical (a) and electrical (b) equivalents of a PZT transducer [3, 60, 61].

Capacitance C_1 will represent stiffness (equivalent to the spring), inductance L_1 will represent mass, and resistance R_1 will represent mechanical losses during vibration (equivalent to the damper). Additionally, capacitance C_0 refers to the PZT crystals and respective cabling [3]. Note that, in this simplified model, thermal dissipative elements are neglected.

Every transducer is designed to function at a determined nominal working frequency, given by f_N. Nonetheless, this frequency value will come with a small tolerance [3].

The working interval in which the transducer's frequency can vary is studied in relation to its electrical impedance, being fundamentally limited by its resonant and anti-resonant working regimes. The resulting impedance-frequency function is known as the transducer's impedance curve, represented by Z.

The peak minimum impedance point corresponds to the resonant regime, while the peak maximum impedance refers to the anti-resonant regime. Figure 42 shows a general representation of said curve.

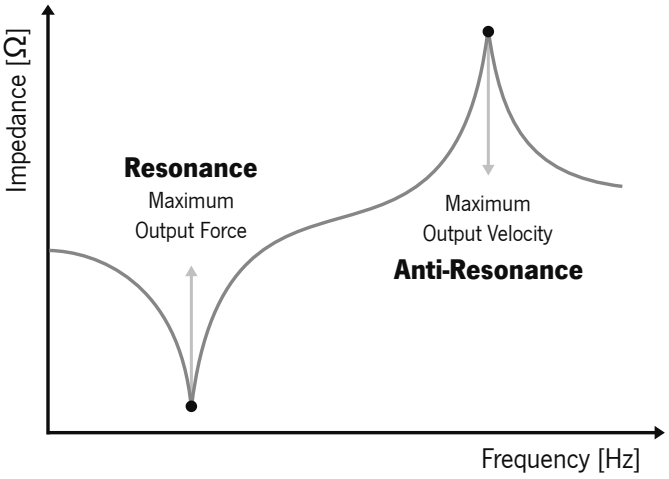

Figure 42: General impedance curve of a piezoelectric transducer [3, 60].

The frequency value at the resonant regime is known as the transducer's resonant frequency, represented by f_R. At this point, the transducer's behavior will coincide with the BVD circuit present in Figure 41 (a), being frequently referred to as "in series resonance". Alternatively, the frequency value at the anti-resonant regime corresponds to the anti-resonant frequency, given by f_A. At this point, the transducer's behavior is represented by the BVD circuit present in Figure 41 (b), which can also be referred to as "parallel resonance".

An electromechanical analogy relating electrical current to force and voltage to velocity can be established. Consequently, given the nature of the corresponding circuit, it can be understood that the transducer will be able to deliver maximum output force (or pressure) and relatively low velocity at resonance. This regime would be the theoretically most effective frequency at which the transducer could operate, resulting in maximum vibration amplitude.

On the other hand, at the system's anti-resonant regime, maximum output velocity and minimum output force will be delivered (minimum vibration amplitude) as the transducer's mechanical and electrical components are not in phase [60].

Frequencies below the resonant frequency f_R and above the anti-resonant frequency f_A correspond to a purely capacitive behavior of the transducer, with current leading the voltage by a phase angle ϕ. Between analyzed nodes, however, the transducer's behavior is purely inductive, with current lagging the voltage, allowing all energy to be used for vibration generation.

Figure 43 includes a rundown of the presented information regarding the behavior of a PZT transducer, including impedance Z and phase angle ϕ variation in relation to its working frequency.

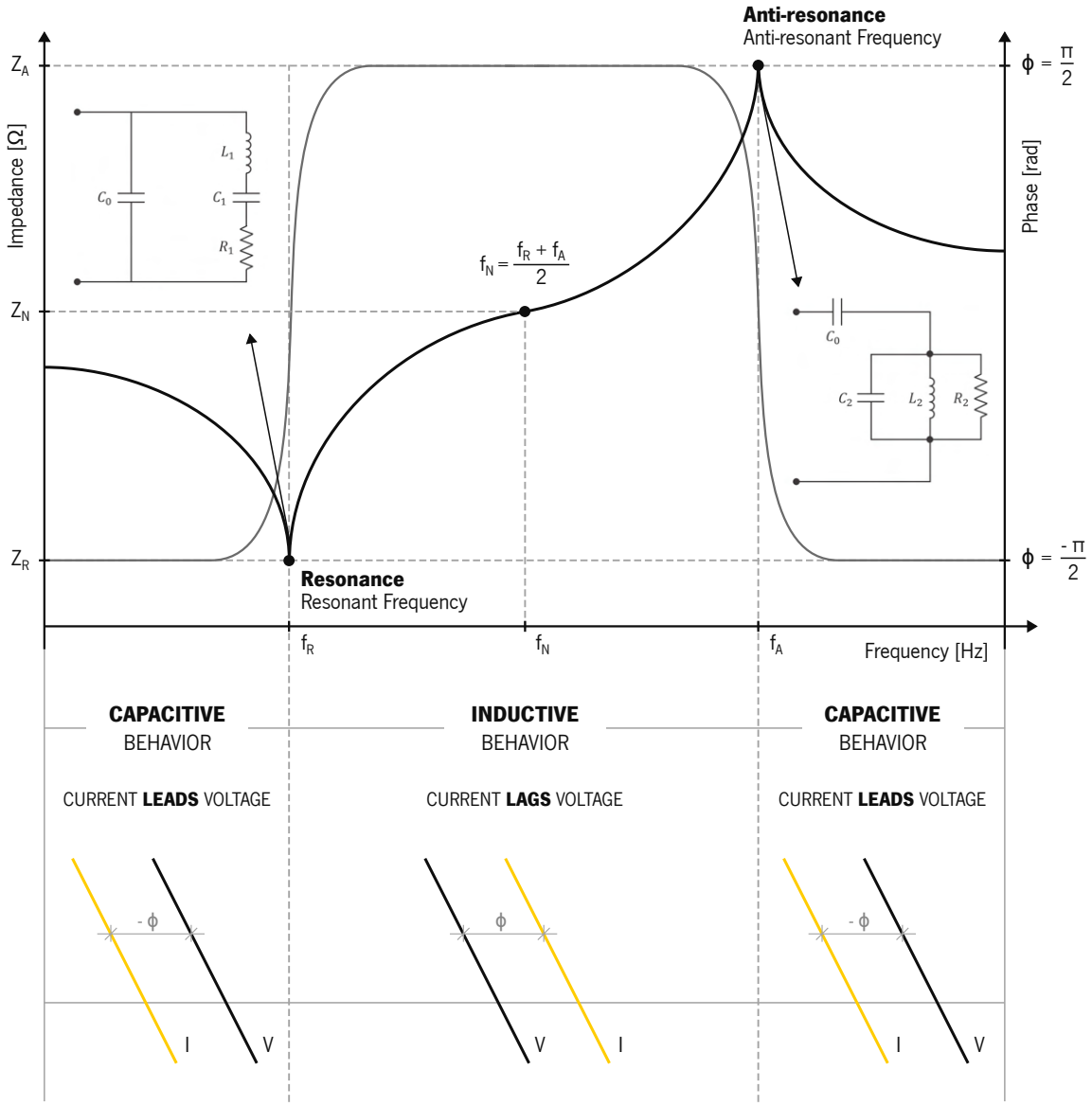

Figure 43: Technical summary of a PZT transducer's operation: frequency, impedance, and phase.

The transducer is then naturally designed to work within the inductive interval, where its energy efficiency is maximum. Outside of this range, issues start to appear in the form of heat (reactive energy), consequently leading to system failure, as current needs to flow for voltage to be established.

Note that, however, applied current intensity and voltage are fundamentally regulated at the ultrasonic generator, and the force that the transducer will output is controlled by the input power [3].

The phase angle ϕ variation is attributed to the transitions between capacitive and inductive behaviors of the transducer. Transition nodes are coincident with the resonance and anti-resonance frequencies, f_R and f_A, each one associated with a specific BVD circuit.

While, in theory, a system would perform best at the analyzed resonant frequency f_R, given the maximum output force (and consequent maximum vibration amplitude), a small frequency deviation could cause the transducer to operate in its capacitive zone, which would prove fatal for the system.

Hence, the optimal working frequency area for the transducer is shown in Figure 44, with the red and green colors indicating the least and most favorable scenarios, respectively.

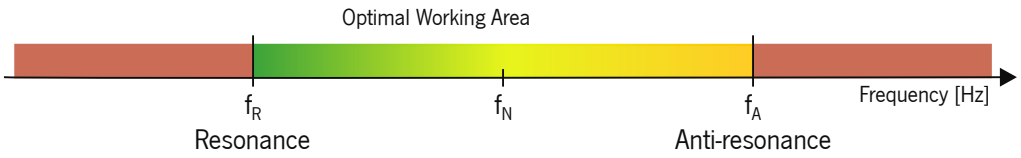

Figure 44: Color scale of a PZT transducer's optimal working area.

To ensure optimal performance, the system needs to be tuned so that its eigenfrequency coincides with the transducer's inductive zone while approaching resonance for amplified vibration efficiency.

2.1.4.3 Sonotrode Considerations

There is a great deviation in the UAM field regarding the designation of the vibration-amplifying components and consequent cutting tool assembly. Such ambiguity must be clarified. Nevertheless, a prior understanding of certain concepts is necessary.

Maximum vibration amplitude values will vary harmonically depending on the direction in which the oscillation is applied, system geometry, and consequent energy absorption. In 1D ATS type systems, said variation will also occur in the axial direction.

The resulting harmonic profile will be determined by the location of the nodal points (nodes and antinodes), corresponding to minimum and maximum displacements, respectively. These will essentially determine how much energy is absorbed by the system or transferred to the tool.

A general representation of the variation profile with nodal point locations is present in Figure 45. Harmonic wavelength is represented by λ, which is essentially the same as period T.

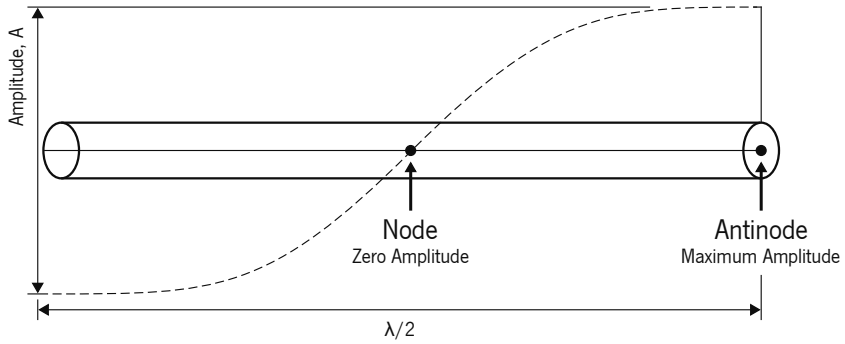

Figure 45: Schematic representation of nodes and antinodes.

The transducer's piezoelectric membranes will coincide with the location of a node. Thus, at this point, there will theoretically be no displacement in working conditions [3, 5]. As a consequence, amplitude values at the face of a transducer are insufficient to achieve reasonable cutting rates, stating the need for an amplifying component to be designed [14].

Oscillations produced by the transducer are directly transferred to an adjacent component known as a booster. The amplified wave is then transferred to the sonotrode (alternatively known as a horn), which acts as the tool holder, driven by the booster. Using a booster component may not be a necessity depending on the required application. In some cases, the sonotrode is designed to comprise the booster's effect.

While component length will determine the frequency of said profile, the change in oscillation amplitude will be determined by the variation of the specified component's outer diameter D. Maximum amplitude will be increased with a reduction in diameter, as shown in Figure 46.

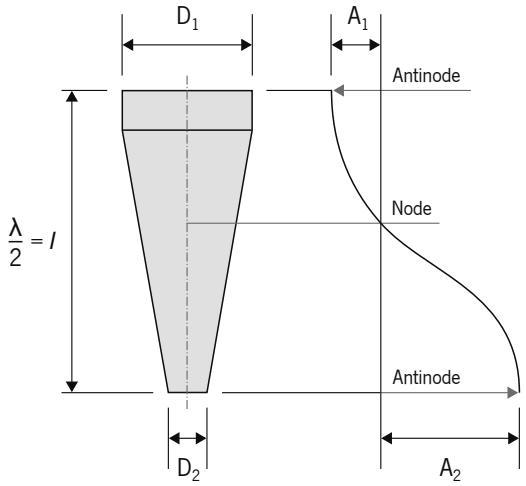

Figure 46: Sonotrode amplitude profile variation [3, 62].

Evidently, such design requirements are a consequence of the maximum desired vibration amplitude at the free end of the tool [14]. Accordingly, for desired results to be achieved, correct design and optimization of the sonotrode is a critical demand, taking both wavelength λ and outer diameter D into consideration.

The increased importance of this component in the development of UAM systems has led to the conduction of intensive research over the years, ultimately resulting in the creation of generic theoretical sonotrode design guidelines, with relation to outer diameter reduction and overall sonotrode length. These are presented in Figure 47.

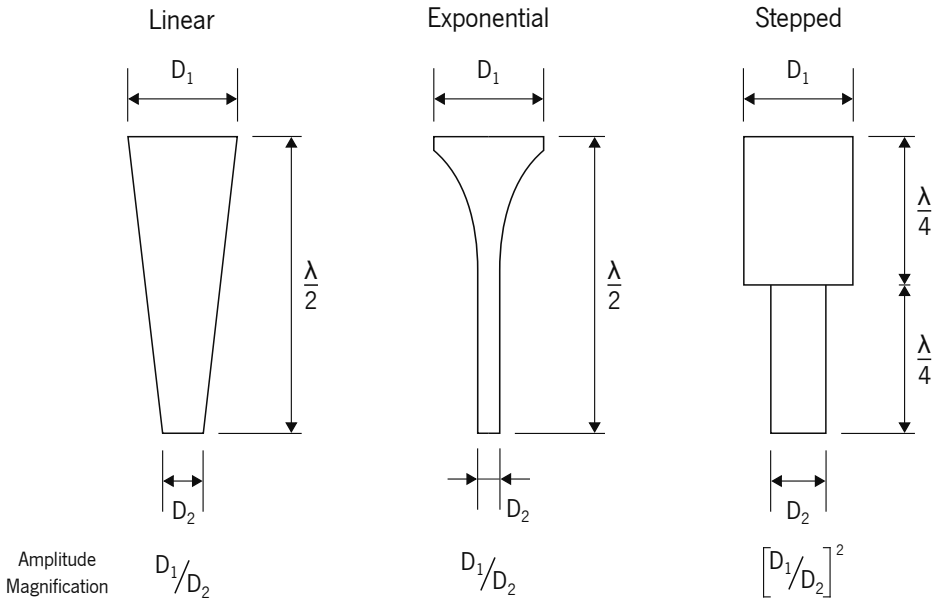

Figure 47: Theoretical sonotrode design guidelines [3].

Despite the importance of adhering to the discussed guidelines and considerations, sonotrode design will ultimately depend on the specific characteristics of each UAM system. Therefore, a thorough analysis should be conducted for each individual case to determine the most appropriate design. Moreover, material choice is also of great importance in sonotrode design, as good acoustic transmission properties and high fatigue resistance under working conditions are required [14].

One of the key aspects to be taken into consideration prior to the UAM system development is that the design will be fundamentally challenging due to hardware structures and PZT materials' capacity limitations [26]. Moreover, excessive amplitude values will result in increased internal stresses in both the tool and sonotrode, reducing their service life if the fatigue strength is surpassed [21].

3 UAM System Project

The development of new and improved machining systems is essential to meet the ever-increasing demand for high-quality products in the manufacturing industry. Concerning UAM, and given the technology's challenges and limitations, specifically regarding the milling operation, good practice should result from the analysis of previously developed systems, with the intent to optimize them.

Consequently, the basis for this work was an existing milling system with ultrasonic assistance, in which reverse engineering was employed as a key tool in its enhancement. The disassembly and rigorous examination of every involved component allowed for the identification of the system's shortcomings and limitations, revealing several key issues to be addressed for design optimization and performance improvement. As a result, reverse engineering leverage resulted in the development of a more effective and advanced UAM system for milling applications.

3.1 Existing System Analysis

The foundation for the improved system has been a project known as AdvUSMachining, developed by professors *Hélder Puga* and *Vítor Carneiro*, with the main objective to produce and implement a prototype of an ultrasonic assisted cutting tool, consisting in a 1D ATS UAM system, with vibration along the tool's axis. Figure 48 includes a representation of the presented system.

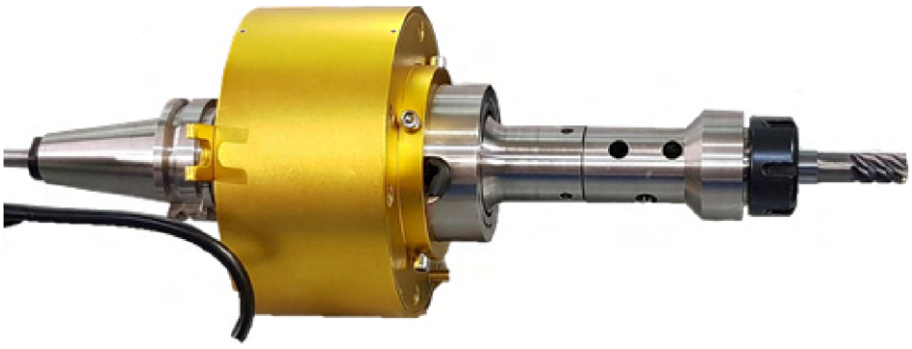

Figure 48: Developed AdvUSMachining system.

It's important to specify that the *AdvUSMachining* project was developed under the MAISTec initiative, a *"collective and integrated action to reinforce the transfer of scientific and technological knowledge"*, promoted by several recognized Portuguese scientific entities: SANJOTEC (Associação Científica e Tecnológica), ISQ (Instituto de Soldadura e Qualidade), UA (Universidade de Aveiro), and TECMINHO (Associaço Universidade-Empresa para o Desenvolvimento).

The presented system comprises a complete reimagination of a traditional tool holder, in which energy transmission from the ultrasonic generator occurs through a component known as a slipring. The harmonic wave is converted into mechanical vibrations by a PZT transducer, transferring them to the sonotrode, which includes a conventional collet chuck to hold the cutting tool.

A schematic representation of the system's constituting elements is shown in Figure 49.

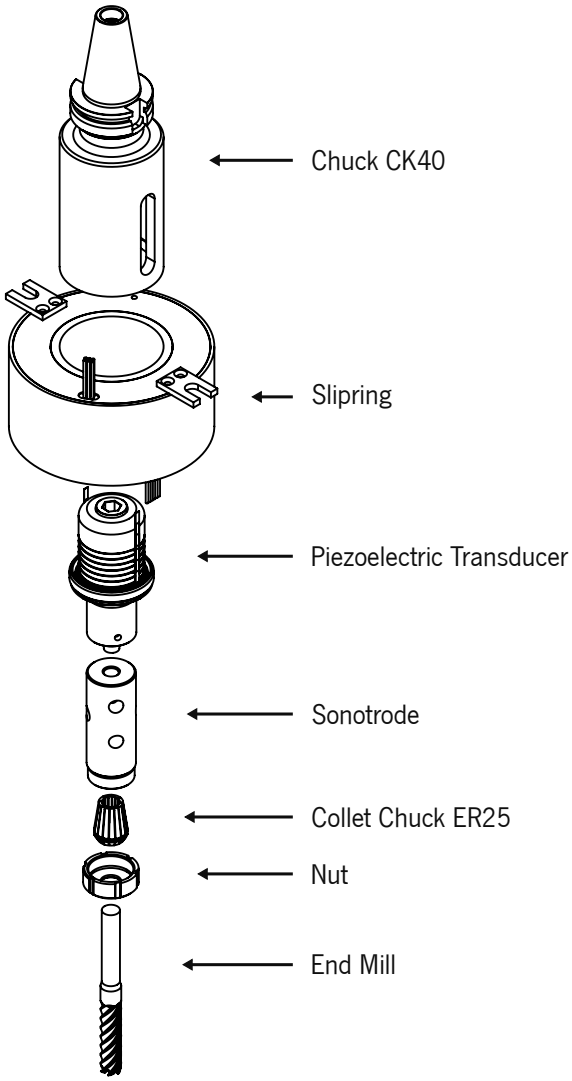

Figure 49: Components of the *AdvUSMachining* system.

A slipring consists of an electromechanical component that allows the conversion of the electrical power and signal from a stationary to a rotating component or system. In the analyzed case, it allows for the harmonic wave from the ultrasonic generator to be transferred to the piezoelectric transducer without causing cabling issues with spindle rotation. Evidently, this will be an essential mechanism for the system, given that the deformation only occurs when the piezoelectric crystals are electrically excited.

The working principle of this component derives from the two parts that constitute it: the stator (the exterior, stationary part, which will be connected to the generator) and the rotor (the interior, rotating part, which will be connected to the transducer). The electrical connection between both sections is ensured by a set of conductive rings.

A schematic representation of a generic slipring's working principle can be observed in Figure 50.

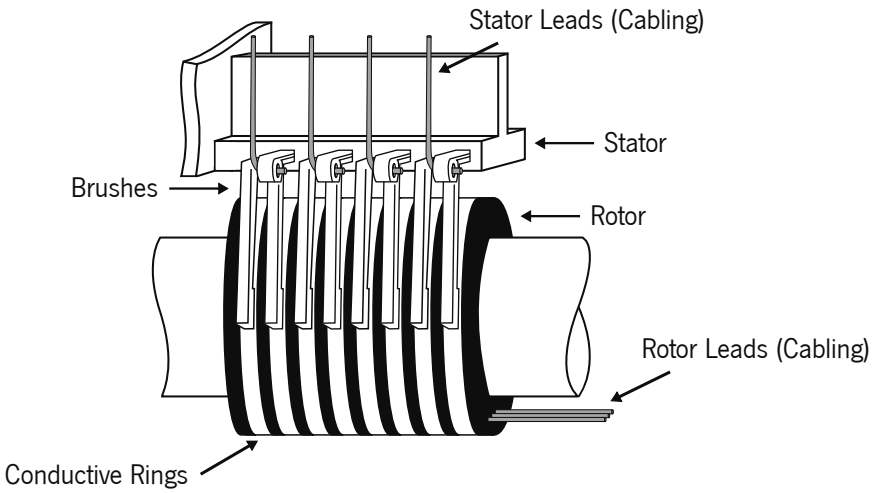

Figure 50: Schematic representation of a slipring's operating principle.

The rotor leads will, however, still need to be connected to the transducer. In this specific case, the cabling passes through a strategically cut side hole in the transducer's cover. As a result, the slipring and the rest of the system will rotate together. With regards to the PZT transducer itself, a commercially available model with general characteristics was used, comprising a nominal frequency value of 20 kHz.

The complete system assembly and the list of components involved can be examined in the system's technical drawing presented in Annex I. Geometrical aspects are also included.

Although project results demonstrated most of the already stated UAM benefits, such as improved surface and dimensional finish, diminished cutting forces, and reduced production time, some key issues were identified that severely hindered the system's performance.

3.1.1 Analyzed Issues and Key Parameters

Besides all the theoretical considerations on UAM system development presented in the previous chapter, with special attention to the fact that the system's eigenfrequency should coincide with the PZT transducer's optimal working frequency spectrum, there are other types of obstacles that only become apparent when a prototype for the system is fabricated.

For instance, a greater number of components within the system will lead to an increase in the number of connections between them, as well as an increase in the number of contact points. Therefore, it is imperative that all fastening joints in the ultrasonic system adhere to strict tolerances. Any deviation may result in localized heating when high-frequency values are achieved.

Undoubtedly, the most critical aspect to consider is the fixation of the tool, which has appeared to be an issue that limited the efficiency of the presented system given the utilization of a collet chuck holder, which essentially consists of a specialized type of clamp designed to have great versatility (being adaptable to more than one tool diameter), repeatability and accuracy, in gripping the cutting tool.

Figure 51 shows a general collet chuck holder.

Figure 51: General collet chuck holder [63].

Although one of the most widely used systems, collet chucks are unsuitable for UAM applications due to their intrinsic tool alignment issues, characteristic of the utilized clamp system. This will evidently cause nodal point variation. Moreover, since these are low-cost tool fixation systems, the materials used for their construction often lack high mechanical properties. Consequently, the contact zone between the collet and the cutting tool will heat up locally, softening the affected surfaces, gradually becoming more compliant, and absorbing more energy. Contact will be damped, causing a reduction in vibration frequency.

As noted in Subchapter 2.1.4.3, vibration amplitude is directly related to the variation in the outer diameter of the sonotrode. However, the significant difference in the external diameter of the system along its longitudinal axis poses an additional and noteworthy drawback.

The external diameter of the used slipring of 158 mm will force a reduction of approximately 76% relative to the outer diameter of the sonotrode, measuring only 38.1 mm. This exaggerated and sudden reduction ratio presents multiple potential issues for the system. Not only may it compromise system stability and consequently reduce its overall efficiency, but it may also lead to an over-amplification of vibrations, resulting in an increase in internal stresses and a reduction in the system's service life, as previously stated. Therefore, diameter uniformity is a crucial factor in ensuring the stability of the system.

Figure 52 shows a visual representation of the outer diameter reduction.

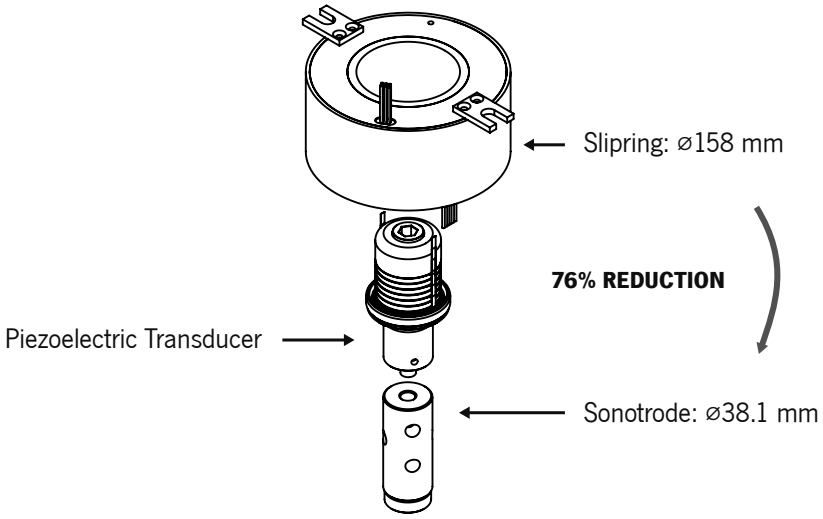

Figure 52: Outer diameter reduction in the *AdvUSMachining* system.

Furthermore, tool deflection must also be addressed. The intensity of the tool-workpiece contact will be amplified with the system's overall length, as torque τ is equal to the product between applied force F and the lever arm's length d, as per Equation 33.

$$\tau = F \cdot d \tag{33}$$

In this context, the lever refers to the distance between the zone where vibration is generated and the zone where the tool-workpiece contact occurs. The greater the distance, the greater the torque generated. However, longer overall system length, as well as longer tool shanks, can increase the likelihood of tool deflection beyond acceptable values, causing geometrical issues and potential accelerated tool wear.

In systems where the vibration and feeding directions coincide, the deflection will be further amplified with the ultrasonic vibration, regarding not only the length of the system but also the employed DOC. The latter should also not be neglected for axial vibrating 1D ATS systems, such as *AdvUSMachining*, as a greater DOC will intensify tool wear by abrasion due to the combined effect of oscillatory movement and friction between tool and workpiece surfaces.

Larger surface contact areas are also one of the reasons why the UAM technology is mainly used as a finishing operation. Increased DOC values will lead to augmented heat zones, specifically the three main deformation areas where heat is accumulated during the cutting process, Q_1, Q_2 and Q_3. Although, initially, this might seem as favorable for the cutting process, due to the localized increase in the workpiece's material ductility, the relative forces on the tool flanks will be intensified.

Since it is desirable to minimize deflection, UAM technology is not suitable for roughing passes, as larger contact surfaces will magnify tool deflection when in conjunction with ultrasonic vibration. Furthermore, special attention is required to the tool's length, which evidently must conform to the sonotrode guidelines presented in the previous chapter. This is important to ensure that the free end of the tool coincides with a nodal point, maximizing the efficiency of the system.

3.1.2 Proposed Solutions

One potential solution to the tool holder problem involves the use of a shrink-fit tool holder, which consists of a metal component that is heated to high temperatures using an induction coil, recurring to the material's thermal expansion for tool insertion. The material is then quickly cooled, causing thermal contraction and applying uniform pressure on the tool shank, creating a tight grip and providing a precise and uniform fixation [2].

Shrink-fit tool holders are known for their enhanced clamping forces and accuracy while having reduced undesired vibrations during machining. A holder of this type can be observed in Figure 53.

Figure 53: General shrink-fit holder [64].

A holder of this kind would provide several advantages for the developed UAM system. By being designed in conjunction with the sonotrode as the same piece, it would reduce the number of required components and minimize the number of joints and points of contact in the system. This would aid in system uniformity and stability, crucial for the precision and accuracy needs of the machining process.

Additionally, a shrink-fit holder would provide excellent clamping force and rigidity due to the tight fit between the holder and the tool shank, which would ensure efficient transmission of ultrasonic vibration to the cutting tool. Furthermore, its characteristic high accuracy and repeatability would be essential in achieving consistent machining results.

However, it is important to note that there are inherent limitations with these types of holders, being a significantly more expensive alternative than, for example, the previously used collet chuck, given their required material's superior mechanical properties. Moreover, specialized equipment is needed for the heating process, and each holder is designed to fit a specific tool diameter, as strict dimensional and tolerance requirements must be followed to ensure proper tool fixation. Nonetheless, despite its higher associated cost, the acquired benefits would greatly outweigh the limitations.

Optimizing the external diameter of the developed UAM system is crucial to ensure maximum system standardization. One possible solution would be to reimagine the energy transmission system, possibly involving the utilization of a smaller or different kind of slipring that would allow for a more compact design.

Limiting outer diameter reduction from this component to the sonotrode would greatly improve system stability and maximize efficiency. Additionally, the system design would need to be updated to incorporate the newly introduced component, which could include adjustments to the placement and positioning of various elements in the system.

Minimizing system deflection is also crucial in achieving maximum system efficiency and should therefore be taken into account. The length of the tool must be carefully selected while considering the overall length of the system, which is intrinsic because of the number of components needed for the application of ultrasonic vibration. The objective is to ensure that the tool is as short as possible while still being long enough to be capable of performing the desired machining operation.

In addition, it is essential to follow the suggested sonotrode guidelines presented in the previous chapter to ensure that the tool is inserted into the holder in such a way that the free end of the tool coincides with a nodal point. By decreasing the tool's length and ensuring that it is inserted into the holder correctly, its deflection can be significantly controlled.

A summary of analyzed key issues and respective proposed solutions can be observed in Table 3.

Table 3: Analyzed key issues and proposed solutions regarding the *AdvUSMachining* system.

Issue	Cause	Proposed Solution
Localized heating	Inadequate tool holder	Tool holder reimagination
Lack of system stability	External diameter inconsistency	Diameter ratio standardization
System deflection	Extended overall length	Tool length regulation

3.2 System Development and Optimization

The reverse engineering process applied to the existing UAM system has provided the foundation for the development of an improved and optimized design. By thoroughly examining and analyzing the system's components, key parameters, and associated issues, the updated model has been developed to address and mitigate these factors, ensuring that every critical aspect has been considered in its creation, resulting in a more efficient and effective UAM system.

Figure 54 shows a diagram of the parameters used in the project of the updated UAM system.

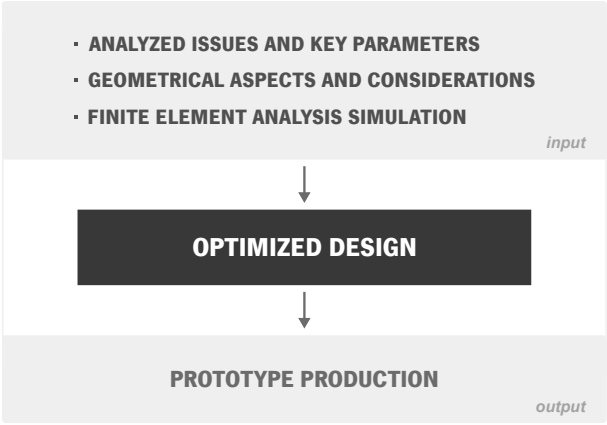

Figure 54: Outer diameter ratio in the *AdvUSMachining* system.

The core of the project development was to take the obstacles presented and introduce them as input for the CAD design of a new initial prototype, carried out using the 3D CAD software *Solidworks*. However, some information for the complete development of the prototype needed to be obtained, such as identifying the system's eigenfrequencies and plotting the referring impedance curve to ensure that the transducer would produce vibration within its optimal working spectrum.

A side-by-side development was conducted regarding the simulation of some components, such as the sonotrode configuration and consequent tool insertion, through Finite Element Analysis (FEA). The comprehensive data obtained through simulation proved to be vital in achieving the final 3D prototype, which enabled subsequent part manufacturing and system assembly while allowing the identification and mitigation of potential design flaws. Overall, the project's development involved a highly integrated and iterative process that required careful consideration of multiple factors.

The discussion shall begin with an assessment of the energy transmission system and its geometrical implementation. An in-depth analysis of the remaining components will follow, including the PZT transducer, the shrink-fit tool holder, and the cutting tool itself. Finally, an overall view of the updated design is presented, ensuring that the system is fully optimized.

3.2.1 Energy Transmission System

The utilization of a component such as a slipring has proven to be the optimal choice for the energy transmission method in developed UAM system. Its geometry perfectly aligns with the expected assembly requirements, and its applicability is relatively straightforward. Additionally, this component can be easily obtained off the shelf, allowing the geometry of the system to be designed around it, consisting of a practical choice.

The primary challenge was to identify a slipring with a suitable size so that the system's outer diameter could be uniformed, diminishing the existing 76% reduction ratio between the slipring and the sonotrode, which must match the diameter of the PZT transducer.

As previously mentioned, a commercially available PZT transducer was used in the *AdvUSMachining* system, having general characteristics and a nominal frequency value of 20 kHz. The transducer can be observed in Figure 55, together with its CAD representation and constituting elements.

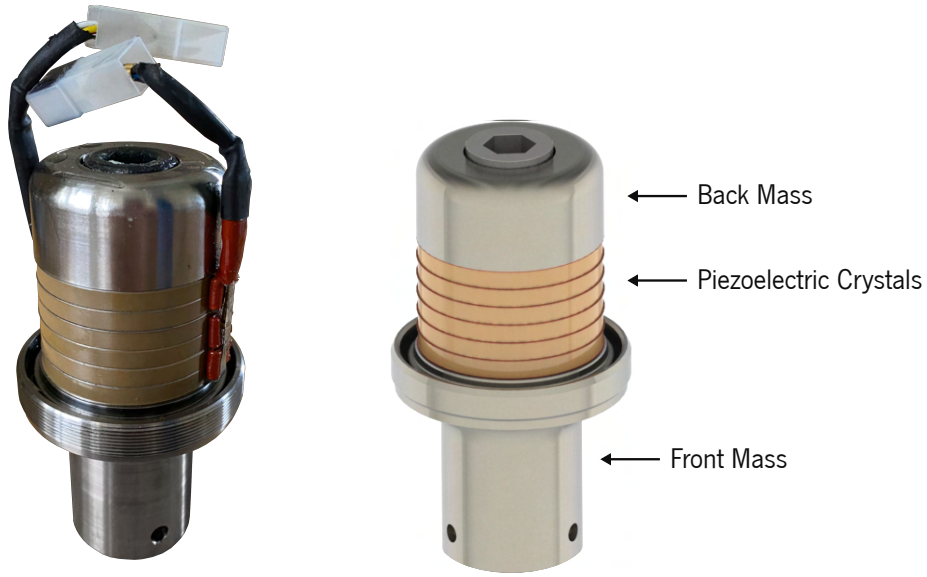

Figure 55: (a) Used PZT transducer; (b) Respective CAD model.

The delicate nature of the PZT crystals evidently requires an adequately designed casing for any component that comes into contact with the transducer, ensuring its optimal operation. Since the slipring was located over this casing in the previous ultrasonic machining system, the choice of this component was fundamentally limited to a geometry with a sufficiently large inner diameter to fit the transducer housing. Therefore, to achieve full optimization of the system's external diameter by selecting a smaller slipring, its application zone had to be reimagined.

Updating the slipring's location in the most plausible way would require the upper piece of the system to be completely redesigned, originally acting as both the spindle adapter and as the transducer's accommodation. A representation of this is shown in Figure 56, which consists of a section view of the system.

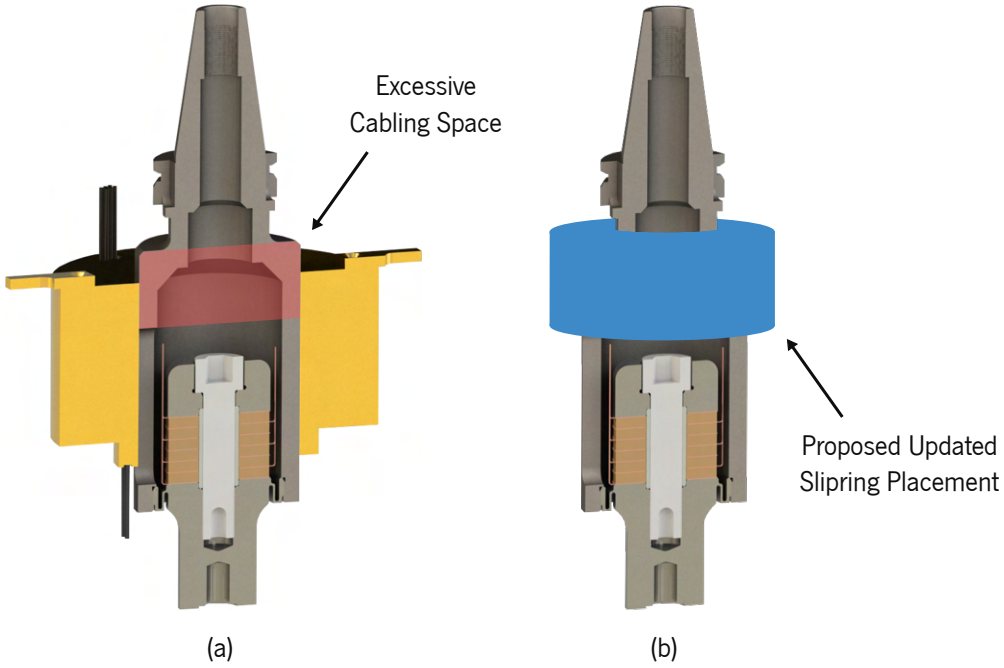

Figure 56: (a) Original slipring placement; (b) Proposed updated location.

Manifestly, the red area that was originally designated for the connection between the transducer and the slipring can be significantly minimized. This reduction will lead to a decrease in the outer diameter of the system's body, allowing for the application of a slipring with a smaller inner diameter.

Based on the information provided by slipring manufacturer *Senring Electronics*, one of the most renowned in the industry, the outer diameter of commercially available models can go as low as 86 mm, with an inner diameter of 40 mm. From now on, and for simplification purposes, the acronyms ID and OD will be used for the inner and outer diameters of the slipring, respectively.

The slipring coinciding with the dimensions presented above is referred to as *H4086* and consists of an excellent solution to enhance the uniformity and stability of the system considering the external diameter of the transducer's case of 80 mm. Nevertheless, decreasing the external diameter of the system's body in the analyzed area to properly accommodate the new model will impede the system's assembly due to the presence of larger diameters in the original upper piece, restricting the slipring's entry.

Thus, a potential solution to overcome this issue involves dividing the component into two separate pieces that can be connected by an internal thread passing through the slipring's aperture.

A representation of this is shown in Figure 57, along with the incorporation of the *H4086* slipring.

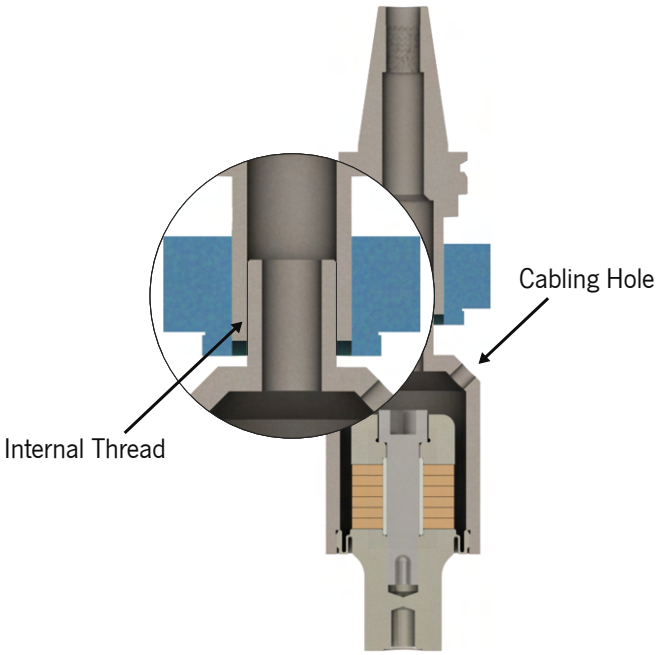

Figure 57: Upper chuck separation into two separate pieces.

In the updated version, system uniformity is granted by the smaller slipring while still comprising a hole in the transducer's accommodation destined for the cabling connection.

It is worth noting that the manufacturer provides two distinct versions of the *H4086* slipring regarding the type of involved electrical circuits. A two-circuit, 5 A slipring of this kind is referred to as *H4086-02S*, while a two-circuit version of 10 A is called *H4086-0210*. As a result of the nature of the transducer used, the latter is required for optimum operation. In addition, it is important to mention that extensive research has been conducted on various slipring manufacturers. However, none of the identified slipring models, besides one presented by *Senring*, met the necessary requirements for the UAM system. Therefore, this was the chosen model for the project.

Table 4 summarizes the selected slipring model's characteristics.

Table 4: Characteristics of the selected slipring [65].

Manufacturer	*Senring Electronics*	
Model	H4086-0210	
Circuit type	2 circuits, 10 A	
Dimensions $[mm]$	ID	40
	OD	86
	Length	32

The slipring was thus acquired from the manufacturer and is shown in Figure 58.

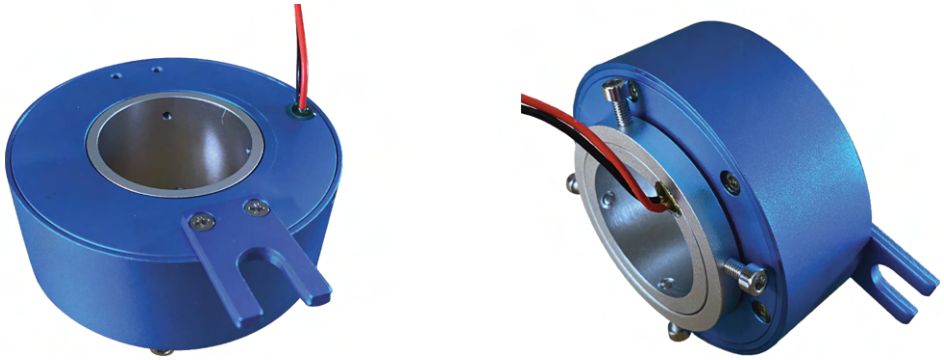

(a) Top View (Stator Cabling) (b) Bottom View (Rotor Cabling)

Figure 58: Acquired slipring, *Senring*'s *H4086-0210* model.

The orientation of the above-presented views has been chosen to align with the desired electrical connections for the system. Specifically, the stator cabling is intended to be connected to the ultrasonic generator, while the rotor cabling is intended to be connected to the transducer through the designed hole illustrated in Figure 57.

Notwithstanding, the redesign of the upper area of the system is not yet complete, as some technical considerations remain with the introduction of the internal screw thread. The nominal diameter selected for the thread was 30 mm, with a pitch of 2.0 mm, resulting in the *M30x2.0* thread designation. Evidently, some geometrical adjustments were necessary to facilitate the correct machining of the thread and to ensure proper assembly.

In addition, to ensure proper fixation of the two separate parts of the chuck in the high-speed rotating system, the transducer's case was modified to include three equidistant stud bolts in the perpendicular plane to the above-described thread, serving to enhance the overall stability and reliability of the assembly.

As a result, raised flaps were designed to accommodate these components. The decision to use flaps instead of a complete raised brim was due to the limited space available for the rotor cabling, as illustrated in Figure 58 (b). Thus, the flaps were strategically positioned to balance the system in accordance with the three employed bolts.

Despite involving meticulous consideration of various technical factors, which required a time-consuming and challenging process of creative thinking, the design process for the slipring's relocation has resulted in a highly refined and robust alternative that delivers enhanced fixation and reliability while ultimately making the assembly vastly more compact to meet requirements for system uniformity and maximum optimization.

The 3D CAD model of the redesigned components can be seen in Figure 59.

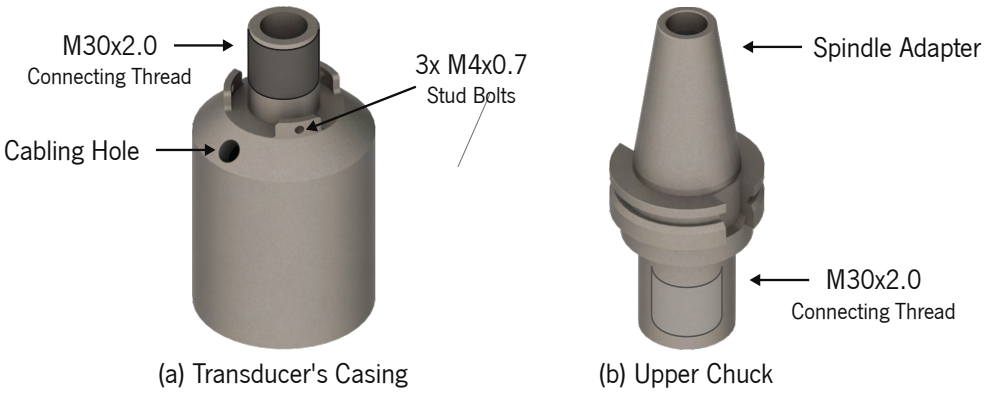

Figure 59: Redesigned components for slipring relocation.

Clearly, a better understanding of the redesigned area can be gained by analyzing the corresponding technical drawings of the individual components. To this end, the slipring's datasheet and technical drawings for the transducer's case and upper chuck are provided in Annexes II, III, and IV, respectively.

Moreover, an analysis of the updated diameter reduction ratio was also performed to further exhibit the stability achieved compared to the original system. Figure 60 shows the updated diameter ratio between the selected slipring and the front mass of the transducer, which coincides with the outer diameter of the originally used sonotrode. This analysis provides valuable insight into the effectiveness of the redesign.

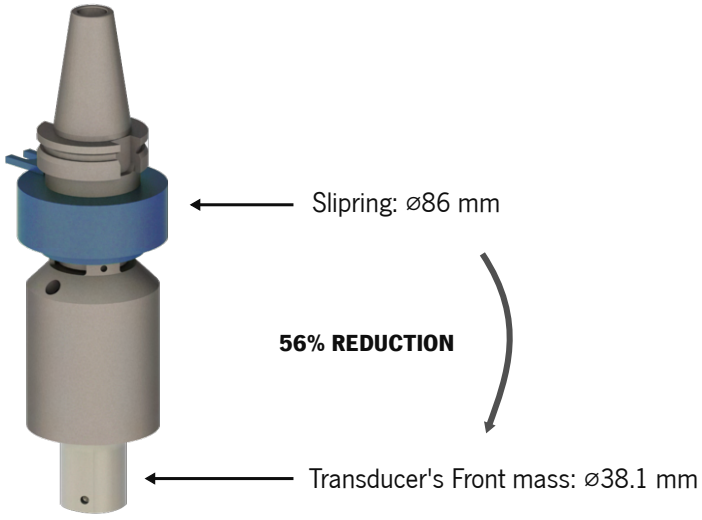

Figure 60: Updated external diameter reduction.

As illustrated, the updated model has led to a significant reduction in the original ratio, decreasing from 76 % to 56 %, while further minimizing the sudden reduction due to the updated geometry in the transducer's accommodation, resulting in a more gradual and less noticeable reduction.

3.2.2 Modal Analysis for Sonotrode Configuration

The correct optimization of the sonotrode is essential to include a different type of tool fixation while ensuring that the vibration produced by the PZT transducer is transferred as desired. As suggested in 3.1.2, a shrink-fit holding system would ultimately be an excellent alternative for this matter, as it would purposely solve the great issue of localized heating in the tool's fixation area, causing the efficiency of the original system to be immensely compromised. Accordingly, and given that the acquired benefits of this method severely outweigh its drawbacks, this was the approach chosen for the updated UAM system.

By designing the sonotrode and tool holder as a single component without the need for a booster, system uniformization could be achieved while minimizing the number of components and connections potentially causing efficiency losses. To ensure optimal amplitude control, theoretical sonotrode guidelines were also taken into consideration. Ultimately, the redesigned component must provide accurate and consistent tool fixation while ensuring maximum efficiency in transferring vibration to the cutting tool. Hence, simulation has proven to be a large part of the overall system's design.

As mentioned in Chapter 1, computational methods play a crucial role in simulating projected systems, eliminating the need for building numerous prototypes, and one of the commonly employed tools is FEA which, as the name suggests, involves dividing the geometry of the component being simulated into a mesh of finite elements with smaller volumes to calculate their respective loads, because it is computationally easier to solve many simpler problems with well-defined geometries than to solve one complex problem with a more intricate geometry. The resulting simulation is constructed from each element's study.

The analysis shall focus on three different studies. The first two are iterative and will facilitate the development of the optimized geometry. Firstly, the eigenfrequency of the vibrating assembly along the required direction needs to be calculated, along with the amplitude's profile from the PZT crystals to the edge of the cutting tool. Second, the system's impedance graph must be plotted to ensure that the obtained eigenfrequency belongs to the optimal spectrum of the transducer's working frequency. Finally, upon obtaining the optimized sonotrode geometry, a thermal study must be performed to simulate the material's expansion for cutting tool insertion.

For the purpose of conducting said simulations, the selected software was *COMSOL Multiphysics*, which is a widely used tool for diverse engineering applications. An initial sonotrode 3D model was designed to start the iterative process. Analyzing the transducer's front mass, with an already presented outer diameter of 38.1 mm, it was evident that this would coincide with the sonotrode's upper area.

The lower part demanded greater attention to detail. A tool needed to be selected as each shrink-fit holder is specifically designed for a required diameter. After careful consideration, it was decided that the system would be developed around a 10 mm, 4-blade end mill for both availability and versatility reasons.

The sonotrode was then designed based on the generic geometric guidelines of the tool holder manufacturer *HAIMER*. The specific chosen model was *Power Mini Shrink Chuck*, selected considering parameters such as maximum spindle velocity, clamping range, tool change time, and required maintenance, and its technical drawing is represented in Figure 61.

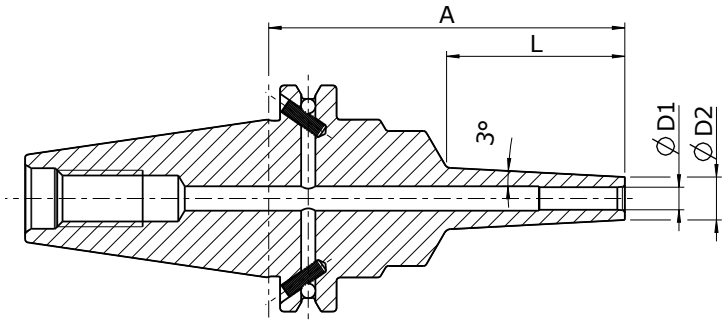

Figure 61: *HAIMER*'s *Power Mini Shrink Chuck* holder [66].

Although the final design would ultimately be determined by the simulation results, the geometric characteristics of this model were used as a starting point to develop the optimized component.

An initially stepped sonotrode/shrink-fit holder was respectively designed and is shown in Figure 62.

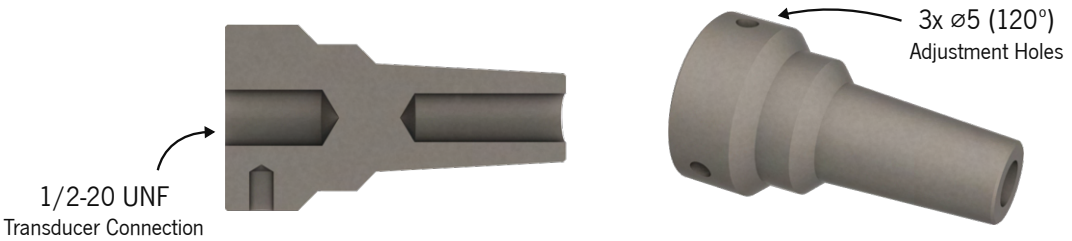

(a) Section View (b) Perspective View

Figure 62: Initially designed sonotrode/shrink-fit holder.

The designed component geometry bears a striking resemblance to the presented basis model. Nonetheless, some adjustments were necessary to make it suitable for the specific application. A hole was added to the location where it is supposed to connect with the transducer's front mass, complete with an internal thread that replicates the one present in the transducer. The purpose of this is to enable the connection between the two components through an internally positioned stud bolt.

Three additional adjustment holes were placed equidistantly around the same area, serving the purpose of securing the sonotrode/transducer link using a torque wrench, with a torque τ of 35 Nm, required for a stable connection during the system's operation. Otherwise, the rotation of the spindle could potentially cause component disassembly, resulting in tragic consequences. The technical drawing for the initial sonotrode design can be consulted in Annex V.

3.2.2.1 Simulation Parameterization

As with any engineering software, defining the problem prior to simulation is a critical step. Incorrect problem definition may result in simulation failure even before the simulation is executed. In this practical case study, several key aspects must be defined in *COMSOL*, including the geometry to be simulated, materials and their properties, types of mechanical and electrical connections, meshing options, the desired study and its own specific variables. It is essential to carefully consider and accurately specify these parameters to ensure a successful simulation process.

Defining the system geometry for simulation should be the initial step in variable definition. Although it may seem straightforward to consider the fully assembled UAM system, simplifying the analysis to the minimum necessary components is good practice due to the computational time and power required for such simulations. For eigenfrequency calculation and impedance plot determination, only the transducer, sonotrode, and cutting tool components are necessary, as the vibration is generated at the transducer and directly transferred to the tool. This focused subassembly enables efficient and accurate simulation without compromising results, reducing calculation time while retaining every essential data point.

Moreover, it is clear that a fully comprehensive study should incorporate the simulation of several tool lengths in order to select the most appropriate alternative when in conjunction with the optimized sonotrode configuration. Albeit, as the acquisition of the latter is already an extensive iterative process, it was decided that, for the scope of this thesis, the study would be restricted to a predefined tool length, as it is fundamentally simple to acquire a specific tool for the optimized system, as long as its desired dimensions belong in the range of the manufactured standards.

Several cutting tool catalogs were thoroughly researched to determine the most suitable tool length. Based on such information, 75 mm has been defined as the selected length, once again, for availability and versatility reasons. Accordingly, a tool with the specified dimensions was designed to be assembled into its respective location. Note that the tool's fillets were excluded for the purpose of simulation model simplification. The simulated geometry should then consist of the subassembly presented in Figure 63.

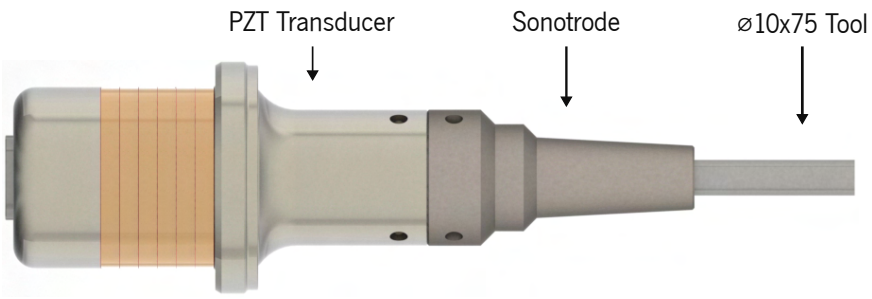

Figure 63: Considered simulation subassembly.

Subsequently, the materials of the imported geometry should be specified individually, including every constituent of the PZT transducer, the sonotrode/shrink-fit holder, and the cutting tool. Figure 64 provides a schematic diagram of the components, while Table 5 shows their corresponding selected materials.

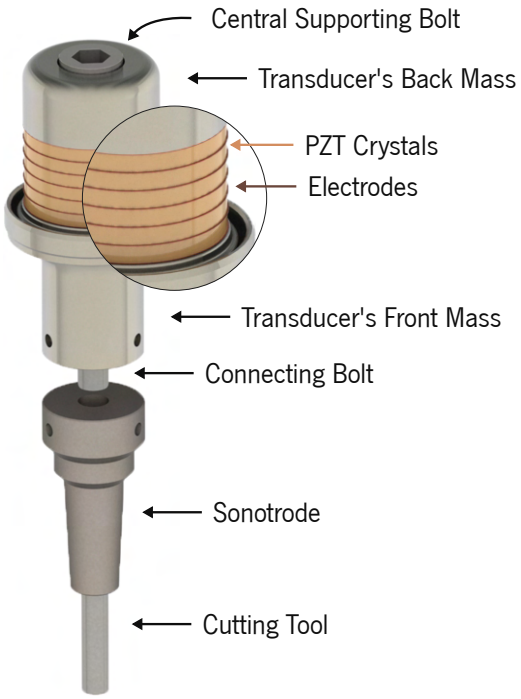

Figure 64: Specified components for material definition.

Table 5: Assigned materials to simulated components.

Material Assignation	
Central supporting bolt	AISI 1045
Transducer's back mass	AISI 316L
Piezoelectric crystals	Lead Zirconate Titanate
Electrodes	UNS C70600
Transducer's front mass	Ti6Al4V
Connecting bolt	AISI 1045
Sonotrode	AISI 316L
Cutting tool	AISI 1045

The optimal material choice for the sonotrode would be *Ti6Al4V*, coinciding with the transducer's front mass and contributing to system uniformity while being supported by a comprehensive analysis of commonly used materials in similar tool holders. However, given the potential cost savings associated with the use of an alternative material, the selection of *AISI 316L* was deemed appropriate once an optimized geometry was obtained. This decision balances performance, cost, and production considerations.

The next step in parameterization should be modeling the piezoelectric effect of the transducer in *COMSOL*, which can be done using its built-in physics modules *Solid Mechanics* and *Electrostatics*.

The *Solid Mechanics* module is responsible for computing various mechanical parameters, such as stress, strain, and displacement, based on Navier's equations. On the other hand, the *Electrostatics* module not only calculates the electrical and displacement fields but also determines the potential distribution under conditions where the electrical charge distribution is explicitly prescribed [3].

Accordingly, an equivalent electrical circuit is used by the software to describe the piezoelectric effect at the transducer. For this, however, the polarization direction of the PZT ceramics needs to be accurately defined, and respective voltage values for the electrodes between them as well.

The transducer under consideration consists of six PZT crystals that are arranged in a stacked configuration. Seven electrodes are incorporated into the design to facilitate the application of an electric field, strategically placed between the crystals to ensure effective and efficient operation.

Therefore, each crystal's own individual polarization direction should be defined, making sure that no two adjacent crystals comprise the same direction, as well as defining the terminal and ground electrodes. The two modules then need to be coupled, and the appropriate components need to be selected for the piezoelectric effect to be simulated. Figure 65 schematically represents these parameters.

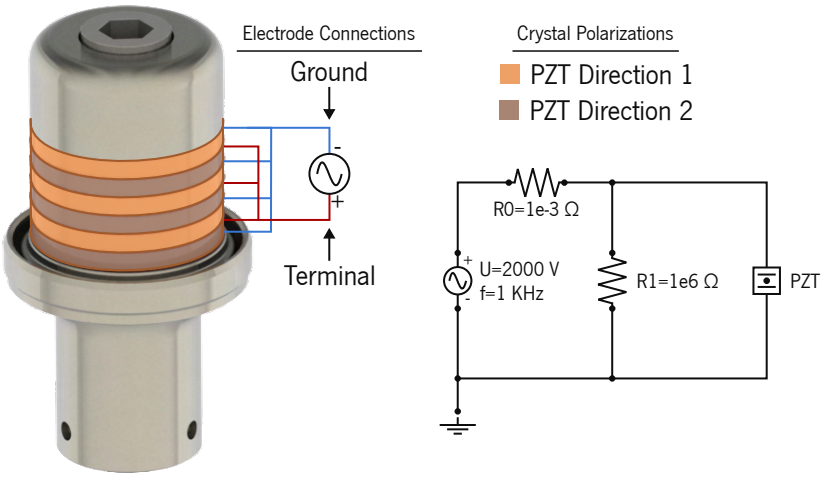

Figure 65: Polarization direction and electrode voltage definition; Respective equivalent electrical circuit.

After introducing these parameters into *COMSOL*, the final aspect to be addressed before defining the desired study is the used mesh and its respective settings. Prior to meshing, however, it is essential to eliminate any unnecessary edges created by the software, as these may sometimes be generated at smooth round surfaces, depending on the imported model. Failing to remove these redundant lines can result in inconsistent and unrealistic node formation, ultimately leading to inaccurate simulation results.

The type of mesh can be manually defined by the user, controlling parameters such as the number of elements, element type and size, among others, or, alternatively, automatically generated by the software. The selected option for the project was to use an automatically generated physics-controlled mesh, which consists of a type of meshing method that is tailored to a specific physical problem or set of equations.

The mesh is constructed based on the underlying physics of the problem being simulated and is designed to capture the relevant features of the solution accurately. Although generating a mesh with varying element size, the overall element scale can be selected from a specific set of 9 categories, ranging from *extremely fine* to *extremely coarse* and as shown in Figure 66.

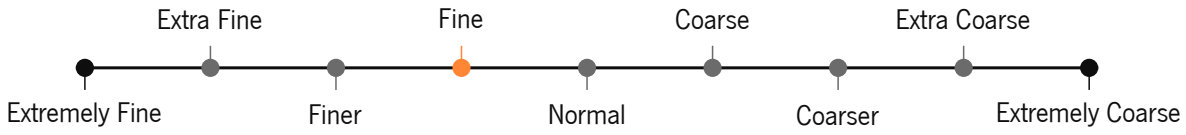

Figure 66: Levels of overall element size in a physics-controlled mesh.

For this specific case, it was determined that reducing the element size to categories below *fine* didn't have any significant benefits on the obtained simulation results. Therefore, this was the selected size.

3.2.2.2 Study 1 - Eigenfrequency

After ensuring that all parameters have been correctly established, the subsequent step in the analysis process is to define the desired study, along with its corresponding settings. The selection of the *Eigenfrequency* study type was based on the suggested options from the previously selected physics modules. The primary study configurations are presented in Table 6.

Table 6: Main selected settings for Study 1 - Eigenfrequency.

Study Settings	
Eigenfrequency solver	ARPACK
Desired number of eigenfrequencies	15
Search for eigenfrequencies around	20000 Hz

Physics and Variables Selection	
Physics Interface	*Discretization*
Solid Mechanics (solid)	Physics settings
Electrostatics (es)	Physics settings
Multiphysics Couplings	
Piezoelectric Effect (pze1)	

As with the previous parameterization, careful consideration and a thorough understanding of the physics and mathematical models involved is crucial for achieving accurate and meaningful results.

Additionally, it is necessary to specify which dimensions of the initially designed sonotrode will be adjusted in accordance to the obtained results. Three main dimensions were defined for this purpose, coinciding with the component's total length, the length of its base, and the depth of the hole destined for the tool, referring to *a*, *b*, and *c*, respectively. These can be observed in Figure 67.

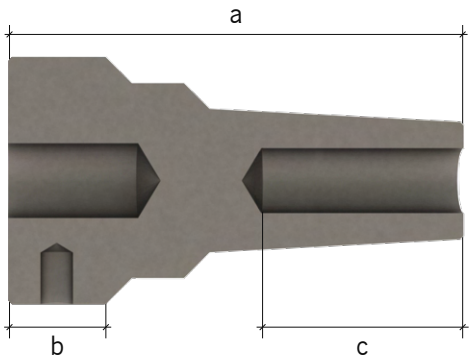

Figure 67: Dimensions of the initial design to be adjusted regarding the simulation results.

Each simulation generated 15 eigenfrequencies within a range centered on the nominal working frequency of the transducer, which was set at 20 kHz. The reference values for the variables *a*, *b*, and *c* were defined as 75, 15, and 30 mm, respectively. Thus, Figure 68 illustrates the eigenfrequency value obtained from the initial simulation, as well as the corresponding displacement profile.

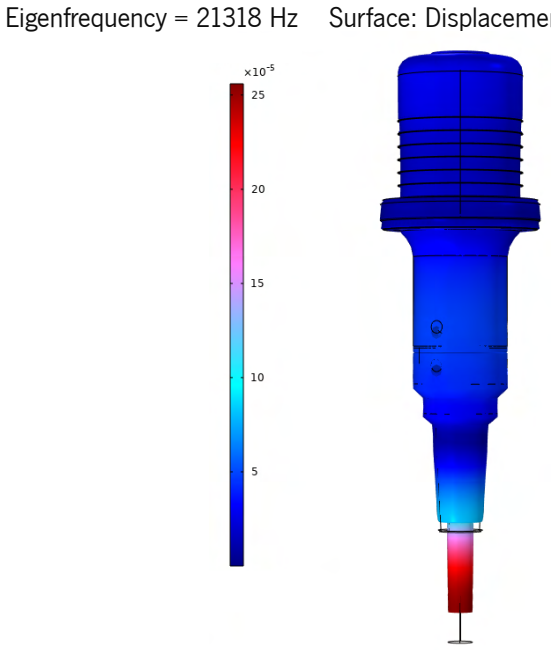

Figure 68: Output of initial frequency study for the proposed stepped sonotrode.

Note that, as already stated, a system may have multiple resonance frequencies depending on the system's several degrees of freedom, each of which affecting the generated vibrations in distinct ways. This is the reason why multiple eigenfrequency values were generated in each simulation. However, the current study only requires the specific frequency value that causes movement along the tool's axis.

As can be observed in the initial simulation, the obtained frequency of 21318 Hz isn't in accordance with the desired working frequency spectrum, as it is crucial to keep in mind that the system's eigenfrequency must be below 20 kHz so that the used transducer can work inductively. Therefore, the sonotrode must be adjusted so that its frequency at resonance decreases.

Several simulations were then performed so that a study was conducted on how the variation of each defined dimension affected the output eigenfrequency. Table 7 depicts the obtained results.

Table 7: Rundown of obtained eigenfrequencies for the stepped sonotrode design.

Simulation	a $[mm]$	b $[mm]$	c $[mm]$	Eigenfrequency $[Hz]$	Simulation Time
reference	75	15	30	21318	2'31"
1	70	15	30	21715	2'45"
2	80	15	30	20951	2'11"
3	75	10	30	21263	2'19"
4	75	20	30	21473	2'23"
5	75	15	25	20523	2'11"
6	75	15	35	22053	2'05"

The tabulated data can be systematically analyzed to ascertain the influence of the individual predefined parameters on the output resonance frequency. Each parameter was varied independently while keeping other dimensions constant. The reference model provided the fixed dimensions in each variation iteration. A plot regarding the variation of each parameter was accordingly drawn as presented in Figure 69. It appears that the total length is inversely proportional to the output frequency values, although parameters *b* and *c* seem to have a contrary effect.

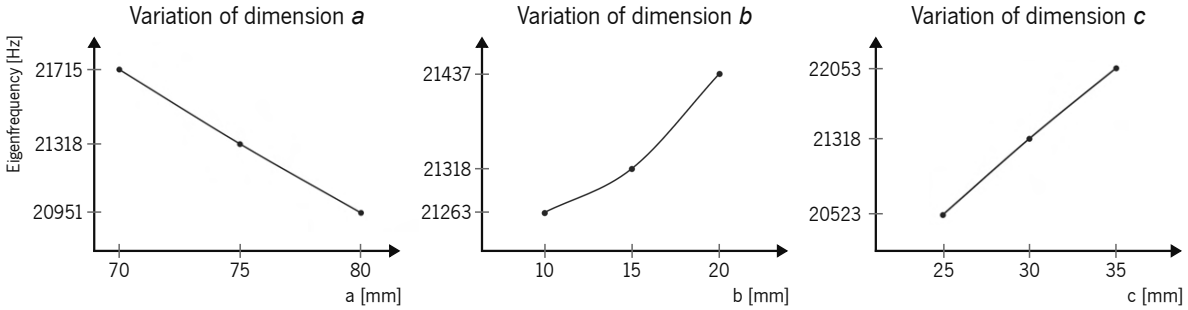

Figure 69: Influence of selected dimensions variation on frequency output (stepped design).

A cursory analysis of the simulation results reveals that the totality of the obtained frequency values is greater than the nominal working frequency of the transducer. As a result, none of the simulated geometries can be integrated into the UAM system without impeding its proper functioning. Furthermore, a comprehensive optimization of the model should also incorporate an investigation into how the dimensions of each step, as well as their respective angles, impact the simulation output. Hence, an alternative, simpler geometry for this component was designed, utilizing the exponential type outlined in the sonotrode guidelines presented in Subchapter 2.1.4.3.

The updated sonotrode design is presented in Figure 70. Similarly to the stepped configuration, the same three dimensions were also selected for analysis in this model.

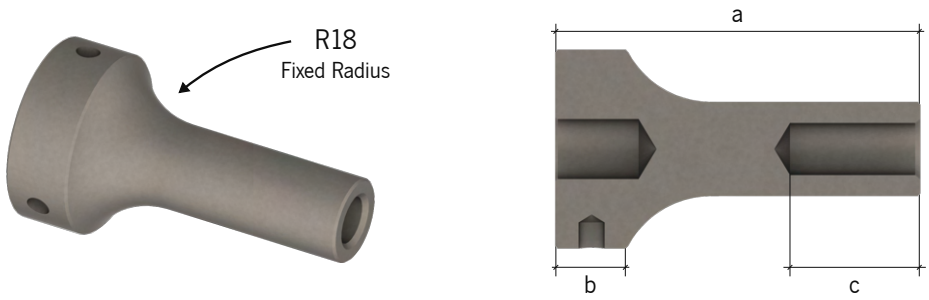

(a) Exponential Sonotrode Configuration (b) Selected Adjustable Dimensions

Figure 70: Influence of dimension variation on frequency output.

Fixing the radius of the fillet at the outset was determined to narrow the focus to the three selected dimensions, thus curtailing the length of the iterative process. The decision to set the radius value to 18 mm was based on visual inspection, resulting in an appealing geometry for the component.

The reference values for *a*, *b*, and *c* were defined as 70, 15, and 25 mm, respectively, based on the analyzed stepped approach resulting frequency trends. While reducing parameter *a* will shorten the overall length of the system, the resulting frequency increase must be compensated by reducing *c*. Nevertheless, Table 8 exhibits independent parameter influence for the exponential alternative.

Table 8: Rundown of obtained eigenfrequencies for the exponential sonotrode design.

Simulation	a [mm]	b [mm]	c [mm]	Eigenfrequency [Hz]	Simulation Time
reference	70	15	25	19764	3'55"
1	65	15	25	20093	3'02"
2	75	15	25	19481	3'52"
3	70	10	25	19985	3'07"
4	70	20	25	19800	2'58"
5	70	15	20	19263	2'41"
6	70	15	30	20297	2'41"

Likewise, the influence that the variation of each parameter has on the output frequency in the updated geometry can be examined in the respective plots presented in Figure 71.

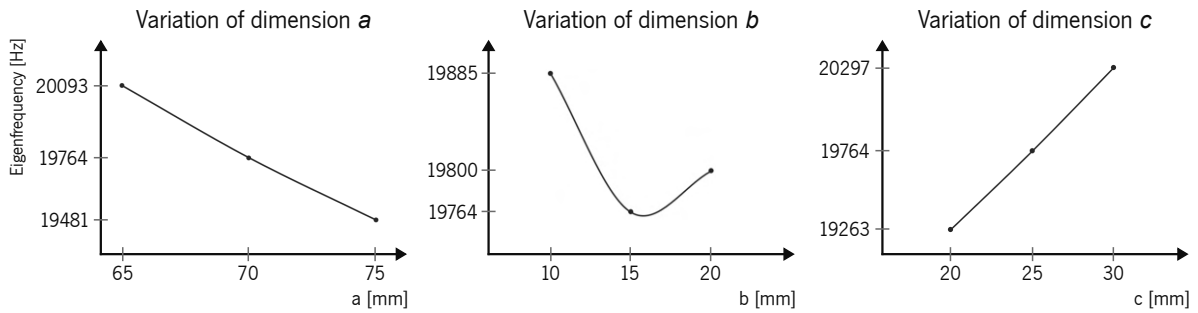

Figure 71: Influence of selected dimensions variation on frequency output (exponential design).

It is noteworthy that the obtained results for the variation of parameter *b* have exhibited inconsistencies, as the three conducted simulations did not provide sufficient data to establish a correlation. Albeit, parameter *a* appears to continue inversely proportional to the obtained eigenfrequency, while parameter *c* appears to maintain directly proportional.

The current design modifications have resulted in a reduction of the output eigenfrequency, which now falls within the optimal range for transducer operation. The initial simulation using the reference values for parameters *a*, *b*, and *c* yielded an output frequency of approximately 250 Hz below the nominal frequency of 20 kHz, which is deemed one of the most effective values of the analysis. However, any frequency within the range of 19.5 to 20 kHz would be considered as acceptable.

In light of these findings, the reference parameters were used as a starting point to make further design improvements, such as the elimination of sharp edges. The value of parameter *b* was also reduced, resulting in the final variables *a*, *b* and *c* with the corresponding values of 70, 14, and 25 mm, respectively.

The resulting optimized geometry can be observed in Figure 72.

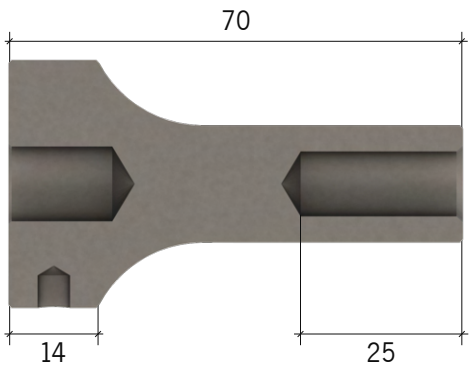

Figure 72: Updated geometry of the exponential sonotrode.

Figure 73 illustrates the obtained eigenfrequency value along with the displacement profile of the tool's axis during simulation. The technical drawing of the updated sonotrode can be consulted in Annex VI.

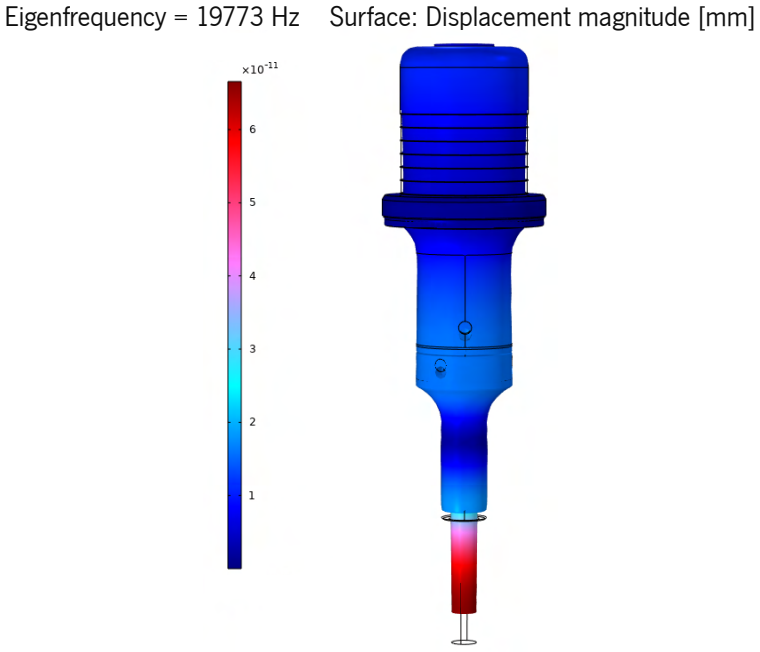

Figure 73: Output of final frequency study for the optimized exponential sonotrode.

Upon examining the presented profile, it is evident that maximum displacement occurs at the free end of the tool, as indicated by the red color. This implies that the vibration amplitude is at its highest at this point, being classified as an antinode, based on the schematic representation in Figure 46 of Subchapter 2.1.4.3. Conversely, a node can be observed just above the point of transition between the tool and the sonotrode, where displacement is at its lowest, indicated by the dark blue color.

While it can be asserted that a tool insertion depth of 25 mm may lead to inadequate fixation given the physical stresses associated with milling operations, this value corresponds to a shaft fixation of one-third compared to the tool's overall length, which is the minimum recommended length to ensure adequate stability. Therefore, it is expected that tool stability will not be compromised during finishing passes.

It should also be noted that the exponential geometry has achieved decreased eigenfrequencies while using a shorter overall sonotrode length in comparison to the stepped model. This represents another advantageous outcome of the updated design, as a reduction in the overall length of the system can consequently be achieved. Thus, taking all the analyzed factors into consideration, such as the advantageous and easy-to-fabricate geometry, the obtained eigenfrequency corresponding to the optimal operation of the transducer in question, and the favorable nodal analysis through the study of the tool's displacement profile, it can be concluded that sonotrode optimization has been effectively achieved.

3.2.2.3 Study 2 - Frequency Domain

The next stage of the research should focus on plotting the impedance curve of the system, aiming to validate the obtained sonotrode geometry. Impedance plotting is a crucial tool in maximizing system performance, as it is necessary to ensure that the attained eigenfrequency is within the optimal working range of the transducer's frequency spectrum, as shown in the guidelines presented in Figure 44.

Further, by plotting the impedance curve, it is possible to obtain important information regarding the energy transfer between the transducer and the applied load, as well as the overall efficiency and effectiveness of the system. This study ultimately aims to confirm that the designed sonotrode geometry will lead to a maximized system performance in terms of efficiency and effectiveness. Additionally, it is expected to provide valuable insight into the system's corresponding anti-resonance frequency.

A *Frequency Domain* study was then selected and defined in *COMSOL*. In similarity to the previous analysis, the desired study characteristics have also been organized and are presented in Table 9.

Table 9: Main selected settings for Study 2 - Frequency Domain.

Study Settings	
Frequency unit	Hz
Range of frequencies	19600 - 20400
Iteration step	10

Physics and Variables Selection	
Physics Interface	*Discretization*
Solid Mechanics (solid)	Physics settings
Electrostatics (es)	Physics settings
Multiphysics Couplings	
Piezoelectric Effect (pze1)	

The desired frequency range must be defined on the basis of the previously obtained eigenfrequency value. To ensure that the entirety of the transducer's inductive interval is captured in the plot, the starting value for the analyzed range should be below the system's resonant frequency, while the other end of the spectrum should be selected after the anti-resonant frequency. However, as the anti-resonant frequency has not yet been discovered, an assumption must be made on where the capacitive zone will start. Furthermore, selecting values outside of the transducer's working interval facilitates the analysis of the capacitive-inductive-capacitive regime changing points.

An iteration step of 10 Hz was chosen to achieve accurate results while not significantly impacting the simulation time, striking a balance between the curve's smoothness and computational efficiency.

The simulation was conducted and the resulting plot is depicted in Figure 74.

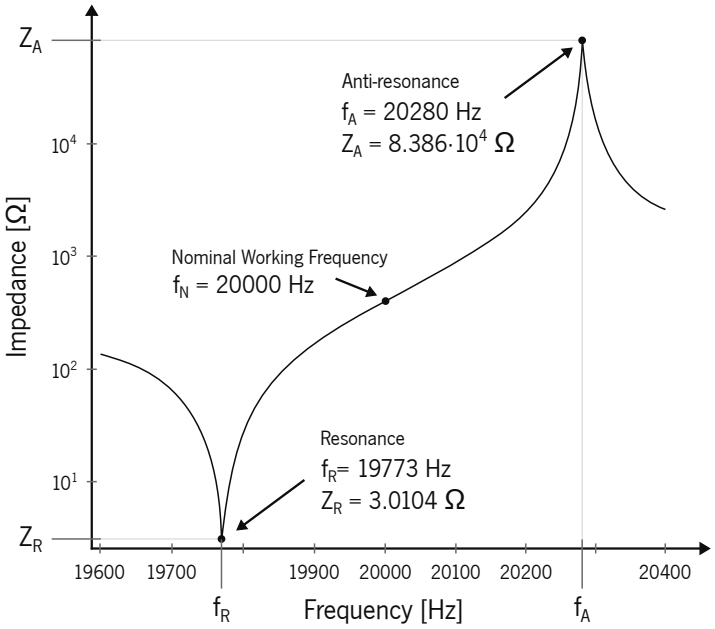

Figure 74: Impedance plot obtained through simulation.

The presented impedance curve shows the resonant frequency, anti-resonant frequency, and their corresponding impedance values. While the impedance values themselves do not carry great significance, they align with the expected minimum and maximum points on the system's characteristic curve.

The analysis concludes that the transducer's nominal frequency falls within the desired inductive area. The resonant frequency of 19773 Hz and anti-resonant frequency of 20280 Hz demonstrate a mean value of 20026.5 Hz, immensely close to the transducer's nominal frequency. While it can be stated that the system should operate closer to its resonant point, the presented curve corresponds to the optimal scenario, allowing for potential losses due to damping. Thus, even if the frequency value is slightly reduced from 20 kHz, there is a substantial gap until the resonant point, allowing proper functioning.

Regarding the simulation time, referring to 1 hour, 56 minutes, and 25 seconds, it was significantly higher than the values obtained for the *Eigenfrequency* study, as extensive computational power was required to simulate the operation of the system within the desired range for the selected reduced iteration step. However, this value is relatively small compared to typical simulations of practical scenarios.

In conclusion, the analysis indicates that the considered exponential sonotrode aligns well with the desired specifications. Moving forward, a thermal expansion study should be conducted, essential to ensure the efficient operation of the entire assembly, as any potential issues in the tool insertion process could compromise the integrity and performance of the system as a whole.

3.2.2.4 Study 3 - Thermal Expansion

While studies 1 and 2 were essential for optimizing the geometry of the sonotrode, the thermal expansion analysis of this component serves purely informative purposes by revealing its reaction to heat and allowing the tool's insertion. Notwithstanding, it constitutes a crucial aspect of the project's success.

During the inductive heating process for shrink-fit purposes, the tool holder is positioned within a coil through which an alternating current power supply is transmitted, producing a magnetic field that causes the component to heat and, consequently, to expand. This process is illustrated in Figure 75.

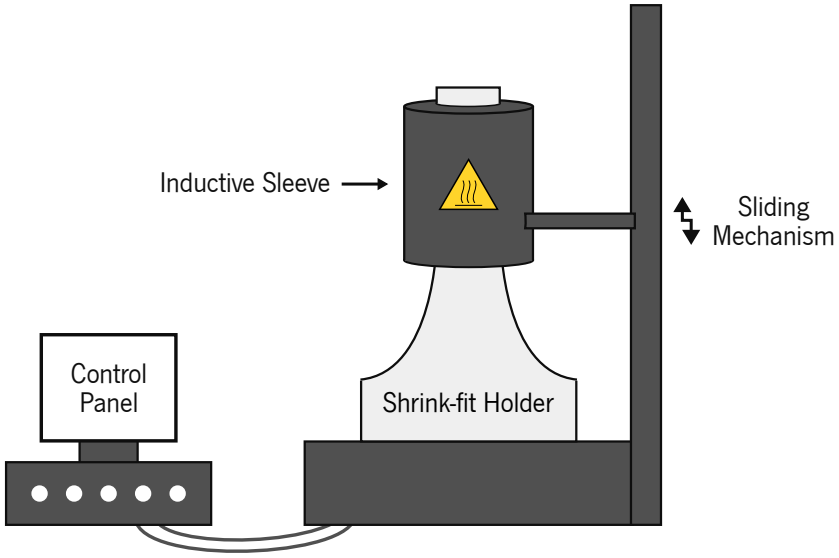

Figure 75: Representation of the inductive heating process.

The primary challenge of this study lies in developing a systematic approach to conducting the simulation, identifying relevant outputs, and performing a robust analysis. To address this challenge, a specific methodology was adopted, which involves selecting particular points on the component and monitoring their coordinates before and after the heat source is employed.

The selected points, denoted P_1 and P_2, belong to the edge of two circumferences drawn at the inner and outer extremities of the shaft hole, respectively. Their initial positions will be recorded based on the model's initial hole diameter, and their radial displacement will be tracked over time until reaching their final position after the heating process is complete.

The obtained displacement values will then be analyzed and, through simple mathematical operations, will allow for the determination of the expanded shaft hole's overall diameter. In addition, by analyzing the two limiting circumferences of the hole, the entire length of the tool's shaft was studied, ensuring that sufficient thermal expansion occurred to allow for the entire tool insertion.

Figure 76 schematically represents P_1 and P_2 and their specific positions within the component.

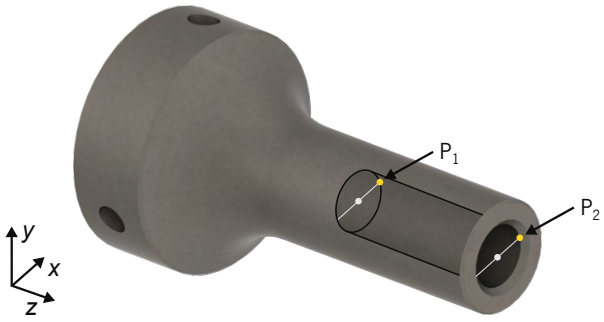

Figure 76: Schematic representation of the analyzed points.

The analysis should begin by selecting the appropriate study and defining the corresponding settings. For the study at hand, the *Solid Mechanics* module was used for displacement analysis, and *Heat Transfer in Solids* was used to simulate the effects of an external inductive heat source.

In *Solid Mechanics*, the parameters included material assignment and respective mechanical properties, potential initial displacement fields, and selection of free and constrained faces for boundary conditions. The material was specified as *AISI 316L*, as indicated in Table 5, and the solid model defined as isotropic. As the sonotrode will originally be in equilibrium, initial displacement fields are nonexistent.

To establish the boundary conditions, the face of the sonotrode intended to make direct contact with the transducer's front mass was constrained, while all remaining faces were left free to allow for expansion. The selection of the constrained face was informed by an analysis of the typical heating process used for shrink-fit tool holders, with the shaft's hole oriented upward.

Accordingly, the respected constrained face is depicted in Figure 77, represented by the yellow color.

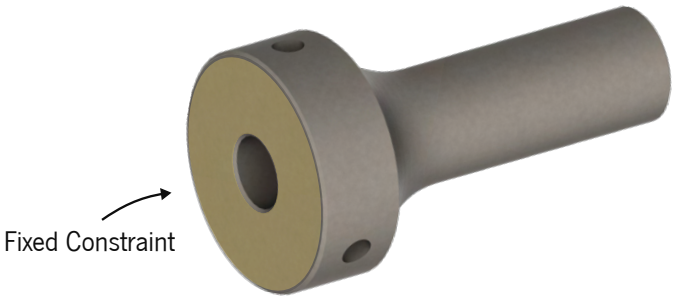

Figure 77: Boundary condition definition for the simulated component.

Regarding *Heat Transfer in Solids*, the main specified parameters were the initial temperature, corresponding to 293.15 K (20 $^{\circ}C$), the boundary heat source (referring to the outer faces of the model in which heat would be employed) and the heat rate, being defined by specifying an applied power.

In practical scenarios, the power output of inductive heat sources can vary significantly depending on the component to be heated, its dimensions and intended application, the specified material, and the type of induction system utilized. Typically, heating systems aim to attain and sustain a predetermined temperature over a specified duration, resulting in a wide range of output powers in the kilowatt range. Following extensive research, the simulation utilized an output power of 5 kW, a value frequently specified in inductive heating machine manufacturer datasheets.

Finally, having specified every parameter specified, a *Time-Dependent* study was selected, and its respective characteristics were also organized and presented in Table 10.

Table 10: Main selected settings for Study 3 - Time-Dependent Displacement.

Study Settings	
Time unit	s
Range of output times	0 - 30
Iteration step	0.01

Physics and Variables Selection	
Physics Interface	*Discretization*
Solid Mechanics (solid)	Physics settings
Heat Transfer in Solids (ht)	Physics settings

Although the simulation is ready to be run, a crucial aspect regarding the sonotrode's geometry needs to be addressed. Specifically, fit dimensioning at the holder/tool contact needs to be considered to ensure proper system assembly and functionality during machining.

To achieve a secure and problem-free connection, it is imperative that there is constant pressure between the fit surfaces. An interference fit is hence necessary. Based on a revision of existing literature, for shrink-fit applications, an S7/h6 shaft basis interference fit is recommended [67, 68]. Therefore, calculations were made to obtain the respective interference values, as shown in Figure 78.

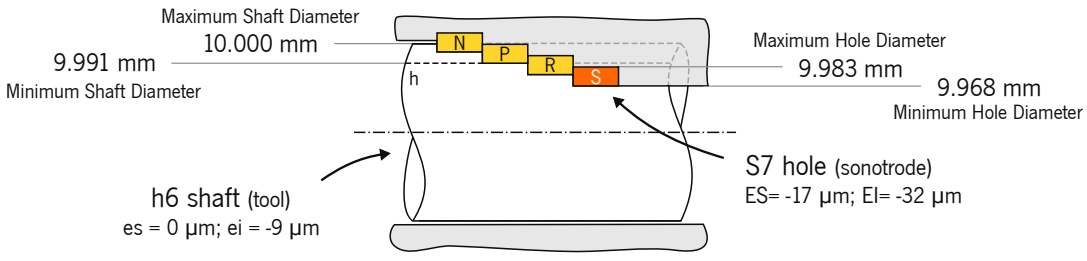

Figure 78: Selected S7/h6 interference fit specifications.

In the context of the thermal expansion study, it is essential to focus on the minimum diameter of the analyzed interference fit. This is because if the sonotrode expands enough to accommodate tool insertion with the minimum hole diameter, it can naturally accommodate the maximum possible hole diameter as well. Therefore, to ensure accurate simulation results, the imported model to the simulation software should have a hole diameter of 9.968 mm, and the focus of the study should be on determining the time required for the diameter to exceed the maximum possible diameter for the tool's shaft, 10 mm.

The simulation was conducted and point displacement was plotted, as illustrated in Figure 79.

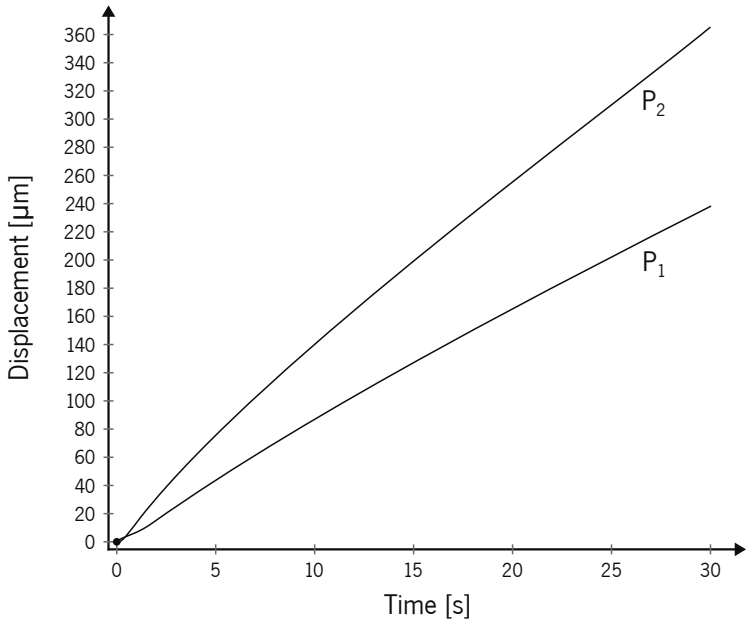

Figure 79: Point displacement plot obtained through simulation.

Upon initial observation, it is evident that the displacement value at P_2, corresponding to the hole's outer extremity, is greater than that at P_1 over the entire analyzed time range. This discrepancy was anticipated, given the distinct geometries of the component at the two corresponding locations. The region containing P_1 is significantly more constrained in comparison to the region encompassing P_2. However, a more comprehensive analysis of the displacement values is required.

By subtracting the minimum possible hole diameter, 9.968 mm, from the nominal diameter of the tool's shaft, 10 mm, and dividing the obtained value by 2 (since displacement acts as a function of the circumferences' radii), it is possible to obtain the minimum required displacement for tool insertion. Accordingly, the obtained value corresponds to 16 μm, as shown by variable δ_{min} in Equation 34.

$$\delta_{min} = \frac{(10 - 9.968) \cdot 10^3}{2} = 16 \quad [\mu m] \tag{34}$$

A detailed view of the first 10 seconds of the analyzed time range is provided in Figure 80.

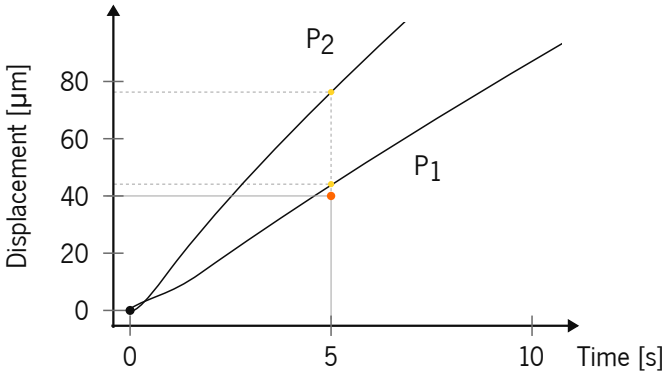

Figure 80: Detail of point displacement plot obtained through simulation.

As illustrated above, the displacement at both analyzed points increases to at least 40 μm after being heated for a mere 5 seconds. Thus, it can be inferred that a 5-second interval is more than sufficient for the sonotrode to expand adequately to allow for tool insertion.

Due to the significantly reduced time interval, the analysis did not proceed to calculate the exact time at which the minimum required displacement was reached, as it was considered unnecessary. It is important to note that, however, the stated conclusions for the study assume the use of a 5 kW induction coil.

Overall, it can be concluded that the sonotrode has been fully optimized, and it should be able to perform its intended function effectively and reliably.

3.2.3 Optimized Design

Having finished all three proposed simulations and obtaining the optimized geometry for the sonotrode/shrink-fit tool holder component, the system's efficiency is expected to be at its maximum potential. Thus, the system is deemed ready for production, subsequent assembly, and testing.

The significant changes of the updated system compared to the original *AdvUSMachining* design should be emphasized. Most notably, the optimized version is significantly more compact, being expected to greatly increase the efficiency of the tool's vibration with the applied harmonic load.

The external diameter ratio from the slipring to the sonotrode has been reduced from 76% to 56%, allowing a reduction from 158 mm to 86 mm in the system's maximum external diameter. Additionally, the overall system length has also been reduced from 500 mm to 417 mm, including the cutting tool.

Finally, the updated sonotrode doubles as a shrink-fit holder, considerably improving the tool fixation mechanism while reducing the number of involved components and enhancing system uniformity.

Figure 81 shows the system in its entirety, including an exploded view to allow clear visualization of every component involved. The corresponding technical drawing is presented in Annex VII.

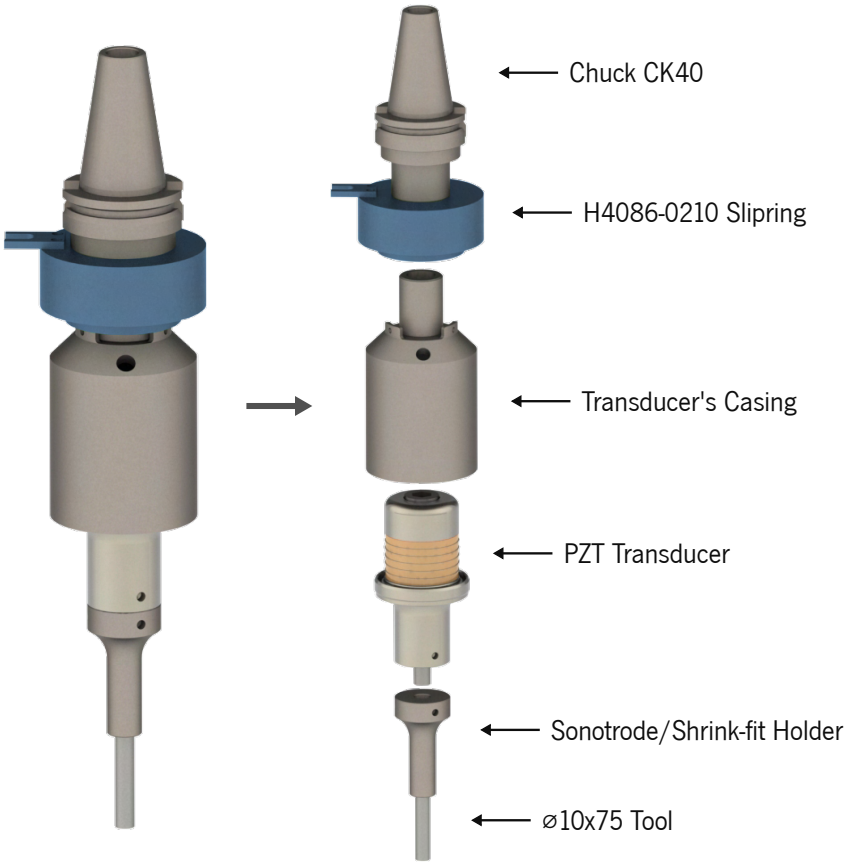

Figure 81: CAD representation of the assembled system.

3.3 Part Production and System Assembly

The final phase of the project involves the manufacturing of previously developed components and their subsequent assembly with the remaining system, including the PZT transducer, reutilized from the original system and the commercially acquired counterparts: slipring, cutting tool, and connecting bolts.

Despite the theoretical optimization of the system through the incorporation of innovative technologies such as ultrasonics into conventional milling processes and extensive iterative simulation, it would be incorrect to assume that the study is complete. Geometric or dimensional incompatibilities or assembly issues may still arise, potentially affecting the desired outcome and possibly rendering the system useless.

Thus, the proper development of a physical prototype is critical to complement the virtual alternative, even if the latter is numerically proven. In this regard, the first step of this phase should involve the organization of all involved components, along with their acquisition method.

For this, Table 11 was created.

Table 11: Rundown of the developed system's components and their respective origin.

Component	Origin / Acquisition method
Piezoelectric transducer	Reutilized from the original system
Slipring *(Senring H4086-0210)*	Commercially available
Cutting tool (4-blade end mill)	Commercially available
Connecting bolts	Commercially available
Chuck CK40	Needs to be manufactured
Transducer's casing	Needs to be manufactured
Sonotrode/Shrink-fit holder	Needs to be manufactured

After organizing all the required information, disassembling the original system, and acquiring all the necessary components, the production order was issued for the three respective components: the chuck, the transducer's casing, and the sonotrode. Every necessary machining operation was carried out by precision machining company *PropreciSion*. The selected material for both the chuck and the transducer's case was *AISI 304*, as was the case with the original *AdvUSMachining* system.

The production of the components was relatively straightforward due to the provided 3D CAD models, accompanied by their respective technical drawings. However, extra care was taken during the threading process to ensure that the assembly and proper functioning of the system would not be posteriorly compromised. Additionally, the desired S7 tolerance on the sonotrode/shrink-fit holder was carefully inspected to prevent any potential compromise of the subsequent tool fixation.

The machined components are depicted in Figure 82.

(a) Chuck CK40 (b) Transducer's Casing (c) Shrink-fit Holder

Figure 82: Machined components ready for assembly.

After production is finished and the components are ready, the thermal induction process should be performed, allowing for the cutting tool to be introduced into the machined sonotrode/shrink-fit holder. To perform the thermal induction process, a *START.2* model thermal induction machine from *Elco* manufacturer was utilized with the assistance of the metalworking company *Resultamper*. It is worth noting that although the technical specifications provided by the equipment manufacturer were thoroughly analyzed, no information regarding the power of the inductive coil was found.

Said equipment can be observed in Figure 83.

Figure 83: Utilized heat induction system, *Elco*'s model *START.2* [69].

As anticipated, the tool was successfully inserted into the sonotrode. Three heating cycles were performed consecutively, each lasting for two seconds. The intermittent heating was implemented to prevent potential material warping, which could have caused the system to be inoperable. Additionally, this method facilitated the proper insertion of the tool to the bottom.

Figure 84 illustrates the resulting subassembly of the two components.

Figure 84: Shrink-fit holder/cutting tool assembly.

The complete assembly of the system was the final step in the proposed project. The slip ring was carefully inserted into the lower section of the chuck, and the piezoelectric transducer was placed into its designated casing. These two components were then connected via the M30 thread, ensuring proper alignment and tightness.

Additionally, the shrink-fit holder, already containing the cutting tool, was connected to the front mass of the transducer through the corresponding internal stud bolt. This connection was tightened to the previously established torque specification.

The entire assembly process was successfully executed without any identifiable issues. The completed assembly is depicted in Figure 85, along with the respective CAD model for comparison purposes.

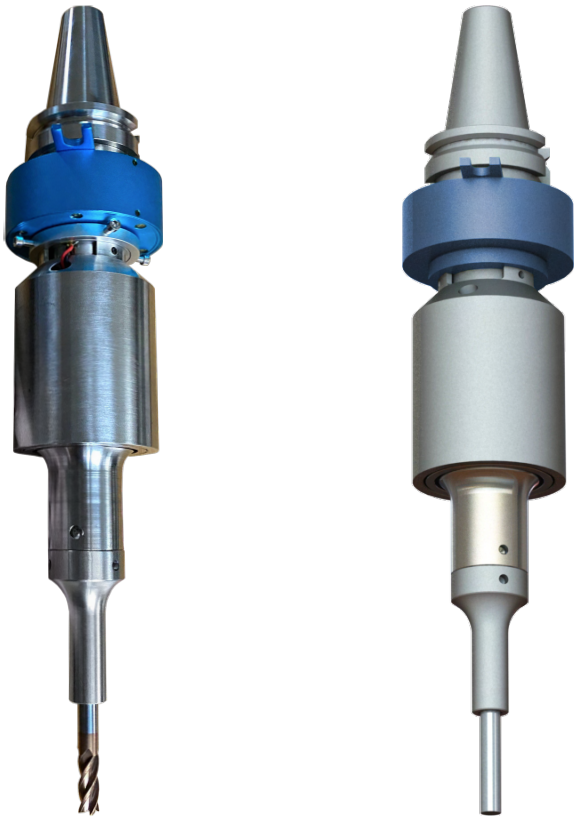

(a) Developed UAM system (b) Respective CAD representation

Figure 85: Developed system after complete assembly compared to its 3D CAD model.

Having assembled the developed UAM milling system, the project has been successfully completed.

4 Conclusions and Future Work

The completion of a project necessitates a thorough analysis of the accumulated data to derive relevant conclusions. The notion that the conclusions chapter solely comprises the obtained information, such as, for the present study, simulation results, and the prototype of the developed UAM system, is erroneous.

This specific chapter is thus a critical component of any research project, wherein the researcher must interpret the findings and contextualize them within the broader field of study. Therefore, in this concluding step of the document, the aim should be to provide a comprehensive analysis of the research outcomes and highlight their significance in advancing our understanding of the subject matter.

For this matter, there are three main questions that the study shall address, as depicted in Figure 86.

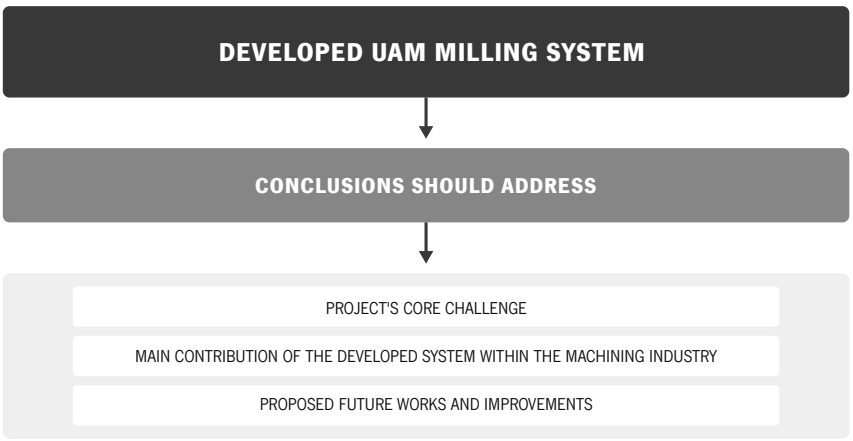

Figure 86: Rundown of the main topics the conclusions should focus on.

Nevertheless, prior to exploring the three presented questions, it is essential to provide an overview of the entire project, which will serve as a comprehensive summary of each completed phase. This review will serve as a useful reminder of the completed work while also facilitating the emergence of insights and responses to the aforementioned topics.

The significance of machining processes and their operations in modern industry cannot be overstated, as these methods are fundamental to the production of countless components for specific applications. Despite their importance, however, the constant technological evolution in diverse areas creates a bottleneck to the application of these technologies, as emerging materials with superior mechanical properties pose significant challenges to conventional machining processes. As previously highlighted in the introductory chapters of this thesis, alternative machining technologies such as UAM offer a viable solution to overcome these limitations.

These alternative methods aim to optimize every factor affecting machinability by refining existing machining techniques through the application of innovative engineering concepts. The objective is to improve productivity, enhance part quality, and reduce costs in comparison to conventional methods.

As demonstrated in Subchapter 2.1.1, UAM offers several advantages over traditional machining methods, including the possibility of using improved machining parameters, reduced cutting forces, longer tool lives, and improved surface finish. Its ability to facilitate chip breaking and reduce burr formation is particularly useful in precision manufacturing applications, and its potential for machining difficult-to-machine materials makes it one of the most promising alternative machining technologies.

Despite the lack of existing research on the topic of UAM for milling applications, this presents a great opportunity to explore and advance this technology. The potential for improved machining efficiency through the application of engineering concepts and the development of viable technologies is not only interesting from an academic and engineering standpoint but also fundamental for practical applications.

The comprehensive theoretical introduction to the technology and the clarification of its underlying principles in the overview section prior to project development were critical to the study. Understanding the complex nature of vibration application and all involving concepts such as resonance, frequency, and amplitude allowed the simplification of the subsequent project development process.

Additionally, the presented kinematic analysis, as well as the individual study of the functionality of each component and how they interact within the system as a whole, granted that the development phase was able to proceed with greater efficiency and accuracy.

4.1 Project Overview

Each phase of the project development process made significant contributions toward the optimization of the updated system. It was evident from the outset, during the analysis and reimagination of the *AdvUSMachining* system, that the updated version would require solutions to address the apparent issues such as the excessive dimensions and non-optimal geometry of the original design, poor material uniformity, and the suboptimal choice of the tool fixation area, ultimately leading to decreased operational efficiency.

The revised UAM system features a more compact design, achieved through the reduction of both the mean external diameter and the variation in external diameter ratio. Specifically, the external diameter ratio between the slipring and the sonotrode has been reduced from 76% to 56%, resulting in a maximum external diameter reduction from 158 mm to 86 mm. Furthermore, the overall length of the system has been reduced from 500 mm to 417 mm to minimize tool flexion when subject to the machining forces within the cutting process.

Figure 87 presents a visual comparison of the overall dimensions of both systems, highlighting the compactness achieved through the updated geometry.

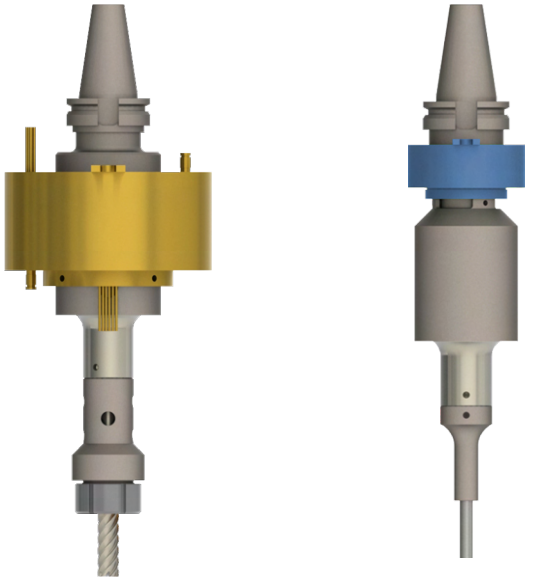

(a) AdvUSMachining (b) Developed UAM System

Figure 87: Visual comparison of studied systems.

The resulting system's geometry presents a significantly more viable alternative, rendering it more compatible with practical application scenarios. This achievement is evidenced by the separation of the upper area of the system into two distinct components in the slipring application area, which facilitates a smoother and more adjustable assembly process through the internally threaded connection. Moreover, the reimagination of the tool fixation method not only enhances the system's operational efficiency but also represents a notable innovation, resulting in a unique stable system that stands apart from the existing research on the application of ultrasonic technology to conventional machining processes.

The design of a sonotrode as a shrink-fit tool holder has yielded several advantages, including a secure and reliable fixation capability owing to the excellent clamping force provided by these types of components. Moreover, this design has led to a reduction in the number of components required for the system, minimizing the points of contact and potential undesired damping effects. However, one potential area for improvement pertains to the material optimization of this component. Matching the sonotrode material with that of the transducer's front mass, *Ti6Al4V*, could enhance the system's uniformity and deliver additional benefits stemming from this material's superior mechanical properties. Further experimentation could facilitate optimization and contribute to the system's overall effectiveness.

The optimized geometry for this component was determined through an extensive simulation process consisting of three distinct studies, with each one playing a fundamental role in the development of the finalized updated model.

The iterative simulation process facilitated the determination of the desired eigenfrequency for the system and subsequent optimization of the sonotrode until optimal operation was achieved, with the transducer working inductively at its nominal frequency of 20 kHz within the optimal working spectrum of the system's impedance curve.

The resulting impedance curve for the updated sonotrode configuration indicated a resonance frequency, f_R, of 19773 Hz, corresponding to an impedance Z_R of 3.0104 Ω. The anti-resonance point corresponded to a frequency value, f_A, of 20280 Hz, with an impedance Z_A of 20280x10^4 Ω.

A displacement profile analysis was conducted to evaluate the vibration amplitude of the tool, which revealed that the selected sonotrode configuration complied with the proposed guidelines for ultrasonic machining systems. Specifically, the antinode was found to coincide with the free end of the tool, thereby maximizing the system's efficiency.

In study 3, it was determined that a heating period of only 5 seconds using a 5 kW induction coil would suffice to achieve the desired expansion values. Albeit, to avoid potential warping of the *AISI 316L* holder, the heating process was done in three consecutive two-second intervals. For this matter, the simulated heating time can be considered a secondary variable since the obtained value did not affect the validity of the optimized system.

It's worth noting, however, that the use of *Ti6Al4V*, with its superior properties, including high strength-to-weight ratio and excellent corrosion resistance, would not only further enhance the smooth insertion of the tool but also significantly mitigate the risk of material warping.

The three studies conducted demonstrate the validity of the developed system, and the corresponding components were successfully produced for subsequent system assembly. It is imperative to acknowledge the significance of this aspect of the project, as the assembly of the physical model may reveal hidden issues or obstacles. Nevertheless, the production process and procurement of commercially available components were seamless, and the assembly was accomplished without any complications.

Overall, the design process of the updated system involved meticulous consideration of various technical factors, necessitating a time-consuming and challenging process of creative thinking. However, this effort has yielded a highly refined and robust system that delivers enhanced fixation and reliability while meeting the requirements for maximum optimization.

The updated differentiated system represents a significant improvement over the previous iteration, demonstrating the importance of careful attention to detail and exhaustive evaluation of technical aspects. Through the incorporation of new and advanced features, the updated version aims to achieve superior performance, providing improved precision and stability for high-speed rotating applications.

4.2 Core Challenges and Resulting Outcomes

As with any academic research study, the extensive investigative aspect of the project is time-consuming but essential for gaining a basic understanding of the technology's concepts.

In this particular case, the development of the optimized UAM system required a thorough grasp of engineering concepts related to the machining industry, such as machining processes, machinability, advanced materials, and their specific properties and applications. Moreover, a comprehensive understanding of the fields of ultrasonic vibration and modal analysis was also necessary. In addition, proficiency in CAD and numerical simulation were critical for the project's success. Therefore, the extensive nature of the project resulted in a completely optimized physical prototype that is distinct from those typically found in academic research. However, the complexity of the theme and the extensive nature of the project presented significant challenges throughout its completion.

Another major obstacle encountered was the scarcity of theoretical research in the area of applying ultrasonic vibration to conventional milling processes, being primarily explored through empirical methods, with most systems of this type being utilized in other machining operations, such as turning and grinding.

Despite its complexity, the development of a physical model, supported by numerical simulation, and the subsequent demonstration of its validity hold significant importance for the fields of ultrasonics and machining. This distinctive system, which seamlessly incorporates both technologies, represents a valuable contribution to the industry. The successful creation of a functional prototype underscores the potential of this technology and highlights its promise for future use.

In terms of future research, several areas warrant further exploration. Firstly, it is essential to test the practical implementation of the system by assembling it in a milling center and conducting finishing passes on different workpiece materials and geometries. During this testing phase, it is vital to monitor machining parameters such as cutting speed, feed rate, and depth of cut.

In addition, a system for measuring cutting forces during operation could be introduced, allowing for a comparison of values obtained with and without vibration. The quality of the machined surface could also be studied by analyzing the surface roughness, and the wear of the tool can also be monitored. These proposed studies will provide valuable insights into the system's efficiency and effectiveness, contributing to a comprehensive understanding of both its performance and potential to transform the milling process.

Finally, the equipment could be further improved by developing an external system that uses control theory methods to constantly adjust the employed vibration frequency to optimal values by analyzing feedback on the system's reactive energy. This would lead to a self-regulating device that could open up new possibilities for improving the machining process even further.

Bibliography

[1] M. Komaraiah and P. N. Reddy. "Rotary ultrasonic machining— a new cutting process and its performance." In: *International Journal of Production Research* 29 (11 1991), pp. 2177–2187. issn: 1366588X. doi: 10.1080/00207549108948077.

[2] H. Puga. *Maquinagem Aplicada*. Universidade do Minho, 2020.

[3] J. L. C. F. Grilo. "Ultrasonic assisted machining - Cutting tool optimization." 2017.

[4] W. Grzesik. *Advanced Machining Processes of Metallic Materials*. 2017.

[5] D. Carson, R. Diemer, and M. Short. *Ultrasonic Assisted Machining - Introducing Intense Vibrations to Enhance Metalworking*.

[6] A. Adeyinka. *Predictive Model for Thermal Response During Dry Machining of Al 6082-T6 using Fem Operations Research and Management View project Finite Element Method, Machining View project*. 2020. url: https://www.researchgate.net/publication/342661400.

[7] J. Iverson. *6 Factors Maximize Profitability in High-Precision Machining*. Oct. 2015. url: https://www.mmsonline.com/articles/6-factors-help-maximize-profitability-in-high-precision-machining.

[8] J. Pujana, A. Rivero, A. Celaya, and L. N. L. de Lacalle. "Analysis of ultrasonic-assisted drilling of Ti6Al4V." In: *International Journal of Machine Tools and Manufacture* 49 (6 May 2009), pp. 500–508. issn: 08906955. doi: 10.1016/j.ijmachtools.2008.12.014.

[9] M. C. Kuşhan, S. Orak, and Y. Uzunonat. "Ultrasonic Assisted Machining Methods: A Review." In: *International Journal of Advanced Engineering Research and Applications (IJA-ERA* (3 2017). issn: 2454-2377. url: www.ijaera.org.

[10] M Knight. *Composite Materials From: Durability of Composites for Civil Structural Applications, 2007 Composite Materials VI Uses of Composites*. 2003.

[11] T.-D. Ngo. *Introduction to Composite Materials*. 2020. url: www.intechopen.com.

[12] F. Feucht, J. Ketelaer, A. Wolff, M. Mori, and M. Fujishima. "Latest machining technologies of hard-to-cut materials by ultrasonic machine tool." In: vol. 14. Elsevier, 2014, pp. 148–152. doi: 10.1016/j.procir.2014.03.040.

[13] X. Xiao, K. Zheng, W. Liao, and H. Meng. "Study on cutting force model in ultrasonic vibration assisted side grinding of zirconia ceramics." In: *International Journal of Machine Tools and Manufacture* 104 (May 2016), pp. 58–67. issn: 08906955. doi: 10.1016/j.ijmachtools.2016.01.004.

[14] T. B. Thoe, D. K. Aspinwall, and M. L. H. Wise. *Review on Ultrasonic Machining*. 1998.

[15] H. Gong, F. Z. Fang, and X. T. Hu. "Kinematic view of tool life in rotary ultrasonic side milling of hard and brittle materials." In: *International Journal of Machine Tools and Manufacture* 50 (3 Mar. 2010), pp. 303–307. issn: 08906955. doi: 10.1016/j.ijmachtools.2009.12.006.

[16] X. Liu, W. Wang, R. Jiang, Y. Xiong, K. Lin, J. Li, and C. Shan. In: *Chinese Journal of Aeronautics* (4). issn: 10009361. doi: 10.1016/j.cja.2020.08.009.

[17] H. L. Ascroft, S. Barnes, A. Dahnel, N. F. H. A. Halim, H. Ascroft, A. N. DAHNEL, and N. A. F. Huda. *Ultrasonic Assisted Machining*. 2016. url: https://www.researchgate.net/publication/305687889.

[18] D. E. Brehl and T. A. Dow. *Review of vibration-assisted machining*. July 2008. doi: 10.1016/j.precisioneng.2007.08.003.

[19] A. Maurotto and C. T. Wickramarachchi. "Experimental investigations on effects of frequency in ultrasonically-assisted end-milling of AISI 316L: A feasibility study." In: *Ultrasonics* 65 (Feb. 2016), pp. 113–120. issn: 0041624X. doi: 10.1016/j.ultras.2015.10.012.

[20] Boeing. *Aero - Boeing 787 from the Ground Up*. 2008.

[21] C. Ni, L. Zhu, C. Liu, and Z. Yang. "Analytical modeling of tool-workpiece contact rate and experimental study in ultrasonic vibration-assisted milling of Ti–6Al–4V." In: *International Journal of Mechanical Sciences* 142-143 (July 2018), pp. 97–111. issn: 00207403. doi: 10.1016/j.ijmecsci.2018.04.037.

[22] F. Ning and W. Cong. *Ultrasonic vibration-assisted (UV-A) manufacturing processes: State of the art and future perspectives*. Mar. 2020. doi: 10.1016/j.jmapro.2020.01.028.

[23] C. Nath, G. C. Lim, and H. Y. Zheng. "Influence of the material removal mechanisms on hole integrity in ultrasonic machining of structural ceramics." In: *Ultrasonics* 52 (5 July 2012), pp. 605–613. issn: 0041624X. doi: 10.1016/j.ultras.2011.12.007.

[24] S. Kumar, S. Das, B. Doloi, and B. B. *Rotary Ultrasonic Machining–New Strategy of Cutting and Finishing*. Ed. by D. S., K. G., D. B., and B. B. 2020. doi: 10.1007/978-3-030-43312-3_3.

[25] Z. Yang, L. Zhu, G. Zhang, C. Ni, and B. Lin. *Review of ultrasonic vibration-assisted machining in advanced materials*. Sept. 2020. doi: 10.1016/j.ijmachtools.2020.103594.

[26] W. X. Xu and L. C. Zhang. "Ultrasonic vibration-assisted machining: principle, design and application." In: *Advances in Manufacturing* 3 (3 Sept. 2015), pp. 173–192. issn: 21953597. doi: 10.1007/s40436-015-0115-4.

[27] B. Zhao, P. Li, C. Zhao, and X. Wang. "Fractal characterization of surface microtexture of Ti6Al4V subjected to ultrasonic vibration assisted milling." In: *Ultrasonics* 102 (Mar. 2020). issn: 0041624X. doi: 10.1016/j.ultras.2019.106052.

[28] X. H. Shen, J. H. Zhang, H. Li, J. J. Wang, and X. C. Wang. "Ultrasonic vibration-assisted milling of aluminum alloy." In: *International Journal of Advanced Manufacturing Technology* 63 (1-4 Nov. 2012), pp. 41–49. issn: 02683768. doi: 10.1007/s00170-011-3882-5.

[29] A Sharman, X. P. Li, M Rahman, P. Bowen, R. Dewes, and D. Aspinwall. "Ultrasonic assisted turning of gamma titanium aluminide." In: Proceedings of the 13th International Symposium for Electromachining Isem XIII ; Conference date: 01-01-2001. Jan. 2001, pp. 939–951.

[30] I. Llanos, Ángela Campa, A. Iturbe, P. J. Arrazola, and O. Zelaieta. "Experimental analysis of cutting force reduction during ultrasonic assisted turning of Ti6Al4V." In: vol. 77. Elsevier B.V., 2018, pp. 86–89. doi: 10.1016/j.procir.2018.08.227.

[31] M. M. A. Zarchi, M. R. Razfar, and A. Abdullah. "Influence of ultrasonic vibrations on side milling of AISI 420 stainless steel." In: *International Journal of Advanced Manufacturing Technology* 66 (1-4 Apr. 2013), pp. 83–89. issn: 02683768. doi: 10.1007/s00170-012-4307-9.

[32] Y. S. Liao, Y. C. Chen, and H. M. Lin. "Feasibility study of the ultrasonic vibration assisted drilling of Inconel superalloy." In: *International Journal of Machine Tools and Manufacture* 47 (12-13 Oct. 2007), pp. 1988–1996. issn: 08906955. doi: 10.1016/j.ijmachtools.2007.02.001.

[33] Z. W. Zhong and G. Lin. "Diamond Turning of a Metal Matrix Composite with Ultrasonic Vibrations." In: *Materials and Manufacturing Processes* 20 (4 July 2005), pp. 727–735. issn: 1042-6914. doi: 10.1081/AMP-200055124.

[34] J. Ahn, H. S. Lim, and S. min Son. "Improvement of Micromachining Accuracy by 2-Dimensional Vibration Cutting." In: 1999.

[35] M. Xiao, K. Sato, S. Karube, and T. Soutome. "The effect of tool nose radius in ultrasonic vibration cutting of hard metal." In: *International Journal of Machine Tools and Manufacture* 43 (13 Oct. 2003), pp. 1375–1382. issn: 08906955. doi: 10.1016/S0890-6955(03)00129-9.

[36] F. H. Japitana, K. Morishige, and Y. Takeuchi. In: *Precision Engineering* (4). issn: 01416359. doi: 10.1016/j.precisioneng.2004.12.011.

[37] J.-D. Kim and E.-S. Lee. "A study of the ultrasonic-vibration cutting of carbon-fiber reinforced plastics." In: *Journal of Materials Processing Technology* 43 (2-4 June 1994), pp. 259–277. issn: 09240136. doi: 10.1016/0924-0136(94)90025-6.

[38] V. I. Babitsky, A. V. Mitrofanov, and V. V. Silberschmidt. "Ultrasonically assisted turning of aviation materials: Simulations and experimental study." In: vol. 42. Apr. 2004, pp. 81–86. doi: 10.1016/j.ultras.2004.02.001.

[39] N. Suzuki, H. Yokoi, and E. Shamoto. "Micro/nano sculpturing of hardened steel by controlling vibration amplitude in elliptical vibration cutting." In: *Precision Engineering* 35 (1 Jan. 2011), pp. 44–50. issn: 01416359. doi: 10.1016/j.precisioneng.2010.09.006.

[40] S. Xu, T. Kuriyagawa, K. Shimada, and M. Mizutani. *Recent advances in ultrasonic-assisted machining for the fabrication of micro/nano-textured surfaces*. Mar. 2017. doi: 10.1007/s11465-017-0422-5.

[41] M. A. Kadivar, J. Akbari, R. Yousefi, A. Rahi, and M. G. Nick. "Investigating the effects of vibration method on ultrasonic-assisted drilling of Al/SiCp metal matrix composites." In: *Robotics and Computer-Integrated Manufacturing* 30 (3 June 2014), pp. 344–350. issn: 07365845. doi: 10.1016/j.rcim.2013.10.001.

[42] J. L. Overcash and J. F. Cuttino. "Development of a Tunable Ultrasonic Vibration-Assisted Diamond Turning Instrument." In: 2003.

[43] V. I. Babitsky, V. K. Astashev, and A. N. Kalashnikov. "Autoresonant control of nonlinear mode in ultrasonic transducer for machining applications." In: vol. 42. Apr. 2004, pp. 29–35. doi: 10.1016/j.ultras.2004.01.004.

[44] V. I. Babitsky, A. N. Kalashnikov, and F. V. Molodtsov. "Autoresonant control of ultrasonically assisted cutting." In: *Mechatronics* 14 (1 Feb. 2004), pp. 91–114. issn: 09574158. doi: 10.1016/S0957-4158(03)00014-X.

[45] J. Meireles. *Dinâmica de Estruturas*. Universidade do Minho, 2020.

[46] J. L. Humar. *Dynamics of Structures*. Second. A. A. Balkema, 2001.

[47] J. He and Z.-F. Fu. *Basic Vibration Theory*. Ed. by J. He and Z.-F. Fu. 2001. doi: https://doi.org/10.1016/B978-075065079-3/50003-6. url: https://www.sciencedirect.com/science/article/pii/B9780750650793500036.

[48] Y. Hara, M. Zhou, and A. Li. *Constant Vibration Amplitude Method of Piezoelectric Transducer Using A PLL (Phase Locked Loop) You may also like Piezoelectric energy enhancement strategy for active fuzzy harvester with time-varying and intermittent switching*.

[49] E. Shamoto, N. Suzuki, T. Moriwaki, and Y. Naoi. *Development of Ultrasonic Elliptical Vibration Controller for Elliptical Vibration Cutting*.

[50] J. Gao, H. Caliskan, and Y. Altintas. "Sensorless control of a three-degree-of-freedom ultrasonic vibration tool holder." In: *Precision Engineering* 58 (July 2019), pp. 47–56. issn: 01416359. doi: 10.1016/j.precisioneng.2019.05.005.

[51] P Legge. "Ultrasonic drilling of ceramics." In: *Ultrasonics* 2 (3 July 1964), p. V. issn: 0041624X. doi: 10.1016/0041-624X(64)90264-1.

[52] E. Shamoto and T. Moriwaki. "Study on Elliptical Vibration Cutting." In: (1994). doi: https://doi.org/10.1016/S0007-8506(07)62158-1.

[53] E. Shamoto, N. Suzuki, R. Hino, E. Tsuchiya, Y. Hori, H. Inagaki, and K. Yoshino. "A new method to machine sculptured surfaces by applying ultrasonic elliptical vibration cutting." In: vol. 2005. 2005, pp. 84–89. isbn: 0780394828. doi: 10.1109/MHS.2005.1589969.

[54] Y. Wang, H. Gong, F. Z. Fang, and H. Ni. "Kinematic view of the cutting mechanism of rotary ultrasonic machining by using spiral cutting tools." In: *International Journal of Advanced Manufacturing Technology* 83 (1-4 Mar. 2016), pp. 461–474. issn: 14333015. doi: 10.1007/s00170-015-7549-5.

[55] C. T. Group. *Ultrasonics - Ultrasonic Generators*. 2012. url: https://techblog.ctgclean.com/2012/01/ultrasonics-ultrasonic-generators-introduction/.

[56] R. E. Berg. *ultrasonics*. Encyclopedia Britannica, Oct. 2017. url: https://www.britannica.com/science/ultrasonics.

[57] H. Shekhani. *Macroscopic PZT Properties*. Jan. 2015. url: https://www.learnpiezo.com/.

[58] C. P. Hampton. *Failure Analysis of a 30 kHz Ultrasonic Welding Transducer*. 2010.

[59] D. Damjanovic. "Ferroelectric, dielectric and piezoelectric properties of ferroelectric thin films and ceramics." In: *Reports on Progress in Physics* 61 (9 Sept. 1998), pp. 1267–1324. issn: 0034-4885. doi: 10.1088/0034-4885/61/9/002.

[60] M. Interconsulting. *Piezoelectric Transducers Modeling and Characterization*. 2004. url: http://mastersonic.com.

[61] D. Berlincourt, D. Curran, and H. Jaffe. *Piezoelectric and Piezomagnetic Materials and Their Function in Transducers*. 1964. doi: 10.1016/B978-1-4832-2857-0.50009-5.

[62] ZVEI. *Ultrasonic Assembly of Thermoplastic Mouldings and Semi-finished Products: Recommendations on Methods, Construction and Applications*. 2006.

[63] T. 16285. *BT50 ER40 Collet Chuck*. url: https://allindustrial.com/techniks-16285-bt50-er40-collet-chuck-x-80mm-length/.

[64] HAIMER. *Shrink Fit Tool Holder*. url: https://www.grainger.com/product/HAIMER-Shrink-Fit-Tool-Holder-Compatible-46LM03.

[65] Senring. *H4086 Series SlipRing Catalog*.

[66] HAIMER. *Tool Holders Catalog*. 2020. url: https://www.haimer-usa.com/services/media-center/brochures.html.

[67] mES. *Fit Tolerances and Specifications*. url: https://www.mec-engineering-spreadsheets.com/documentation-area/fit-tolerances-and-applications/.

[68] Schaeffler. *Technical Pocket Guide*. Vol. 2nd Edition. 2018.

[69] Elco. *Shrinking Equipments*. url: https://www.elco.eu/en/catalogue.